UNIVERSITAT POLITÈCNICA
DE CATALUNYA

Dynamical behavior of delay-coupled semiconductor lasers

Cristina Martínez González

Memòria presentada per a optar a grau de Doctor per la Universitat Politècnica de Catalunya

Directors:

Jordi García Ojalvo
M. Carme Torrent Serra

Departament de Física i Enginyeria Nuclear
Universitat Politècnica de Catalunya

Terrassa, 2008

Durant aquests anys he conegut i treballat amb molta gent, el que considero la part més interessant del fet de realitzar una tesi. Voldria agrair la paciència, el bon fer i l'acolliment que he rebut de tothom, començant pels meus directors de tesi en Jordi García Ojalvo i la M Carme Torrent. La seva paciència no té límits i la manera de ser i ajudar als seus estudiants fa que tots els tinguem un apreci que va molt més enllà d'una pura relació laboral. M'han ajudat sempre que els he necessitat i en els moments de baixa moral científica (que creieu-me, han estat molts) m'han suportat estoicament. Per això i per que els consideraré per sempre més uns amics, moltes gràcies per ser com sou.

Aquesta gran experiència no hagués estat possible sense la intervenció d'en Ramon Vilaseca, que em va considerar per treballar amb el Jordi i la Carme sense tenir referències meves anteriors. Trobar persones que et donen aquest vot de confiança és realment gratificant.

Agrair també a tota la gent de les subseccions de Terrassa, tant a la gent ubicada a l'Escola d'Enginyeria Superior com a la d'Enginyeria Tècnica. En especial a l'administrativa del departament, la Montse, amb la que hem compartit bons moments i que sempre s'ha preocupat de facilitar-me les coses.

I would like to specially thank to Ingo Fisher his attentions during my stay in Brussels. The best part of my stay was the possibility of learning from his experience. Thanks a lot, Ingo, you're a great scientist and a better person. Ha sigut una molt bona experiència treballar amb el grup de la Vrije Universität, i em van demostrar que la hospitalitat no té fronteres. Gracias a todos los españoles que vivían allí y que hicieron mi estancia más que agradable, especialmente a Amaia.

Els companys de feina han sigut molt més que companys. Gràcies al Xavi vaig

començar la tesi ja que em va animar a parlar amb el departament, sense ell ni hagues començat. Gracias a Elena, por alegrarme la estancia en Terrassa (y por esos tiramisús que son un don de dios), y a Sergio, Luís y Gemma por soportarme durante el tiempo que vivimos juntos. Moltíssimes gràcies Gemma per ajudar-me a superar l'insuperable en l'univers matemàtic (no sé què hagués fet sense tu). Moltes gracies Marc per el teu companyerisme, i al Jordi Sellares per ajudar-me sempre amb els meus problemes (profunds) amb el Linux. A Muriel, Crina y Cristina por todo lo que hemos compartido juntas, por las charlas existenciales y las no existenciales. Moltes gràcies als nou vinguts (els dos Jordis, Toni, Lorena, Belen i Núria) que tot i que vau arribar quan ja acabava espero continuar col.laborant amb vosaltres. Y por último, que siempre se deja lo más importante, a Javier y a Pablo que han sido unos compañeros sensacionales, científicamente y personalmente. Ni que decir tiene que la experiencia en el laboratorio de Javier me salvó de hundirme en la desesperación. Quiero agradecerles a los dos que hicieran de los congresos, cenas y cursos lo mejor de mi tesis. Ya no volvieron a ser lo mismo desde que os fuisteis.

Agrair també a totes les persones amb les que he coincidit en els congressos durant la tesi i que per uns quants dies han estat grans companys en terres extranyes.

Sobretot agrair als companys de Girona el seu recolzament continu tots aquests anys, sense el qual no hagués estat possible acabar. Gràcies Marta, Gàlia (gràcies per acompanyar-me durant les hores de biblioteca), Santi i Roger, que es pot dir dels millors amics que es poden tenir, sou uns amics de veritat.

També, com no, agrair a la Carlota i la Miriam que m'han demostrat que les amistats poden durar per sempre, i encara que estiguem lluny els retrobaments són com el primer dia.

Y para acabar, quiero dar gracias a mis padres, que sacrifican todo por mí, mi hermano y cuñada que me han ayudado siempre, a mi abuela que siempre ocupará buena parte de mi corazón, y sobretodo a mi marido que es el que realmente ha llevado el peso de esta tesis, soportando todos mis altibajos (Jessè, você merece um monumento).

Cristina Martínez González

Contents

Part I

INTRODUCTION

Chapter 1

Dynamics of solitary semiconductor lasers

1.1 Historic overview and types of semiconductor lasers

The importance of *semiconductor lasers* in present industrial applications is the result of a very active field of research in the previous century. Theories developed in first half of the century settled the bases to describe the interaction between radiation and matter. For instance, Planck (see e.g. Kuhn, 1978) described in 1900 the spectrum of the electromagnetic radiation emitted by a black body, and Einstein in 1917 (Hawks and Latimer, 1995) proposed the existence of stimulated emission, through the interpretation of Lenard's experiment on the photoelectric effect. Nevertheless, the experimental implementation of the stimulated emission to obtain light

amplification did not materialize until decades later. A first stage of development started with Gordon, Zeiger, and Townes (1954), who showed that the electromagnetic radiation could be amplified in the microwave range using the concept of stimulated emission, leading to the *maser* (microwave amplification by stimulated emission of radiation). First steps towards the extension of the concept to optical frequencies were made by Dicke (1958), and Proktov (1958). Schawlow and Townes (1958) settled the theoretical mechanism to pump an optical resonator, using an excited gas enclosed into a Fabry-Perot interferometer as an amplification system. The *laser* (light amplification by stimulated emission of radiation) was finally obtained by Maiman (1960), with a ruby laser showing pulsed operation. Javan *et al* (1961) subsequently built the first He-Ne gas laser.

In 1960 Agrain suggested that the radiative combination of electrons and holes in a semiconductor material could give rise to a maser in the infrared frequencies (see Russell (1987)). Dumke (1962) pointed to GaAs (which has direct bandgaps) as amplifying medium. Experimental investigations published simultaneously by Nathan *et al* (1962) in IBM, Hall *et al* (1962) in General Electric, and Quist *et al* (1962) from MIT Lincoln Laboratories showed laser amplification in GaAs diodes. The electron-hole recombination in the depletion region of the p-n junction produced the optical gain, and the polished facets perpendicular to the junction plane provided optical feedback, by forming a resonant cavity.

Kroemer (1963) and Alferov and Kazarinov (1963) suggested that semiconductor lasers could be improved (increasing the carrier lifetime) if a semiconductor material was clamped between two layers of semiconductors with a wider bandgap. This was the first theoretical proposal of heterostructure lasers, with two different

semiconductor materials, in contrast with homostructure lasers, which have a single semiconductor. In these early years it was difficult to match the lattice constants of the two semiconductor materials to build a heterostructure. In 1969 a semiconductor pulsed laser that could work at room temperature was built. Until 1970 it was not possible to have heterostructure lasers operating continuously at room temperature (Hayashi *et al*, 1970).

Later, in 1971, the first gain-guided structure was manufactured, and during the following years index-guided structures were developed, where a lateral confinement was forced by an index difference on both sides of the stripe.

In 1975 it was possible to build a laser with emission wavelength of 1.1 μm, in 1977 the wavelength reached 1.3 μm and in 1979, 1.5 μm. More recent advances include quantum well, distributed feedback, and vertical-cavity surface emitting lasers, which we will explain in the next section.

The simplest semiconductor laser consists of a semiconductor p-n junction, as showed in Fig. 1.1, operated in forward bias (a positive voltage is applied to the p side of the junction with respect to the n side). Energy bands are continuous across the junction, because the semiconductors on the two sides have the same bandgap. The current applied in the p-n material produces the injection of electrons from the conduction band of the n-type material to the p-type material, while holes are injected in the opposite direction.

When an electron and a hole are in the same region, they can recombine, giving rise to spontaneous emission, which is necessary to initiate the stimulated emission. The key of lasing is the transition of an electron from an occupied state at a high energy level to an empty state at a lower energy, due to the stimulated emission process.

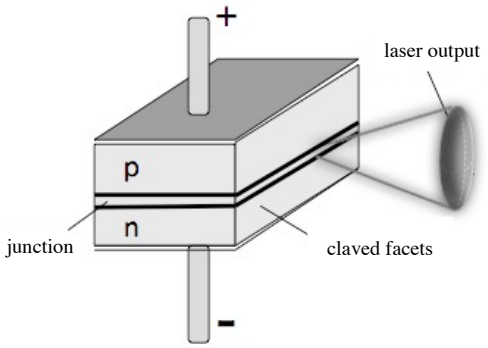

Figure 1.1: *Schematic semiconductor laser diode. Lasing occurs in the plane of the junction.*

The cleaved facets of the device act as mirrors, reflecting photons back into the laser cavity where they interact with excited electrons. The cavity is designed to resonate at a frequency corresponding to the energy of stimulated emission, amplifying the photons that propagate at the same direction. Lasing occurs when the amplification or gain is higher than the losses inside the cavity. This occurs at a given threshold value of the pump current, and emission occurs in the plane of the junction.

Figure 1.2 shows the most common types of semiconductor lasers:

- Homostructure: it consists in a p-n union, with cleaved facets. There is no defined region in which the recombination can take place, and carriers can diffuse before recombination occurs. As a result, the threshold current is very high.

- Heterostructure: reduces considerably the threshold current. The active region (where the recombination processes take place) is sandwiched between two oppositely doped semiconductors with higher bandgap and lower refractive index compared with the active layer. This difference in the bandgap

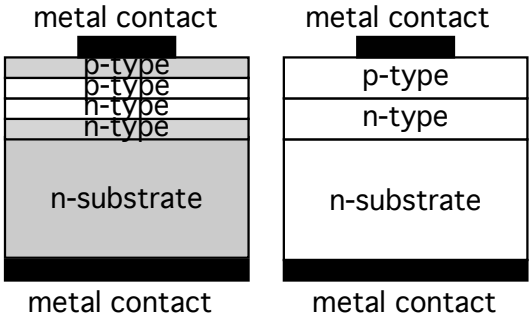

Figure 1.2: *Schematic heterostructure (left) and homostructure (right) semiconductor lasers. In heterostructure lasers, a layer of low bandgap material (white) is sandwiched between two high bandgap layers (grey). Homostructure lasers consist in a p-n union of same type of semiconductor materials.*

confines the electron and holes to the active layer, where they can recombine to produce the optical gain. At the same time the difference in the refractive index transforms the active region in a waveguide.

There are several different heterostructures, but the two basic ones are the single-heterostructure and the double-heterostructure, depending on whether the active region is surrounded by one or two cladding layers of higher bandgap. Because of the index steps on both sides of the active layer, the wave guide in the double heterostructure geometry is much more effective than in the single one. The active layer in a double heterostructure laser (DH) is typically between 100-300 nm.

When the active region of a DH is thin enough (< 50 nm), the structure becomes a quantum well (QW). In quantum well lasers the vertical variation of the electron's wavefunction, and thus its energy, is quantized (Liu, 2005). The conduction and valence bands are divided in subbands corresponding to the quantized levels. A higher number of electrons can occupy these subbands, which implies that for a

given injection current, the gain is much higher than in the QW lasers because it is easier to reach the transparency (minimum number of carriers to have gain or amplification equal to the losses inside the cavity, Sec. A.2.3 of Appendix A). This leads to low threshold currents and allow higher modulation speed.

The energy distribution of the electrons in the QW structures is narrower than that in the standard double herostructures. Therefore, the optical gain concentrates on a certain energy (wavelength). As a result, quantum well lasers have a narrower laser linewidth.

Semiconductor lasers can also be classified according to the direction of emission with respect to the junction. The optical field in a semiconductor laser can propagate either horizontally or vertically with respect to the junction, and can thus be emitted parallel or perpendicular to the junction. We can thus classify semiconductor lasers into edge-emitting if the light is emitted through the side surfaces perpendicular to the junction plane, or surface-emitting laser diodes, if the light is emitted through a surface parallel to the junction interface.

Edge-emitting laser diodes can be classified according to their geometry in:

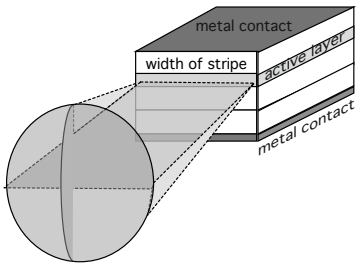

Figure 1.3: *Broad area edge-emitting laser (adapted from Liu (2005)).*

- Broad-area geometry. These lasers do not have a particular restriction in the

propagation or guiding of the optical wave (in the direction parallel to the junction). This leads to multiple transverse modes in the emission profile.

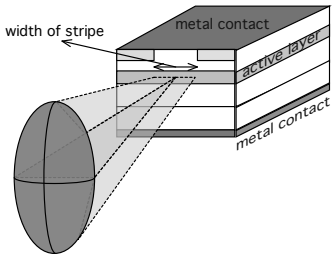

Figure 1.4: *Stripe edge-emitting laser (adapted from Liu (2005)).*

- Stripe-geometry. Almost all laser diodes have a stripe geometry. It restricts the carriers and the optical field in a confinement area parallel to the junction. Due to the different vertical and lateral guiding structure, the emission profile is strongly asymmetric, with different vertical and lateral divergence angles. The width of the stripe is still much larger that the thickness of the active layer, and the output light of the laser has the perpendicular divergence angle higher than the parallel one, resulting in a beam with an stronger elliptic section (Fig. 1.4). This restriction can allow transverse single mode operation along the junction plane.

Stripe-geometry lasers can be classified depending on the way of confinement of the propagating wave into (Agrawal and Dutta, 1986):

- Gain-guided: the current injection is restricted over a narrow region along the junction plane. A stripe of concentrated carriers forms the active layer along the longitudinal direction, which results in a stimulated amplification

of the optical field along it. The lateral variation of the optical gain restricts the propagation to the stripe. An undesirable characteristic of these type of lasers is the antiguidance effect. In semiconductor lasers an increase in the carrier density produces a decrease in the refraction index (see Sec. A.4 in Appendix A), which spreads the optical field laterally instead of confining it. It is necessary a very narrow stripe to compensate the spread of the gain.

- Index-guided: the active region is buried into higher-bandgap layers. The refraction index step is larger than the carrier-induced effects along the junction plane, producing a very low antiguidance effect. As a result, the lasing characteristics of these lasers are determined by the rectangular waveguide that confines the mode inside the buried active region. Due to this confinement the size of the emitting profile and its divergence are smaller.

Depending on the type of cavity, there are three different kinds of edge-emitting semiconductor lasers (Fig. 1.5):

- FP: Fabry-Perot lasers with a resonant cavity formed by cleaved end facets.
- DBR: distributed Bragg reflector lasers, with Bragg reflectors as end mirrors.
- DFB: distributed feedback lasers, which use a grating as a feedback mechanism.

The small dimensions of semiconductor lasers, the high efficiency in converting electrical current into coherent light, the very small power supply requirements, and the effective cost production, make them attractive devices for industrial applications. Examples of technical applications are CD/DVD storage, laser printing,

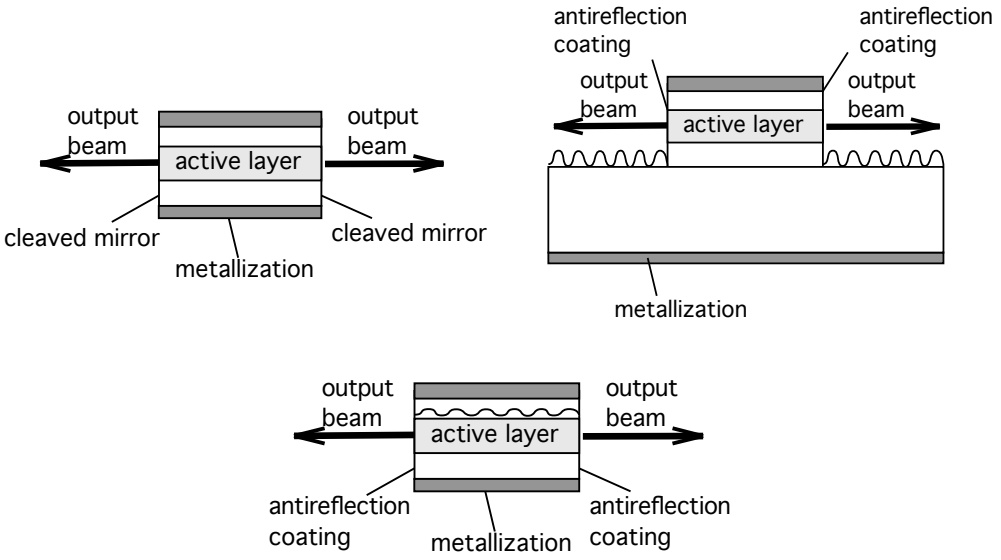

Figure 1.5: *Basic cavity structures for edge-emitting laser diodes. Left: Fabry-Perot laser diode (FP), right: distributed Bragg reflector semiconductor laser (DBR), and bottom: distributed feedback semiconductor laser (DFB).*

scanning, surgery, or material processing. Fiber-optics telecommunications is also a very important application of semiconductor lasers.

There are many differences between semiconductor lasers (SL) and other kinds of lasers. SL have a high gain, generated by the population inversion between the conduction and valence bands, the shape of the beam section is elliptical, and its divergence tends to be large. The gain spectrum is large (many THz). The short cavity (several hundreds of μm) means that the longitudinal mode spacing is much larger than that of a conventional solid state laser (on the order of GHz). The typical reflectivities of the cleaved facets (around 30%) are sufficient for lasing action, due to the very high gain of the material. These devices also react easily to external perturbations as optical feedback or optical injection, which produce changes in

the dynamics of the output power, linewidth, and stability. Semiconductor lasers evolve on fast time scales, the parameters of the device are well known, and are experimentally well controllable. All these characteristics make semiconductor lasers interesting devices to study nonlinear dynamical effects.

1.2 Rate equations

To understand the basic semiconductor laser dynamics, it is necessary to obtain time-dependent equations for the evolution of the field amplitude and carrier density. We summarize in this subsection the mathematical derivation of a rate equation model for a semiconductor laser.

There are two different ways to describe the dynamics of semiconductor lasers: deriving the rate equations directly from the Maxwell equations, or introducing a field equation approach inside the gain medium expression to derive the rate equations.

In the first case, from the Maxwell equations describing the electromagnetic field in a medium, it is possible to arrive with some approximations, to the semiclassical Maxwell-Bloch equations. This leads to three differential equations: for the optical field, the material polarization, and the population inversion (see Heil (2001) and Dellunde (1996) for a detailed derivation). For semiconductor lasers (class B lasers, whose polarization decay rate is much higher than the decay rates of the population inversion and optical field), one can apply the adiabatic elimination of the polarization, which finally leads to two rate equations describing the variation of the electrical field and the population inversion.

In the second case, introducing a field equation approach inside of the gain medium it is possible to derive the rate equation model (Petermann, 1988). First, it is necessary to derive the gain condition of the material to reach stationary laser oscillation, and then the differential equations for the dynamical variables of the semiconductor laser.

In our case, we will use this second method to derive the rate equations model. We consider a Fabry-Perot cavity laser as described in Fig. 1.6. A plane wave inside the cavity has the stationary-wave expression:

$$E(z,t) = E_0 e^{i\omega t} e^{-ikz} = E(z) e^{i\omega t} \ , \tag{1.1}$$

where E_0 is the amplitude, ω the frequency of a longitudinal mode, and k the wave vector.

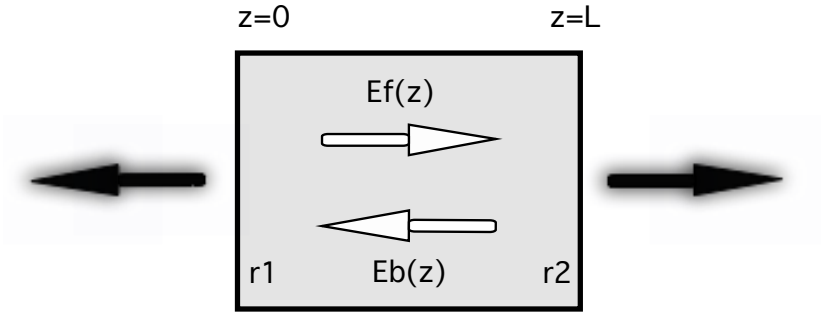

Figure 1.6: *Schematic semiconductor laser cavity. z: facets, r_i: reflectivities of the cleaved facets, $E_f(z)$ and $E_b(z)$: forward and backward traveling complex electrical field, respectively.*

This wave will be amplified in both directions (forward, E_f and backward, E_b),

because of the reflection at the cleaved facets at $z = 0$ and $z = L$ (although we consider the mirror losses uniformly distributed).

Considering the amplification of the material, g, together with the absorption, α_{abs}, the power of the forward (backward) wave into the material is:

$$P_f(z) = P_{f0} e^{gz - \alpha_{abs} z} \ , \tag{1.2}$$

where P_{f0} (P_{b0}) is the power amplitude at the front (rear) facet.

The field amplitude and the optical power are related by: $P(z) \sim |E_0|^2$. Using Eqs. (1.1) and (1.2), and $E_{f0} = \sqrt{P_{f0}}$, the expressions of the forward and backward fields take the form:

$$\begin{aligned} E_f(z) &= E_{f0} e^{\left[-i\frac{\omega}{c} n z + \frac{1}{2}(gz - \alpha_{abs} z)\right]} \\ E_b(z) &= E_{b0} e^{\left[-i\frac{\omega}{c} n (L-z) + \frac{1}{2}(g(L-z) - \alpha_{abs}(L-z))\right]} \ , \end{aligned} \tag{1.3}$$

where E_{f0} and E_{b0} are the amplitudes at the facets, $\kappa = \frac{\omega}{c} n$ is the real part of the wavevector, α_{abs} the absorption coefficient due to the losses inside the cavity, and $n(N)$ is the refractive index, with N the carrier density.

Applying the continuity condition in the reflection at the cleaved facets we arrive to a relation between the forward and backward waves in the material :

$$\begin{aligned} E_f(0) &= r_1 E_b(0) \\ E_b(0) &= r_2 E_f(L) \ , \end{aligned} \tag{1.4}$$

where $r_1 = \sqrt{R_1}$ and $r_2 = \sqrt{R_2}$ are the reflectivities of the cleaved facets.

The amplitudes of the forward $E_f(z)$ and backward $E_b(z)$ fields are related to each other:

$$\begin{aligned} E_{f0} &= r_1 E_b(0) \\ E_{b0} &= r_2 E_f(L) \ , \end{aligned} \tag{1.5}$$

Introducing Eqs. (1.3) into Eqs. (1.5) we arrive to the condition for the stationary laser oscillation:

$$r_1 r_2 e^{\left[-i2\frac{\omega}{c}nL+(gL-\alpha_{abs}L)\right]} = 1 \tag{1.6}$$

The real and imaginary parts of this equation give two different conditions, one referring to the amplitude and the other one corresponding to the phase.

With the phase condition [taking the imaginary part of Eq. (1.6)], we can calculate the different mode frequencies that can be sustained inside the cavity:

$$\omega_{th} = \frac{mc\pi}{Ln} \ , \tag{1.7}$$

where c is the speed of light, L the cavity lenght, n the refractive index, and m is an integer that accounts for the mode number.

For evaluating the spacing between adjacent frequency emission modes, $\Delta\nu = \nu_m - \nu_{m+1}$, one must take into account the dispersion of the refractive index, so that an effective group index

$$\overline{n} = n + \omega\frac{dn}{d\omega} \ , \tag{1.8}$$

must be introduced, yielding:

$$\Delta\nu = \frac{c}{2L\overline{n}} \tag{1.9}$$

Since the group velocity of the optical wave is given by $v_g = c/\overline{n}$, the spacing between adjacent modes corresponds to the inverse of the round trip time delay of the laser cavity:

$$\Delta\nu = \frac{c}{2L\overline{n}} = \frac{1}{\tau_L} \tag{1.10}$$

The amplitude condition of Eq. (1.6), leads to an expression of the gain needed to reach the lasing threshold:

$$g_{th} = \alpha_{abs} + \frac{1}{2L}\ln\left[\frac{1}{R_1 R_2}\right] \ , \tag{1.11}$$

where we have not considered the spontaneous emission in the material: the real gain is slightly smaller than this defined g_{th}.

After deriving the gain condition of the material to reach stationary laser oscillation, we will find a time-dependent equation for the evolution of the variables of a semiconductor laser. By defining the round trip gain, which is the gain experienced by the traveling wave during one round trip inside the cavity, we proceed to get the rate equation which describes the dynamical evolution of the photon number inside the cavity.

The gain in the laser medium for each round trip inside the laser cavity (the round-trip gain), taking into account the reflections at both mirrors (r_1 and r_2), the phase accumulation, the gain, and absorption effects after propagation a distance

$2L$ is:

$$\mathcal{G} = r_1 r_2 e^{\left[-i2\frac{n\omega}{c}L+(gL-\alpha_{abs}L)\right]} \tag{1.12}$$

This quantity depends directly on the optical frequency and indirectly on the carrier number through the refractive index. The field inside the cavity oscillates with a frequency around ω_{th}, which is the lasing frequency at threshold, and the carrier density value is around its value at threshold.

The resonance frequencies of the cavity [Eq. (1.7)] must be integer multiples of $\frac{\pi}{L}$, but at the same time, they depend on the optical frequency and carrier number at threshold, through the refractive index $n(\omega_{th},\ N_{th})$. We therefore expand the term $\frac{n\omega}{c}$ in terms of the optical angular frequency ω_{th} and the carrier threshold N_{th}:

$$\begin{aligned}\frac{n\omega}{c} &\simeq \frac{n_{th}\omega_{th}}{c} + \frac{1}{c}\frac{\partial\,(n\omega)}{\partial\omega}\Big|_{Nth}(\omega-\omega_{th}) + \frac{1}{c}\frac{\partial\,(n\omega)}{\partial N}\Big|_{Nth}(N-N_{th}) = \\ &= \frac{n_{th}\omega_{th}}{c} + \frac{\overline{n}}{c}(\omega-\omega_{th}) + \frac{\omega_{th}}{c}\frac{\partial n}{\partial N}\Big|_{Nth}(N-N_{th})\ ,\end{aligned} \tag{1.13}$$

where we considered the effective refractive index $\overline{n}$ and that the optical frequency at threshold does not change with population inversion variations $\left(\frac{\partial\omega}{\partial N}\Big|_{Nth} \simeq 0\right)$.

We now introduce Eq. (1.13) in the roundtrip gain $\mathcal{G}$ expression given by Eq. (1.12), and split the roundtrip gain into a frequency independent (G_1) and a frequency dependent (G_2) term:

$$\mathcal{G} = G_1 \cdot G_2\ , \tag{1.14}$$

where,

$$G_1 = r_1 r_2 e^{(g-\alpha_s)L} e^{(-i\phi_G)}\ , \tag{1.15}$$

with,

$$\phi_G = \frac{2\omega_{th}L}{c}\frac{\partial n}{\partial N}\Big|_{Nth}(N - N_{th}) \ , \tag{1.16}$$

and,

$$G_2 = e^{-i\left[\frac{2n_{th}\omega_{th}L}{c}+\frac{2\overline{n}L}{c}(\omega-\omega_{th})\right]} \tag{1.17}$$

From the possible emission frequencies derived from Eq. (1.7) we can see that the first term of the exponential in Eq. (1.17) is a multiple of 2π. The second term can also be simplified by taking into account Eq. (1.10) and G_2 can be rewritted as:

$$G_2 = e^{-i[\tau_L(\omega-\omega_{th})]} \tag{1.18}$$

Once we have found a general expression for the round trip gain, we analyze the dynamics of the laser emission. Since the field essentially oscillates at ω_{th}, it is useful to introduce the complex time-dependent electric field:

$$\varepsilon(t) = E(t)e^{i\omega_{th}t} \tag{1.19}$$

where $E(t)$ is the slowly varying envelope of the electric field propagating in the positive direction inside the Fabry-Perot cavity.

The round trip gain is applied on each round trip to the light that travels inside the cavity, yielding an expression:

$$\begin{aligned} \varepsilon(t) &= \mathcal{G}\varepsilon_f(t) \\ \varepsilon(t) &= G_1 e^{i\tau_L\omega_{th}}e^{-i\tau_L\omega}\varepsilon_f(t) \end{aligned} \tag{1.20}$$

The term $e^{-i\tau_L\omega}$ can be considered as an operator in the frequency domain and to be expressed as $e^{-\tau_L\frac{d}{dt}}$ in the time domain, producing a time shift[1] of $(-\tau_L)$ in the electric field:

$$\varepsilon(t) = G_1 e^{i\tau_L\omega_{th}}\varepsilon_f(t-\tau_L) \tag{1.21}$$

Introducing Eq. (1.19) in the above expression, and ignoring the subindex for the forward traveling wave[2] we arrive to an expression for the slowly varying field after one round trip:

$$\begin{aligned} E(t)e^{i\omega_{th}t} &= G_1 e^{i\tau_L\omega_{th}}E(t-\tau_L)e^{i\omega_{th}(t-\tau_L)} \\ E(t) &= G_1 E(t-\tau_L) \end{aligned} \tag{1.22}$$

According to the small variation of the electric field envelope $E(t)$ during one cavity roundtrip, we can make the following approximation:

$$E(t) \simeq E(t-\tau_L) + \tau_L\frac{dE(t)}{dt} \tag{1.23}$$

So that:

$$-\tau_L\frac{dE(t)}{dt} = E(t-\tau_L) - E(t)\ , \tag{1.24}$$

and introducing Eq. (1.22) in the above equation, we obtain:

$$\frac{dE(t)}{dt} = \frac{1}{\tau_L}\left[1-\frac{1}{G_1}\right]E(t)\ , \tag{1.25}$$

---

[1] We can express: $e^{-\tau_L\frac{d}{dt}}\varepsilon(t) \simeq \varepsilon(t) - \tau_L\frac{d\varepsilon(t)}{dt} \simeq \varepsilon(t-\tau_L)$

[2] The boundary condition of the cavity is satisfied: after a round trip the amplitude of the field at $z=0,\ E(t)$, has to coincide with the previous field $E(t-\tau_L)$

where taking into account the expression (1.6) for lasing condition, we can consider G_1 lower than the unity. Therefore, we can expand the expression of G_1 [Eq. (1.15)]:

$$\begin{aligned}\frac{1}{G_1} &= \exp^{\left[-\ln(\sqrt{R_1R_2})-(g-\alpha_s)L+i\phi_G\right]} \simeq \\ &\simeq 1+\frac{1}{2}\ln(\frac{1}{R_1R_2})-gL+\alpha_sL+i\frac{2\omega_{th}L}{c}\frac{\partial n}{\partial N}\Big|_{Nth}(N-N_{th}) \ , \end{aligned} \quad (1.26)$$

and substituting Eq. (1.11) in this expansion:

$$\frac{1}{G_1} = 1-(g-g_{th})L+i\frac{2\omega_{th}L}{c}\frac{\partial n}{\partial N}\Big|_{Nth}(N-N_{th}) \quad (1.27)$$

The gain g in last equation is carrier dependent and it can be linearized around its threshold value g_{th}, leading to:

$$g(N) = g_{th}+\frac{\partial g}{\partial N}\Big|_{N_{th}}(N-N_{th}) \ , \quad (1.28)$$

Using Eq. (1.10), Eq. (1.27) and Eq. (1.28), we can rewrite Eq. (1.25) as:

$$\frac{dE(t)}{dt} = \left[\frac{c}{2\overline{n}}\frac{\partial g}{\partial N}\Big|_{N_{th}}(N-N_{th})-i\frac{\omega_{th}}{\overline{n}}\frac{\partial n}{\partial N}\Big|_{Nth}(N-N_{th})\right]E(t) \quad (1.29)$$

The change of the refractive index caused by an excitation of a medium is related to the change of the absorption through the Kramers-Kronig relation (Yariv, 1989).

The way on which changes in the carrier density alter the refractive index and the absorption of the active layer, is characterized by the linewidth enhancement factor

or α factor[3]. The linewidth enhancement factor is also referred as the amplitude-phase coupling coefficient (Masoller, 1997) and Equation (1.29) can be expressed as:

$$\frac{dE(t)}{dt} = \frac{1+i\alpha}{2}\Big[v_g \frac{\partial g}{\partial N}\Big|_{Nth}(N - N_{th})\Big]E(t) \ , \tag{1.30}$$

We now define the optical gain per unit time as:

$$G(N) = v_g g(N) = v_g g_{th} + v_g \frac{\partial g}{\partial N}\Big|_{Nth}(N - N_{th}) \tag{1.31}$$

The photon lifetime (τ_s) inside the cavity can be considered as the inverse of the total loss rate of the photons γ (see Sec. A.2.2 of Appendix A), which is related with the gain threshold [Eq. (1.11)] by:

$$\gamma = \frac{1}{\tau_s} = \frac{c}{n}\Big[\alpha_{abs} + \frac{1}{2L} ln(\frac{1}{R_1 R_2})\Big] = v_g g_{th} \tag{1.32}$$

We can express the second term in the right of Eq. (1.31) as:

$$v_g \frac{\partial g}{\partial N}\Big|_{Nth}(N - N_{th}) = G(N) - \gamma \tag{1.33}$$

Finally, the field equation takes the form:

$$\frac{dE(t)}{dt} = \frac{(1+i\alpha)}{2}\Big[G(N) - \gamma\Big]E(t) \ , \tag{1.34}$$

where γ is the inverse of the photon lifetime and $G(N)$ is the optical gain. This expression of the gain has to be completed, to take into account that it depends

[3]We can express: $\frac{\partial n/\partial N}{\partial n''/\partial N} = -2\frac{\omega}{c}\frac{\partial n/\partial N}{\partial g/\partial N}$, with n and n" the real and imaginary parts of the refractive index [see Sec. A.4 in App. A for details].

nonlinearly on the population inversion and the optical power ($P = |E|^2$).

It is more useful to express the gain as a function of the population inversion at transparency (N_0), rather than as a function of the population inversion at threshold (N_{th}), because N_0 is a parameter of the semiconductor device. At transparency, the loss in the laser medium balances the gain, and the gain must exceed this value to allow for laser emission. Taking into account the density at transparency we can define the gain at threshold as an expansion around the transparency:

$$g_{th} \simeq \frac{\partial g}{\partial N}\Big|_{N_0}(N_{th} - N_0) \tag{1.35}$$

Then, from Eq. (1.31), the optical gain per unit time can be defined as:

$$G(N) = v_g g(N) = g_N(N - N_0) \ , \tag{1.36}$$

with

$$g_N = v_g \frac{\partial g}{\partial N}\Big|_{N_0} \simeq v_g \frac{\partial g}{\partial N}\Big|_{N_{th}} \ , \tag{1.37}$$

being the differential gain.

This linear dependence is not accomplished for high optical powers, due to the spatial hole burning and the carrier heating effects. The spatial hole burning accounts for the fact that the optical field is not uniform in all the active region (the standing wave inside the cavity forms an interference pattern), and the recombination is higher where the optical field is maximum. If the carrier diffusion is not sufficiently fast to supply these zones with more carriers, this effect will lead to a saturation of the gain coefficient. This can lead to an emission in various frequencies,

because the lasing mode experiences stronger gain saturation than the non-lasing modes. The other contribution to the saturation of the gain consists on the carrier heating effects. This occurs when the electrons of the conduction band are excited to higher energies. This fact hinders the recombination with the holes of the valence band, leading to a saturation of the gain. These two processes lead to a nonlinear gain of the form:

$$G(N, |E|^2) = \frac{g_N(N - N_0)}{1 + s\,|E|^2} \ , \tag{1.38}$$

which accounts for the dependence of the gain with the carrier density and the amplitude of the field. g_N is the differential gain, N_0 is the carrier density at transparency, s is the saturation coefficient, and $|E|^2$ is the output power of the field, or the number of photons inside the cavity.

The dependence of the gain on the population inversion requires the derivation of a differential equation for the carrier density, to have a complete description of the dynamics of a semiconductor laser.

We start with the equation of charge neutrality in the material (Yamada, 1983):

$$\frac{\partial N}{\partial t} = D\nabla^2 N + \frac{I}{e} - \frac{N}{\tau_s} - R_{st}(N, |E|^2) \ , \tag{1.39}$$

The first term of the right side corresponds to the carrier diffusion, where D is the diffusion coefficient. The second term accounts for the generation of electron-hole pairs, which is due to the pumping, being I the injected current and e the elementary charge. The third and last term are related with the loss of carriers. We use several assumptions in order to arrive to a governing equation for the carrier density:

- We neglect the carrier diffusion, because this kind of lasers have a very small

dimension of the active layer compared to the diffusion length ($D\nabla^2 N \simeq 0$).

- We consider the carrier decrease due to spontaneous emission, non-radiative transitions $\left(\frac{N}{\tau_s}\right)$ and stimulated emission processes $\left(R_{st}(N, |E|^2)\right)$. Recombination processes such as spontaneous emission and non radiative recombinations (see Sec. A.2.1 of Appendix A) are related to the carrier lifetime, and the stimulated emission is directly related to the emitted field through $R_{st}(N, |E|^2) = G\,|E|^2$.

- We consider the carrier lifetime as constant above threshold, because the carrier number is clamped to its value at threshold.

- We do not consider inhomogeneities due to the fast carrier diffusion, so that N is space independent. This allows us to replace the partial derivative $(\frac{\partial N}{\partial t})$ by a total one.

With the points considered above the equation for the population inversion reads:

$$\frac{dN}{dt} = C - \gamma_e N - G(N, |E|^2)\,|E|^2 \tag{1.40}$$

where $C = I/e$ is the pump current and γ_e is the inverse lifetime of the carriers $\gamma_e = 1/\tau_e$ (Sec. A.2.1 of Appendix A).

Because it is necessary to consider spontaneous emission processes that initiate the lasing emission, a real semiconductor laser must be described with differential equations that include a noise term. We add an additional term in the field equation that accounts for the independent events of creation of spontaneous emission photons. It is proportional to a complex Gaussian noise $\zeta(t)$, with zero mean ($\langle\zeta(t)\rangle = 0$),

and correlation $\langle \zeta(t)\zeta^*(t')\rangle = 2\delta(t-t')$. The noise term has to be proportional to the population inversion, also, to account for the amount of spontaneously emitted photons.

The final rate equations that describe the dynamics of a semiconductor laser, governing the electric field and the carrier density number are:

$$\frac{dE(t)}{dt} = \frac{(1+i\alpha)}{2}\Big[G(N,|E|^2)-\gamma\Big]E(t) + \sqrt{2\beta N}\zeta(t) \tag{1.41}$$

$$\frac{dN}{dt} = C - \gamma_e N - G(N,|E|^2)\,|E|^2 \ , \tag{1.42}$$

where β is the noise strength.

It is also possible to express these equations as the variation of the photon number and its phase, instead of the slowly varying field, in order to account for the evolution of the dynamics of the laser output power. Defining $E(t) = \sqrt{P(t)}e^{i\phi(t)}$, where $P(t) = |E(t)|^2$ is the photon number, and ϕ the phase of the field, the rate equations can be expressed as:

$$\frac{dP(t)}{dt} = [G(N,P)-\gamma]\,P(t) \tag{1.43}$$

$$\frac{d\phi(t)}{dt} = \frac{\alpha}{2}\Big[G(N,P)-\gamma\Big] \tag{1.44}$$

$$\frac{dN}{dt} = C - \gamma_e N - G(N,P)P \ , \tag{1.45}$$

where the nonlinear gain is now expressed as:

$$G(N,P) = \frac{g_N(N-N_0)}{1+sP} \tag{1.46}$$

In spite of having three degrees of freedom, as shown explicitly here, the system cannot show chaos, due to the fact that the phase ϕ is not affecting the other two degrees of freedom.

The steady-state solutions of this reformulated system of equations are obtained setting the $dP(t)/dt$, $d\phi(t)/dt$, and $dN(t)/dt$ values to zero at Eq. (1.43), Eq. (1.44), and Eq. (1.45) respectively. With this we obtain a solution for the number of photons, P_s, the difference of the optical frequency respect to the stationary value, $\Delta\omega = \omega - \omega_s$, and the density of carriers, N_s (see Buldú (2003) for a detailed calculation). There are two situations to take into account:

- Below threshold: the laser emission is zero and the density of carriers increases linearly with the pump current ($N_s = C/\gamma_e$).
- Above threshold: the photon emission is proportional to the distance of the pump current level from its threshold value. The carrier density is clamped to its threshold value, and the instantaneous frequency is clamped to the stationary value ($\Delta\omega = 0$).

In the boundary between both it is possible to derive an expression for the inversion population at threshold. The expression of the stationary solution for the number of photons [taking $dP/dt = 0$ in Eq. (1.43) and introducing Eq. (1.46)] is:

$$P_s = \frac{g_N(N - N_0) - \gamma}{s} \tag{1.47}$$

Taking $P_s = 0$ in last equation it is possible to express the population inversion at threshold as:

$$N_{th} = N_0 - \frac{\gamma}{g_N} \tag{1.48}$$

Through the study of the stability of the steady-state solutions with a linear stability analysis it is possible to obtain, for the solutions above threshold, an oscillatory approach to equilibrium as a response to a small perturbation. This defines the relaxation oscillations (RO), which are common in any class-B laser (Weiss and Vilaseca, 1991). The relaxation oscillations can be explained if we introduce a step input through the pump current. The carrier density reaches the threshold and emits light. The population inversion decreases, due to the light emission and as consequence, the output power decreases until the population inversion recovers. This produces relaxation oscillations between the field and the carrier density. These oscillations characterize the speed of reaction of the laser to external modulations of the pumping. The relaxation oscillation frequency sets the upper limit of the dynamics, and goes from 1 to 10 GHz typically. The two-dimensional system of Eqs. (1.41) and (1.42) allows only periodic solutions and not chaotic behavior, but the enhancement of the relaxation oscillations in semiconductor lasers through external perturbations such as optical feedback or optical injection causes strong instabilities. The damping rate of these oscillations affects the characteristics of the dynamical response to these external perturbations.

1.3 Optical feedback

As shown above, the dynamics of semiconductor lasers is described by two coupled first-order differential equations, which implies that these lasers cannot become chaotic by themselves. However, in the presence of external influences, the dynamical dimension is increased up to three or more, and then these lasers can experience chaotic behavior. In particular, relaxation oscillations of a semiconductor laser can

be destabilized by optical feedback, which introduces a delayed perturbation into the system. The optical feedback consists in the re-introduction of part of the laser's own emitted radiation through a mirror placed in front of its output facet. Due to the low reflectivities of the laser facets in semiconductor lasers, these devices are strongly affected by external optical feedback.

Early studies showed that the output intensity of the laser can be stabilized by optical feedback (Paoli *et al*, 1975; Hirota and Suematsu, 1979). In the 1970s, researchers began to study in detail the dynamical aspects of these instabilities (Risch and Voumard, 1977). The nonlinear dynamics of the semiconductor lasers began to generate interest and the addition of external cavities to semiconductor lasers showed a rich variety of instabilities (Bogatov *et al*, 1975; Broom *et al*, 1970; Edmonds and Smith, 1970). In particular, a chaotic state of operation was seen to be easily caused by minor amounts optical feedback.

Based on the model of Lang and Kobayashi (1980) of semiconductor lasers with optical feedback, many manifestations of the different regimes of chaotic operation produced by optical feedback have been reported. From the point of view of nonlinear dynamics, semiconductor lasers are highly controllable nonlinear systems, and the sizable feedback sensitivity is very critical for technical applications. In many laser devices such as CD or DVD players, the undesirable feedback effects from external system components might destabilize the laser. Therefore, the very rich chaotic behavior and the large number of instabilities of this type of lasers have been subject to extensive investigations.

1.3.1 Modelling semiconductor lasers with optical feedback

A combination of high gain, strong coupling of the re-injected light, and weakly damped relaxation oscillations makes semiconductor lasers very sensitive to external perturbations. The high asymmetry of the gain profile coming from a positive value of the α-parameter (Sec. A.4 of Appendix A), is a very important factor in the emergence of instabilities arising from optical feedback (Dente *et al*, 1988; Sacher *et al*, 1992; Masoller, 1997; Ryan *et al*, 1994). On the other hand, the spectral linewidth of the laser is reduced considerably through optical feedback from its solitary value, for steady-state conditions.

Increasing the feedback strength the laser also leads to instabilities, including different types of chaotic behavior, and losses of coherence. The latter occurs, for instance, in the coherence collapse regime, where the laser spectrum spreads over the range of GHz. When the feedback strength is further increased, the spectral linewidth becomes very narrow again and the laser stabilizes to a single mode oscillation (Ohtsubo, 2002).

To derive a rate equation model to describe a semiconductor laser with optical feedback, we proceed as in the case of a single semiconductor laser (Sec. 1.2). We place a mirror in front of a Fabry-Perot semiconductor laser, which re-introduces part of the output light into the laser (Fig. 1.7). We consider an ordinary mirror (not diffraction grating or phase-conjugate) and place it at a distance within the coherence length of the laser.

The distance between the laser and the mirror, L_{ext}, determines the roundtrip time of the external cavity, i.e. the time needed by the light to go to the mirror, reflect on it and come back again to the laser, calculated as $\tau_f = 2L_{ext}/c$. This

external cavity imposes boundary conditions to the emitted light of the laser, due to the reflection in the mirror (with reflectivity r_{ext}).

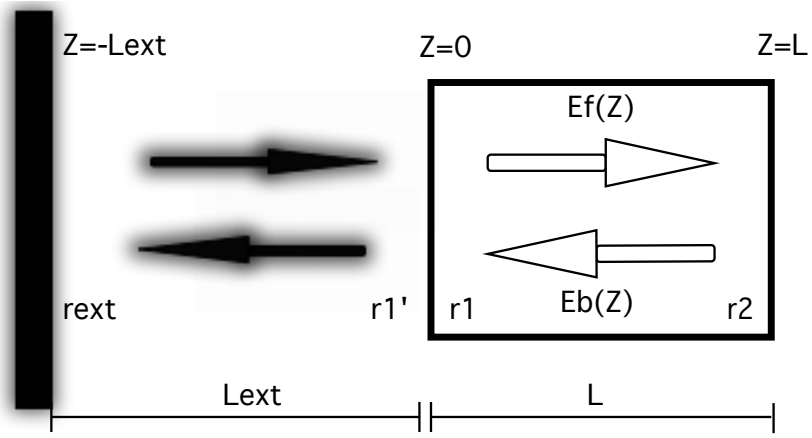

Figure 1.7: *Schematic Fabry-Perot laser cavity with optical feedback. $z = 0$ and $z = L$: facets, r_1 and r_2: internal reflectivities of the cleaved facets, r_1': external reflectivity at the front facet, r_{ext}: reflectivity of the mirror, L: cavity laser length, L_{ext}: external cavity length, $E_f(z)$ and $E_b(z)$: forward and backward traveling amplitude of the complex electrical field.*

We now make some assumptions:

- The feedback strength is weak and we consider only one reflection in the mirror. The external reflectivity is less than a few percents of the output intensity amplitude.

- The external cavity is a long cavity. The round trip frequency of the laser light in the external cavity ($\nu_{ec} = c/2L_{ext}$) is much lower than the relaxation oscillation frequency ν_{RO}. This corresponds to cavity lengths of the order of 1 meter.

- The laser emission, and therefore the re-injected field, are considered mono-

mode.

- The carrier density is not affected directly by the optical feedback. The rate equation that accounts for the carrier density variations, does not change from the solitary laser equations.

- As in the solitary laser case, in previous section, the amplitude reflectivities for the front and the back facets of the laser cavity are the same ($r_1 = r_2$).

- The output field oscillates at a frequency $\omega_0 \simeq \omega_{th}$, as for the solitary case, and we consider the slow varying amplitude of the field in the rate equations (Sec. 1.2).

With these assumptions the rate equations for the amplitude of the complex field and the carrier density read (Lang and Kobayashi, 1980):

$$\begin{aligned} \frac{dE(t)}{dt} &= \frac{(1+i\alpha)}{2}\left[G(N,|E|^2)-\gamma\right]E(t) + \\ &\quad +\kappa_f E(t-\tau_f)e^{-i\omega_0\tau_f} + \sqrt{2\beta N}\zeta(t) \qquad (1.49) \\ \frac{dN}{dt} &= C-\gamma_e N - G(N,|E|^2)\,|E|^2 \ , \qquad (1.50) \end{aligned}$$

where $\kappa_f E(t-\tau_f)e^{-i\omega_0\tau_f}$ is the feedback term, $\omega_0\tau_f$ the feedback phase, ω_0 is the optical frequency emission of the solitary laser, and $E(t-\tau_f)$ the optical field that left the laser cavity a time τ_f before. The feedback strength κ_f is defined as:

$$\kappa_f = \frac{(1-r_1^2)}{\tau_L}\frac{r_{ext}}{r_1} \ , \qquad (1.51)$$

where τ_L is the internal cavity round trip time, r_{ext} the mirror reflectivity, and r_1 the internal facet reflectivity. Experimentally, the feedback strength is calculated by

the reduction of the threshold current observed in the P-I curve (see Sigg (1993)). As in the estimation of the threshold current for a solitary semiconductor laser (see Sec. A.3.1 of Appendix A), the threshold current for a semiconductor laser with optical feedback is determined through the P-I curve. The percentage of the light reinjected into the laser is estimated through the solitary threshold current reduction as:

$$\%\ reduction = \frac{I_{th} - I_{th}^{f}}{I_{th}}\ , \tag{1.52}$$

where I_{th} is the solitary laser threshold current and I_{th}^{f} is the threshold current of the laser with optical feedback.

There are several papers deriving the steady state solutions of Eq. (1.49) and Eq. (1.50) and their stability (Petermann, 1995; Tromborg *et al*, 1984, 1987; Sano, 1994). In this introduction we only explain the method to arrive at the expression of the solutions of a semiconductor laser with optical feedback.

Splitting the field equation (1.49) into the variation of the photon number and its phase, as for the solitary laser case [Eqs. (1.43)-(1.45)], and after introducing the ansatz for stationary solutions $P(t) = P_s$, $N(t) = N_s$ and $\phi(t) = (\omega_s - \omega_{th})t$ in the resulting equations, one finds (Mørk *et al*, 1992; Sano, 1994):

$$P_s = \frac{C - \gamma_e N_s}{g_N(N_s - N_0)} \tag{1.53}$$

$$\Delta N = N_s - N_{th} = -2\frac{\kappa_f}{g_N}\cos(\omega_s \tau_f) \tag{1.54}$$

$$\Delta\omega\tau_f = (\omega_s - \omega_0)\tau_f = \kappa_f \tau_f \sqrt{1+\alpha^2}\ \sin(\omega_s \tau_f + \arctan\ \alpha) \tag{1.55}$$

To see the evolution of the laser dynamics we look at the phase space of the system. When plotting ΔN versus $\Delta\omega\tau_f$, Eq. (1.54) versus Eq. (1.55), we obtain

an ellipse. This ellipse contains the possible solutions in the phase space defined by these two variables, and takes the form:

$$\left[(\omega_s\tau_f - \omega_{th}\tau_f) + \frac{\alpha g_N \tau_f}{2}(N_s - N_{th})\right]^2 + \left[\frac{g_N\tau_f}{2}(N_s - N_{th})\right]^2 = \kappa_f^2 \qquad (1.56)$$

Through a linear stability analysis of the solutions it is possible to know that the lower half of the ellipse is formed by fixed points that are either stable or unstable via a Hopf bifurcation (external modes, due constructive interference between external and internal fields) and the upper half are unstable saddle solutions (antimodes, due to destructive interferences) (Sano, 1994). At least one mode, called the Maximum Gain Mode (MGM), is stable and corresponds to the regime of operation where the carrier density is minimum and the output power is maximum. This value can be obtained from Eq. (1.55), for $\omega_s\tau_f = 0 \bmod 2\pi$ when $\omega_{th}\tau = \kappa_f\alpha/\tau \bmod 2\pi$.

Figure 1.8 represents the solutions of the laser equations with optical feedback. Empty points are stable or Hopf unstable solutions and full circles are unstable saddle points.

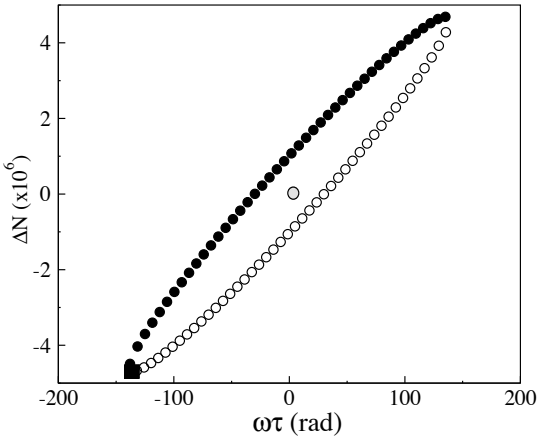

Figure 1.8: *Fixed points for the rate equation model of a semiconductor laser with optical feedback. Solutions on the upper branch (filled circles) are unstable saddle antimodes and on the lower branch are the external cavity modes (empty circles). The maximum gain mode is the filled square and the stable emission without feedback is the grey circle in the center of the ellipse.*

The MGM is always located at the left corner of the ellipse and is represented by a black box in the figure. The solution corresponding to the stable laser emission without feedback is located at the center of the ellipse (grey point). It is possible to have more than one stable MGM point (Levine *et al*, 1995; Masoller and Abraham, 1998) for decreasing values of α, which stresses the importance of this parameter in the stability of the system with feedback. The number of solutions, which increases or decreases in pairs, changes with the values of the parameters (κ_f, α, τ_f, and $\omega_0\tau_f$).

1.3.2 Regimes of optical feedback

The different regimes displayed by a semiconductor laser due to its sensitivity to external optical feedback can be classified in several different ways. If we take into account the reflectivity of the mirror (Tkach and Chraplyvy, 1986; Mørk *et al*, 1992), the feedback effects can be divided into five regimes:

- Regime I: lowest levels of feedback. Narrowing or broadening of the emission line is observed, depending on the phase difference between the emitted and the returning light. The spectral width is wider when the two are out of phase.
- Regime II: small levels of feedback. A splitting of the emission line appears, arising from rapid mode hopping.
- Regime III: very narrow region around small levels of feedback. The mode hopping is suppressed and the laser oscillates with a narrow linewidth.
- Regime IV: moderate feedback levels. The relaxation oscillations become undamped and the linewidth is broadened. In this regime the laser shows chaotic

behavior.

- Regime V: strong feedback regime. The internal and external cavities are like a single cavity and the laser oscillates with a single longitudinal mode.

In this Thesis we are mainly interested in regime IV, with moderate feedback levels, in which the laser shows chaos and can be described by the Lang and Kobayashi model. In this region, another classification can be made. The dynamics of the chaotic behavior of a semiconductor laser subject to optical feedback has been classified by Besnard *et al* (1993) [see also (Heil *et al*, 1998, 1999)], who distinguished three domains of the output intensity behavior depending on the pump current: stationary regime, low-frequency-fluctuation regime (LFF) and coherence-collapse regime (CC).

The coherence-collapse regime appears for moderate to high feedback level with pump currents far above the threshold value. The relaxation oscillations are excited due to the feedback and the spectral linewidth of the laser emission increases up to several GHz. The phase-space trajectory in this regime is completely disordered (Mulet and Mirasso, 1999).

The low-frequency-fluctuation regime appears when the laser operates at pump currents close to the threshold and the feedback level is low or moderate. It consists in sudden power dropouts, followed by a gradual power recovery. These dropouts are irregular in time and their frequency ranges from MHz to hundreds of MHz, i.e. smaller than the relaxation oscillation frequency. Due to this the dropouts are called low frequency fluctuations (LFF). This signal is in fact the envelope of a fast pulsing dynamics that is frequently masked by experimental limitations caused by the limited bandwidth of the monitoring devices (Fig. 1.9). The real dynamics

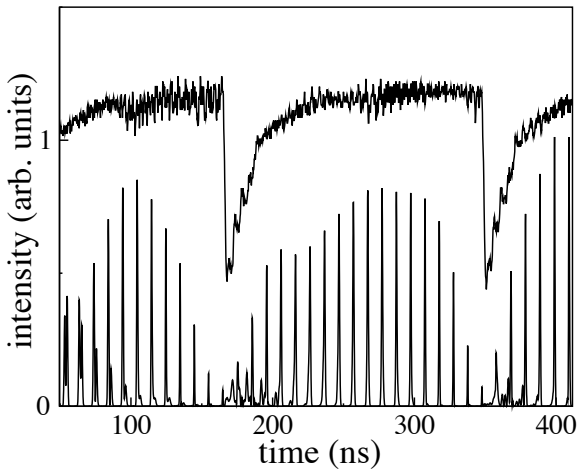

Figure 1.9: *LFF dynamics for filtered (top) and unfiltered (bottom) signals.*

is on the order of ps, as predicted theoretically van Tartwijk *et al* (1995a), and experimentally observed using a streak camera by Fischer *et al* (1996).

In multimode lasers, the fast scale dynamics of LFF does not change appreciably, ruling out that the multimode operation is fundamental for the LFF occurrence (Sukow *et al*, 1999). In the slow dynamics of the LFF regime, the mean time period between dropouts depends on the parameters of the system. The mean time period increases for low pump current, it increases with the feedback strength κ_f, and decreases for increasing values of α. Finally, the larger the feedback time τ_f, the larger the mean time period, but this dependence is less drastic than the pump current or the feedback strength effects. It is also known (Heil *et al*, 1999), that the distribution function of the time interval between dropouts decays exponentially, and that a certain refractory time exists between subsequent dropouts (see next subsection).

The dynamical nature of the LFF regime has been explained in several different ways. Henry and Kazarinov (1986) explained the phenomena as an escape from a potential well due to noise. Mørk *et al* (1988) introduced a model in which the dropouts correspond to a noise-induced switching between a high and a lower power state. The suppression of the noise does not eliminate the LFF and suggested that they were produced by a chaotic attractor. Some years later, Sano (1994) proposed a deterministic model in which the LFF are explained in the phase space defined by $\omega\tau$ and N. The optical feedback causes a decrease in the population inversion, and the laser drifts from the stable emission point towards the maximum gain mode.

The proximity between modes and antimodes increases near the MGM and a collision (crisis) between the trajectory and an antimode becomes likely. When the trajectory approaches the stable manifold of the saddle (antimode), it moves to the unstable manifold and the system initiates a dropout in power, during which the laser turns off and the population inversion increases to the threshold value (because during the dropout the carriers are not depleted) until the system reaches its solitary state. This process is repeated again on each dropout, with the crisis occurring at different points on each trajectory towards the MGM, so that the dropouts occur at irregular times.

1.3.3 Excitability in semiconductor lasers

Excitability properties in semiconductor lasers with optical feedback have been shown experimentally (Giudici *et al*, 1997) and numerically (Mulet and Mirasso, 1999; Eguia, 1998; Eguia and Mindlin, 1999). To consider a system as excitable, some features must be observed:

- In the absence of external perturbations the system is in an equilibrium state.
- Above a certain threshold, perturbations produce a transient excursion away from the equilibrium, leading to a pulse.
- The amplitude of the pulses is approximately independent of the amplitude of the perturbation.
- After the perturbation the system returns to the equilibrium state and is not able to react to another perturbation during a certain refractory time.

In a semiconductor laser with optical feedback, when the pump current is close to its threshold value with a constant output intensity, it is possible to generate dropouts perturbing the pumping current with an external electrical signal. The amplitude of these dropouts is independent of the amplitude of the perturbation. Several experiments (Heil *et al*, 1999) and numerical works (Mulet and Mirasso, 1999) showed that the distribution function of the mean time period of the dropouts reveals the existence of a refractory time during which the next dropout can not occur. This refractory time decreases as the pump current is increased.

In this framework, it is possible to control the low frequency fluctuations by applying an harmonic signal into the pump current of a semiconductor laser. In the low-frequency-fluctuation regime, when we induce a semiconductor laser with external cavity to drop with a certain time period, we entrain the laser. A first study of the effect of external modulation in a semiconductor laser with optical feedback was made by Takiguchi *et al* (1998). They introduced a sinusoidal signal into the pump current and observed the effect of the external frequency on the dropout events. As expected, not all modulation frequencies affected the laser in the same way. Their

work shows that only a range of frequencies above and below that corresponding to the external cavity frequency affects the system. Modulation at the external cavity frequency did not affect the dropouts.

Later, Sukow and Gauthier (2000) made a more specific study of entrainment in semiconductor lasers subject to optical feedback. They were able to make an hypoThesis about the frequencies that entrain the laser. The effect of the modulation is noticeable when the frequency equals the frequency difference between modes and antimodes. The periodic modulation changes the external cavity solutions of the system, impressing side bands on each cavity mode and antimode frequency. A resonance occurs when the modulation frequency is equal to the mode-antimode frequency difference.

A laser with optical feedback, due to the positive value of the linewidth enhancement factor (see Sec. A.4 of Appendix A), experiences a drift towards longer wavelengths (van Tartwijk and Lenstra, 1998). Keeping in mind the elliptic representation of the solutions of the Lang and Kobayashi equations shown in Fig. 1.8 of Sec. 1.3.1, each dropout is associated with a mode-antimode collision (Sano, 1994). This collision occurs between different mode-antimode pairs, and the travel time of the trajectory in phase space is different for each dropout. In this sense, we have a dynamic threshold to produce the dropout events. When the pump current is modulated with a periodic signal, it is possible to make the laser follow the periodicity of the introduced modulation. An optimal amplitude of the periodic signal exists, for which the laser is entrained. For higher amplitudes, the system loses its intrinsic dynamics and for lower amplitudes, it does not react to the introduced signal. Buldú *et al* (2004) made a numerical study of the influence of the cavity

length on the entrainment in semiconductor lasers with optical feedback, showing how the optimal amplitude for the entrainment decreases for decreasing feedback time. There are several studies in how the coupling enhances the entrainment of the system. One experimental work from Buldú *et al* (2002,b) shows that in two bidirectionally coupled lasers coupling increases the entrainment of the system.

It has also been observed that the output pulses can be made more regular by means of the introduction of external noise. When an external noise is introduced in the pump current of the laser with feedback, an increase of regularity in the dropout events occurs for an optimal amplitude of the noise (Giacomelli *et al*, 2000; Buldú *et al*, 2001), which is a clear evidence of coherence resonance (CR) in the system. Experimentally, the laser is biased very close to threshold, so that the system is stable in the absence of external noise. Then, the external noise is added into the dc pump current level, which produces dropouts at irregular times. These dropouts become more regular and frequent as the amplitude of the noise is increased. For large noise amplitudes, the pulses become irregular again. This shows that an optimal amplitude of the noise guarantees a coherent output (Lindner *et al*, 2004).

A general explanation from the point of view of excitable systems is that every time that the external perturbation crosses a threshold value, a pulse is produced. The total time between pulses, t_p, can be decomposed into two independent time intervals: the activation time, t_a, which is the time that the system needs to react to the perturbation, and the excursion time, t_e, which corresponds to the time needed by the system to return to the initial stable state (observed by Palenzuela *et al* (2001) in a Chua circuit).

When the perturbation process is related to a random source, such as a noise, t_a becomes a random variable. The mean value of the activation time depends on the intensity of the external noise (Hänggi *et al*, 1990). An increase of the noise amplitude will decrease the activation time. Taking into account that the excursion time t_e depends on the parameters of the system, an increase of the amplitude of the noise is translated into a decrease of the time between pulses t_p (see Pikovsky and Kurths (1997)).

For low values of the noise amplitude, the time between pulses is dominated by the activation time (because t_a has a high increase for a low values of noise amplitude and we can consider the mean time of t_e as constant). When the noise intensity is large, the activation time is small and the system exhibits a pulse shortly after the system returns from an excursion. For intermediate values of noise, if the excursion time is high enough and the threshold of excitation is small, it causes a maximum regularity of the time between output pulses (Palenzuela *et al*, 2001).

The coherence resonance phenomenon in semiconductor lasers with optical feedback can be explained in a similar manner. If we take into account the ellipse with the solutions (Fig. 1.8), an external perturbation can take the system away from the stable emission and after a collision with an antimode produces a dropout event. For small intensities of the external noise, the excursion time t_e of the system to undergo a dropout is basically independent of noise, and has the role of a refractory time during which no dropouts can be induced. As noise intensity increases, the escape events become more frequent, reducing the mean time period of the dropouts. When the dropout separation is of the order of t_e, for an optimal amount of noise, a regularity of the mean time period between dropouts occurs. For higher values of

the noise amplitude, it produces escapes before the build-up process of the dropout is finished (i.e. before the stable mode is reached), producing an irregularity of the pulses (Buldú *et al*, 2001).

If semiconductor lasers with optical feedback are capable of presenting excitable characteristics such as the coherence resonance phenomenon, it is reasonable to think that stochastic resonance (SR) could also be observed. Stochastic resonance is the enhancement of a system's response to an external harmonic driving for an optimal noise level (Gammaitoni *et al*, 1998). For a certain range of noise amplitudes, when the system is driven by a weak periodic signal, it responds to the introduced signal. In fact, the system is helped by noise to follow the frequency of the periodic signal in a resonance-like behavior. When the noise amplitude is not high enough to produce any effect at the system output, or when it is too high that it overtakes the dynamics of the system, no regularity or entrainment will be observed. Only for intermediate noise values its effect will be sufficient to help the system to follow the weak periodic driving without having a strongly noisy output. Numerical evidence of stochastic resonance in lasers has been shown by Buldú *et al* (2002a). They modulated the laser with a weak external signal while it was operating in the LFF regime, and the addition of the right amount of external noise was seen to help the intensity dropouts to follow the modulation signal by jumping to the sideband impressed by the external modulation, for the correct amount of external noise amplitude (Marino *et al*, 2002).

Chapter 2

Dynamics of coupled semiconductor lasers

Nonlinear systems are classified in two groups, depending on the predictability of their behavior. One group includes systems whose dynamics can be predicted from their initial conditions, including systems with stationary or periodic behaviors. A second group includes systems that are highly sensitive to perturbations in their initial conditions, and whose behavior appears to be random. The latter look like very complex and disordered systems, which can only be described with statistical methods. However, some of these systems can be deterministic, meaning that their future dynamics are fully defined by their initial conditions (assuming they are known with infinite precision), with no random elements involved. This behavior is known as deterministic chaos.

In the decade of the 1980's, investigations were centered in the study of the chaotic behavior of lasers, and in discovering the different routes to chaos in this kind of sys-

tems. In the 1990's investigations were focused in the control of this chaotic behavior and in the synchronization of chaotic systems. The understanding of synchronization as an adjustment of the rhythms of oscillating systems due to a weak interaction was well known from the initial observation of Huygens in 1673 Pikovsky *et al* (2003) in two pendulum clocks. Considerations in chaotic systems, however, started with works on chaotic circuits (Pecora and Carroll, 1990; Cuomo and Oppenheim, 1993).

As mentioned above the trajectory of a chaotic system is very sensitive to small perturbations of its initial conditions. This means that if we take two close, but different, points in phase space and follow their evolution, both trajectories starting from these points eventually diverge. Two identical systems (with the same chaotic attractor), that start at very similar initial conditions, will follow trajectories diverging exponentially with time. Even so, coupled chaotic systems can exhibit synchronized behavior. Synchronizing two chaotic systems requires forcing the trajectories to follow the same path of the attractor at the same time.

An early study of chaos synchronization was carried out by Pecora and Carroll (1990). Later, Pecora *et al* (1997) reported a detailed method to produce chaos synchronization (for a detailed discussion see Uchida *et al* (2005)) in two identical Lorenz chaotic systems. A chaotic signal was transmitted from the drive to the response system completely replacing the corresponding variable in the latter. This leads to synchronized behavior. The stability of this situation was studied taking into account that synchronization occurs when the difference between the variables of each system tends to zero for time tending to infinite. Yamada and Fujisaka (1983, 1984) analyzed synchronization phenomena in chaotic systems with the use

of conditional Lyapunov exponents[1].

A variety of synchronization phenomena has been discovered in various areas of science: in physics (Sugawara *et al*, 1994; Roy and Thornburg, 1994), chemistry (Coffman *et al*, 1986), biology (Strogatz and Stewart, 1993) and physiology (Schäfer *et al*, 1999; Glass, 2001; García-Ojalvo *et al*, 2004).

There are several ways to characterize the different types of synchronization behavior of chaotic systems. Comparing their output, synchronized behavior can be classified as:

- Identical or complete synchronization: two coupled systems $[x_1(t), x_2(t)]$ have an identical output $[x_1(t) = x_2(t)]$.

- Generalized synchronization: the outputs of the two systems are functionally related $[x_1(t) = F(x_2(t))]$.

In systems that interact with a time delay, such as semiconductor lasers, a lag synchronization appears. The outputs of both systems can be equal after an appropriate shift in time. More generally, lag synchronization takes the form: $x_1(t) = F[x_2(t - \tau)]$, where τ is the time needed for the interaction to affect the second system, and depends on the time lag or delay between the signals. We will refer to achronal or lag synchronization when we detect a delay or lag between the synchronized signals. We will talk about zero-lag or synchronous synchronization when there is a coincidence without delay in the signals of the lasers.

[1]Using the eigenvalues (Lyapunov exponents) of the Jacobian matrix (the matrix of partial derivatives of the right hand side of the response system) is possible to obtain a minimal condition to have stability in the system: negative Lyapunov exponents leads to synchronized solution.

2.1 Coupled lasers

The first theoretical prediction of synchronization of chaotic lasers was made by Winful and Rahman (1990). They studied an array of semiconductor lasers coupled by lateral overlap of their output fields, observing that for certain coupling values these outputs can be synchronized. Some years later, experimental synchronization in two solid state lasers was carried out (Roy and Thornburg, 1994). The lasers were drawn to chaos using periodic modulation of their pump currents, and by means of mutual coupling they showed synchronization behavior. Sugawara *et al* (1994) obtained, nearly at the same time, synchronization in unidirectionally coupled CO_2 lasers. This was possible by means of the modulation of a saturable absorber in the cavity of one laser by the chaotic output of the other laser. Synchronization of fiber lasers was carried out by van Wiggeren and Roy (1998), while Goedgebuer *et al* (1998) synchronized chaotic wavelengths of semiconductor lasers. Previous numerical works showed synchronization of solid-state lasers Colet and Roy (1994) and in semiconductor lasers, in which two lasers were driven to chaos by optical feedback, and the output field of one of the lasers was injected into the other one (unidirectional coupling) (Mirasso *et al*, 1996). Another numerical study in the synchronization of semiconductor lasers was made by Annovazzi-Lodi *et al* (1996). In that work, chaos was due to the external injection from the other laser. A work from Takiguchi *et al* (1999) showed the first experimental evidence of synchronization in the case of two unidirectional coupled lasers in the LFF regime. In that work a chaotic signal from a semiconductor laser with optical feedback (driver or transmitter laser) was injected into another semiconductor laser without feedback (receiver laser). Simultaneously, another experimental work from Sivaprakasam and

Shore (1999) showed the synchronization of two unidirectionally coupled semiconductor lasers, both of them with feedback, in a slower time scale. In the following year, Fischer *et al* (2000) reported an unidirectional scheme for synchronization, with feedback only in the master laser, at fast time scales. And at the same year, experimental synchronization of chaotic mode hopping induced by feedback in two unidirectionally coupled DBR tunable lasers was reported by Liu and Davis (2000).

There are several ways to synchronize two semiconductor lasers. The simpler way is to optically inject the output field of one of the lasers with feedback into the other one (unidirectional coupling in open loop configuration), taking advantage of the open front facet of this type of lasers. One of the lasers acts as the driving or transmitter laser and the other one as the receiver laser. In this scheme, there is an extra injected power into the receiver. To compensate it, and so recover the symmetry of the system, it is useful to add feedback in the other laser (unidirectional coupling in closed loop configuration). As we defined in Sec. 1.3.1, the feedback time is the time needed by the light to go to the mirror and return to the laser. When we consider two coupled lasers, the coupling time is defined as the time to travel between both systems. The relations between the feedback and coupling strengths, and the feedback and coupling times, determine the time lag between the synchronized signals.

If the optical output field of each of the two lasers is injected into the other one (mutual or bidirectional coupling), we can have a symmetrical configuration that also leads to a synchronized behavior. In the absence of feedbacks the delay time between the synchronized signals corresponds to the coupling time.

The differences between the unidirectionally and bidirectionally configuration are

not only in the delay time between the synchronized output signals, as we will discuss in the following sections.

2.1.1 Unidirectional injection

In the case of unidirectionally coupled lasers there are two commonly considered configurations. Figure 2.1 (left) shows an open loop configuration, and Fig. 2.1 (right) a closed loop configuration. The former is called open loop because only the transmitter laser has optical feedback (which can show independent chaotic dynamics), and the latter closed loop because both lasers are subject to optical feedback (they can show chaotic dynamics independently, without coupling).

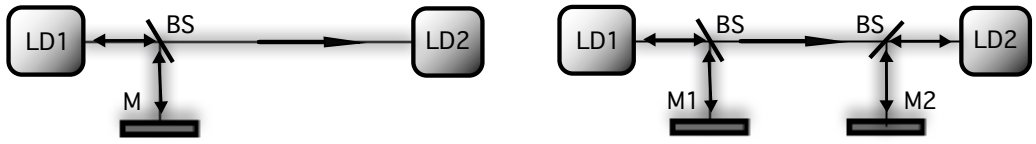

Figure 2.1: Unidirectionally coupled lasers in open loop (left) and closed loop (right) configuration. LD: laser diodes, M: mirrors, and BS: beamsplitters.

From the rate equation model of Lang and Kobayashi describing semiconductor lasers with optical feedback, one can derive the model equations to describe two unidirectionally coupled lasers, each one with feedback, adding a new term to take into account the injected field coming from the transmitter laser (in this case the first laser) (Masoller, 2001):

$$\begin{aligned} \frac{dE_j}{dt} &= \frac{(1+i\alpha_j)}{2}\Big[G_j - \gamma_j\Big]E_j + \kappa_{j,j}E_j(t-\tau_{j,j})e^{-i\omega_j\tau_{j,j}} \\ &+ \delta_{j2}\kappa_{3-j,j}e^{i(\Delta\omega t - \omega_{3-j}\tau_{3-j,j})}E_{3-j}(t-\tau_{3-j,j}) + \sqrt{2\beta N_j}\xi_j(t) \end{aligned} \tag{2.1}$$

$$\frac{dN_j}{dt} = C_j - \gamma_{ej} N_j - G_j \left|E_j\right|^2 \tag{2.2}$$

The subindex $j = 1, 2$ denotes lasers LD1 and LD2, respectively, and the subindex $3 - j$ represents the injecting laser. The Kronecker delta, δ_{j2} ensures that the unidirectional coupling term exists in only the LD2 field equation. E_j represents the corresponding optical field and N_j the carrier number. $\omega_{1,2}$ are the free-running optical frequencies of the two lasers, which sometimes for simplicity will be considered to be the same, so that frequently we consider the detuning zero, $\Delta\omega = \omega_2 - \omega_1 = 0$. The optical intensity (or number of photons inside the cavity) is given by $P_{1,2}(t) = |E_{1,2}(t)|^2$.

The feedback term in the field equation is $\kappa_{j,j} E_j(t - \tau_{j,j}) e^{-i\omega_j \tau_{j,j}}$, where $\kappa_{j,j}$ are the feedback strengths, which are directly related to the threshold reduction due to the reinjected light. The feedback field corresponds to the emitted for each laser at a time $\tau_{j,j}$ before, thus $\tau_{j,j}$ defines the feedback time of each laser. To simplify the notation, we define when possible $\kappa_{j,j} = \kappa_f$, and $\tau_{j,j} = \tau_f$. For the closed loop configuration both feedback terms appear, and for the open loop one of them is eliminated ($\kappa_{2,2} = 0$).

The coupling term $\delta_{j2} \kappa_{3-j,j} e^{i(\Delta\omega t - \omega_{3-j}\tau_{3-j,j})} E_{3-j}(t - \tau_{3-j,j})$ which only appears in the field equation of the second laser, accounts for the injected field coming from the first laser. $\kappa_{3-j,j}$ is the coupling strength that is directly related with the threshold reduction due to injection of the laser. The expression of the injected field takes into account the time needed by the light to travel from first laser to the second, $\tau_{3-j,j}$. Usually, when we use one single path to inject the light coming from one laser to the other, we simplify the coupling notations as: $\kappa_{3-j,j} = \kappa_c$ and $\tau_{3-j,j} = \tau_c$.

As we mentioned before, synchronization in semiconductor lasers usually shows a lag between both signals $P_2(t) = P_1(t - \Delta\tau)$, due to the finite time needed by the light to travel to the receiver laser. We will discuss in more detail which value corresponds to $\Delta\tau$ depending on the type of synchronization and the relation between the feedback and coupling times, and their respective strengths.

In closed loop configuration, when $\kappa_{1,1} = \kappa_{2,2} = \kappa_f$, and $\tau_{1,1} = \tau_{2,2} = \tau_c$ ($\tau_f = \tau_c$), the intensity of the receiver usually synchronizes with the driver with a lag corresponding to the coupling time, in a leader-laggard configuration, in which the receiver follows the dynamics of the transmitter: $P_2(t) = P_1(t - \Delta\tau)$, $\Delta\tau = \tau_c$. However, when $\kappa_{1,1} = \kappa_{2,2} + \kappa_c$, the two lasers receive the same amount of light, and the receiver synchronizes with the driver as: $P_2(t) = P_1(t - \Delta\tau)$, where $\Delta\tau = \tau_c - \tau_f$. This situation is called anticipated synchronization when $\tau_f > \tau_c$, i.e. when the feedback time is larger than the coupling time, and the receiver anticipates the transmitter (Locquet *et al*, 2001, 2002,a). When $\tau_f < \tau_c$, i.e. if the coupling time is larger than the feedback time, the receiver lags the dynamics of the transmitter (Tang and Liu, 2003). In this behavior it is possible to observe zero-lag or isochronal synchronization when $\tau_c = \tau_f$ (Gross *et al*, 2006).

In the case of anticipated synchronization, it is possible for the receiver to be influenced by the transmitter before the transmitter is affected by its own feedback, and the receiver advances the dynamics of the transmitter. This type of synchronization was first predicted theoretically by Voss (2000), numerically reported in semiconductor lasers by Masoller (2001), and observed experimentally in unidirectionally coupled lasers by Liu *et al* (2002). A similar type of synchronization has been observed in different experimental configurations by Sivaprakasam *et al* (2001),

and Tang and Liu (2003) (see Calvo *et al* (2004) for detailed discussion).

The stability of the synchronized solutions depends on the parameters of the system (see Locquet *et al* (2002,a); Vicente *et al* (2002) for details). A broad experimental study of the general behavior of this system was made by Peil *et al* (2002).

The open loop configuration is less sensitive to parameter mismatch between the lasers than the closed loop configuration (Locquet *et al*, 2002). In the open loop case the system can show good synchronization for both $\tau_f = \tau_c$ and $\tau_c \neq \tau_f$. For $\tau_f = \tau_c$, the outputs show a leader-laggard configuration: $P_2(t) = P_1(t - \Delta\tau)$, where $\Delta\tau = \tau_c$. For $\tau_c \neq \tau_f$ a good synchronization arises in two different cases: for $\kappa_c > \kappa_f$ and for $\kappa_c = \kappa_f$. When the coupling strength is higher than the feedback strength the signals synchronize with a $\Delta\tau = \tau_c$. When the coupling and feedback strengths coincide an anticipated or retarded synchronization appears. The lag in this case is $\Delta\tau = \tau_c - \tau_f$, and is anticipated or retarded depending on whether $\tau_c > \tau_f$ or $\tau_c < \tau_f$ (see Appendix B).

Recently, in unidirectionally coupled lasers in open loop configuration, another synchronization phenomenon was observed. Buldú *et al* (2006) observed experimentally and numerically spontaneous synchronization events between the lasers, in an episodic synchronization regime. When the output light of a laser driven to the low-frequency-fluctuation regime (due to optical feedback) is injected into a second laser that is detuned with respect to the first, episodic synchronization appears. The periods of synchrony correspond to the recovering of the dropout event. When the output intensity of the laser is traveling towards the maximum gain mode the synchronization of the system is lost, and recovered again when the driving laser

switches off.

2.1.2 Bidirectional injection

Synchronization phenomena in mutually (or bidirectionally) coupled semiconductor lasers has also been widely studied. Periodic oscillations in mutually coupled semiconductor lasers were first observed by Hohl *et al* (1997), and two years later a quasiperiodic synchronization was observed in the same system by the same group (Hohl *et al*, 1999). Later, Heil *et al* (2001), observed experimentally synchronization in two single mode semiconductor lasers mutually coupled face to face in the low frequency fluctuation regime. In that case, the output light of one of the lasers was injected into the second laser and vice-versa. In this mutual coupling scheme, both lasers showed low frequency fluctuations due only to the mutual perturbation.

Figure 2.2 shows the schematic setup of a face-to-face coupling configuration. In this case a chaotic behavior is displayed in both output intensities due only to the mutual interaction, and the addition of external mirrors is not necessary to drive the

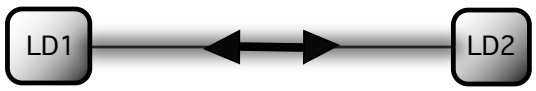

Figure 2.2: Bidirectionally coupled lasers.

lasers to chaos. In this configuration, synchronization in a leader-laggard behavior was observed with a time lag between both signals equal to τ_c, corresponding to

the flight time between the lasers. Heil *et al* (2001) showed that if the lasers have the same optical frequencies, a spontaneous switching of the role of leader occurs between both lasers. When one of the lasers is detuned to a higher optical frequency, this laser becomes the leader of the dynamics. The zero-lag solution in this system is not stable. In the classification made above, the synchronization is always a lag synchronization, in the sense that we have a time shift ($\Delta\tau = \tau_c$) between the signals corresponding to the coupling time.

Recently, the zero lag state has been experimentally (Klein *et al*, 2006) and numerically (Vicente *et al*, 2007) reported for mutually coupled lasers. To stabilize this isochronal solution it is necessary to subject each laser to optical feedback. Klein *et al* (2006) and Vicente *et al* (2007) show that for symmetric values of strengths and equal delay times it is possible to observe a stable zero lag solution in the system.

Further investigations of variations of this configuration have been made in the last decade. The leader-laggard relation in mutually coupled lasers with one feedback was also studied by Sivaprakasam *et al* (2001, 2002). Rees *et al* (2003) studied the role of the detuning in the choice of the leader. In that case they used the terminology "anticipated synchronization" to refer to common lag synchronization, with a change of the leader of the dynamics, due to the fact that the time shift between the signals was in all cases equal to τ_c. Other experimental studies of bidirectionally coupled lasers with one feedback were made by Martínez-Avila *et al* (2007) and González *et al* (2007).

A model that represents two semiconductor lasers bidirectionally coupled each one with feedback is a modification of the Lang and Kobayashi equations (Mulet

et al, 2002):

$$\begin{aligned}\frac{dE_j}{dt} &= \frac{(1+i\alpha_j)}{2}\Big[G_j-\gamma_j\Big]E_j+\kappa_{j,j}E_j(t-\tau_{j,j})e^{-i\omega_j\tau_{j,j}} \\ &+ \kappa_{3-j,j}e^{i(\Delta\omega t-\omega_{3-j}\tau_{3-j,j})}E_{3-j}(t-\tau_{3-j,j})+\sqrt{2\beta N_j}\xi_j(t) \qquad (2.3)\\ \frac{dN_j}{dt} &= C_j-\gamma_{ej}N_j-G_j\left|E_j\right|^2 \qquad (2.4)\end{aligned}$$

The model is the same as in the previous section, but now the injection term appears in both field equations. To model two bidirectionally coupled lasers coupled face-to-face without feedbacks we must take $\kappa_{j,j}=0$. As in the previous equations, the coupling strength $\kappa_{3-j,j}$ leads to a threshold reduction due to injection from the other laser. In this Thesis we will find situations in which we separate the paths of the light in both directions, and we will control the amount of light along each path. In this situation the coupling strengths in both directions can be different, as well as the coupling times. When we consider a unique path for both directions, as in the general case described in Fig. 2.2, we will use a simplified notation, as explained above for the unidirectional configuration: $\kappa_{1,2}=\kappa_{2,1}=\kappa_c$ and $\tau_{1,2}=\tau_{2,1}=\tau_c$.

2.2 Chaotic communications

The possibility of synchronizing chaotic systems suggests that these systems might be useful for communication purposes. In particular the broadband spectral behavior of chaotic systems makes this approach useful for encryption. The basic idea of using chaotic signals as carriers for message transmission was introduced by Pecora and Carroll (1990, 1991). A message was added to one of the chaotic variables of the

driver, and the resulting signal was transmitted to the receiver together with another signal to drive the synchronization of the receiver system. It was possible to recover the message by the subtraction of the synchronized signals at the receiver. In an experimental work reported by Cuomo and Oppenheim (1993), and Cuomo *et al* (1993) in electronic circuits, the transmission was easily carried out. They showed that the receiver can synchronize with the transmitter even with an added message in the driven signal. The message can be recovered by the subtraction of both signals (the transmitted and the receiver signals), due to the fact that only the chaotic part of the transmitted signal is synchronized with the receiver signal. The privacy in the transmission depends on the dimensionality of the chaotic attractor, and its efficiency requires having matching parameters of the systems that allow a stable and reliable synchronization.

A first optical system for chaotic communications was suggested by Colet and Roy (1994) using solid state lasers. High dimensional chaotic systems, such as semiconductor and fiber lasers, seemed more suitable to encrypt messages, and a couple of years later Mirasso *et al* (1996), and Annovazzi-Lodi *et al* (1996) showed in numerical studies that semiconductor lasers were good optical systems for high speed data transfer. Later, message transmission and its posterior recovery was experimentally reported with two coupled doped fiber ring lasers by van Wiggeren and Roy (1998). Nearly at the same time, the first experimental observation of data transmission with semiconductor lasers was made by Goedgebuer *et al* (1998). That work used the synchronization of two semiconductor lasers with electro-optical feedback, with the aim of transmitting a message taking advantage of the high-dimensional wavelength chaos generated. Much experimental research was performed in the following years in the synchronization of semiconductor lasers and the detection of subnanosecond

synchronization in the low-frequency-fluctuation and coherence collapse regimes. With this aim, Fischer *et al* (2000) introduced a periodic signal through the transmitter's pump current, observing a sharp peak in the RF spectrum corresponding to the signal frequency. The RF spectrum of the receiver was almost identical to the transmitter, with the difference that the sharp peak observed at transmitter spectrum was considerably suppressed at the receiver, denoting synchronization with the chaotic output and filtering of the periodic signal. This filtering process is necessary to recover a message by subtracting the receiver output (chaos) to the injected signal from the transmitter (message+chaos). These experimental results are evidence of the capability of these systems to encode/decode a message through their output intensity.

There are several characteristics that a chaotic system has to accomplish to perform a reliable communication system, which make semiconductor lasers good candidates for secure chaos communications (Peil, 2006):

- From the performance point of view: sufficient bandwidth, high maximum carrier frequency, and good controllability of the key parameters of the dynamics (the internal parameters of the lasers in our case).

- From the privacy point of view: high information entropy, and rapidly decreasing auto-correlation of the dynamics (high dimensional chaos)

- Robust synchronization against small perturbations.

- Well defined relation between transmitter and receiver, to be able to reconstruct the message after the transmission.

- Short period of time needed by the system to get synchronized. Also the possible periods of synchronization loss must be short, in order to minimize the message loss.

- An effective masking method and encryption/decryption rates to make Gbit/s rate transmission possible.

There are four general ways to mask the message in chaotic communication systems.

- The chaos masking method (CM) (Cuomo and Oppenheim, 1993; Uchida *et al*, 2003a), consists in the addition of the message to the chaotic carrier signal.

- Chaos modulation keying (CMK) consists in modulating the carrier signal by the message. It is not only an addition of the message, but a modulation of the signal, for example adding the message to the pump current of a semiconductor laser (Mirasso *et al*, 1996; Annovazzi-Lodi *et al*, 1996).

- Chaos shift keying (CSK) consists in the introduction of the message by switching one of the parameters responsible of the dynamics of the system to generate a data bit (Mirasso, 2002; White and Moloney, 1999). ON/OFF shift keying (OOSK) consists, in particular, in a switch between synchronized and desynchronized states (Heil *et al*, 2002). The message is transmitted only at the synchronized times that correspond to one of the two bit rates, being desynchronized in the other bit (Rogister *et al*, 2001; Mirasso, 2000).

These encoding/decoding methods have been applied to different optical systems. For example, chaotic masking and chaotic modulation have been experimentally

implemented in fiber laser systems (van Wiggeren and Roy, 1998a, 1999), and all of them have been also experimentally demonstrated in semiconductor laser systems (Liu *et al*, 2002a).

Further numerical (Sánchez-Diaz *et al*, 1999; Rogister *et al*, 2001; Liu *et al*, 2002a; Mirasso, 2002; Li *et al*, 2008) and experimental (Sivaprakasam and Shore, 1999a; Uchida *et al*, 2001; Heil *et al*, 2002) works, applied the synchronization and the chaos pass filtering phenomenon of semiconductor lasers to develop different techniques of encrypted data transmission. An experimental work in secure communications was reported by Argyris *et al* (2005) in which a 1Gb/s message was transmitted through a commercial optical communication system based on semiconductor lasers, from two points separated 120 km in the metropolitan area of Athens.

Part II

RESULTS

Chapter 3

Route to chaos via quasiperiodicity in two mutually coupled lasers

Synchronization phenomena are often described in terms of entrainment or locking of frequencies. If two nonidentical oscillators having their own frequencies are coupled together, they may start to oscillate with a common frequency. The injection of an optical field into a laser diode can be viewed as a mechanism for coupling two oscillators, where one oscillator corresponds to the laser that produces the injection field and the other one is the injected laser. Whether they synchronize or not depends on the coupling strength and the frequency detuning (the difference between the optical frequencies of the lasers). The coupling can also be mutual between both units, although its strength need not be identical in the two directions of the interaction. In the symmetrical case, both units perturb the state of each other through

a purely bidirectional coupling (Mulet *et al*, 2002; Heil *et al*, 2001). Synchronization between the subsystems is achieved by adjusting the optical frequencies of the lasers. The laser with higher frequency acts as the leader of the dynamics as discussed in Sec. 2.1.2. When the lasers operate with the same optical frequency (which is accomplished by tuning the temperature and pump currents), a random change in the leader and laggard role appears. To better understand the emergence of this symmetry breaking in the system, we studied the transition from unidirectional to bidirectional injection in two coupled semiconductor lasers. Specifically, we vary in a controlled way the directionality of the coupling, ranging from pure unidirectional injection of the light emitted by one laser into the other one, to quasi-bidirectional coupling. This allows us to see the transition from stable unidirectional injection to chaotic synchronization with a leader in the dynamics, and how this chaotic lag synchronization arises in the system.

3.1 Experimental setup

We consider first the unidirectional case. At very low injection levels the receiver is stable, with an optical power close to that of the solitary laser. If we increase the pump current or the coupling, we can see the transition from stable to oscillatory output. This oscillation becomes more and more unstable if we increase the coupling or, as in our case, by adding another external perturbation. When we depart from the unidirectional coupling state by gradually increasing the injected light coming from the reverse path, chaos arises in the system, with a clear symmetry breaking introduced by the time delay of the coupling paths.

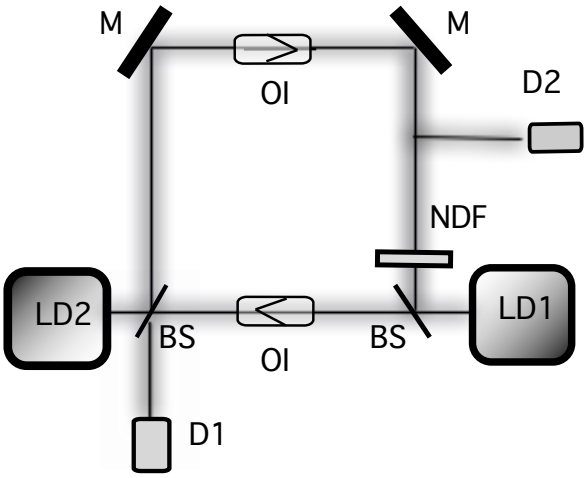

Figure 3.1: *Experimental setup. LD: laser diodes, BS: beamsplitters, OI: optical isolators, and M mirrors. The mutual coupling consists of two separate paths.*

Our experimental setup, shown in Fig. 3.1, consists of two parameter-matched AlGaInP index-guided and multi-quantum well semiconductor lasers (Sharp GHO 6510B2A), coupled by mutual optical injection through two independent unidirectional paths. Both lasers operate with a nominal wavelength $\lambda_n = 654$ nm. The temperature and pump currents of the lasers are controlled with an accuracy of $\pm 0.001^{\circ}$C and ± 0.01 mA, respectively, and are adjusted such that the optical frequencies of LD1 and LD2 (in isolation) are as similar as possible to each other. For temperatures $T_{\mathrm{LD1}} = 18.238^{\circ}$C and $T_{\mathrm{LD2}} = 26.021^{\circ}$C, the threshold currents of the solitary lasers are, respectively, $I^{\mathrm{th}}_{\mathrm{LD1}} = 30.48$ mA and $I^{\mathrm{th}}_{\mathrm{LD2}} = 30.79$ mA. Optical isolators (Electro-Optics Technology, Inc.), labeled OI in Fig. 3.1, are placed in the two injection paths in order to have unidirectional coupling in each path. The amount of light injected into LD1 is controlled by a variable neutral density filter. The delays associated to the two coupling paths are $\tau_{1,2} = 3$ ns (LD1 to LD2) and $\tau_{2,1} = 5$ ns

(LD2 to LD1). The laser outputs are sent simultaneously to a 4 GHz oscilloscope (Tektronix CSA7404), to an optical spectrum analyzer (Ando AQ6317B) and to a RF spectrum analyzer (Anritsu MS2667C).

A good characterization of the lasers spectra is very important before starting a synchronization experiment to know the rate of change of their wavelengths with temperature, and the hops of their modes (see Sec. A.2.4 of Appendix A). We find a rate of change of 0.065 nm/°C for LD1 and 0.047 nm/°C for LD2. We change the temperatures until the wavelengths of the lasers are as similar as possible. With this choice of temperatures ($T_{\mathrm{LD1}} = 18.238$°C and $T_{\mathrm{LD2}} = 26.021$°C), we inject the light of LD1 into LD2. Then, we optimize the alignment of the lasers by maximizing the increase of LD2 output power near its threshold, due the injection of LD1 (measuring the increase in the output power with a PM30-122B-Thorlabs power meter in the detection path). Finally, we change slightly the pump currents to obtain the optimal locking of the injected laser, by matching their optical spectra. These measures place the LD1 and LD2 currents at 28% and 13.2% above their respective threshold values. Figures 3.2(a) and (b) show the optical spectra of the solitary lasers, with a highest peak at 655.1 nm for LD1 and 654.5 nm for LD2. For the indicated values of pump current and temperatures, we obtain the locking of LD2 spectrum with the light coming from LD1 as shown in Fig. 3.2(c).

After the optimization of the unidirectional coupling between the two lasers, we increase the injected light in the opposite direction, from LD2 to LD1. Figure 3.3 shows the RF spectra for increasing back-injection light. Figure 3.3(a) displays the RF spectrum for LD2 after unidirectional injection from LD1. A wide peak is observed corresponding to the combination of the relaxation oscillations (RO) of

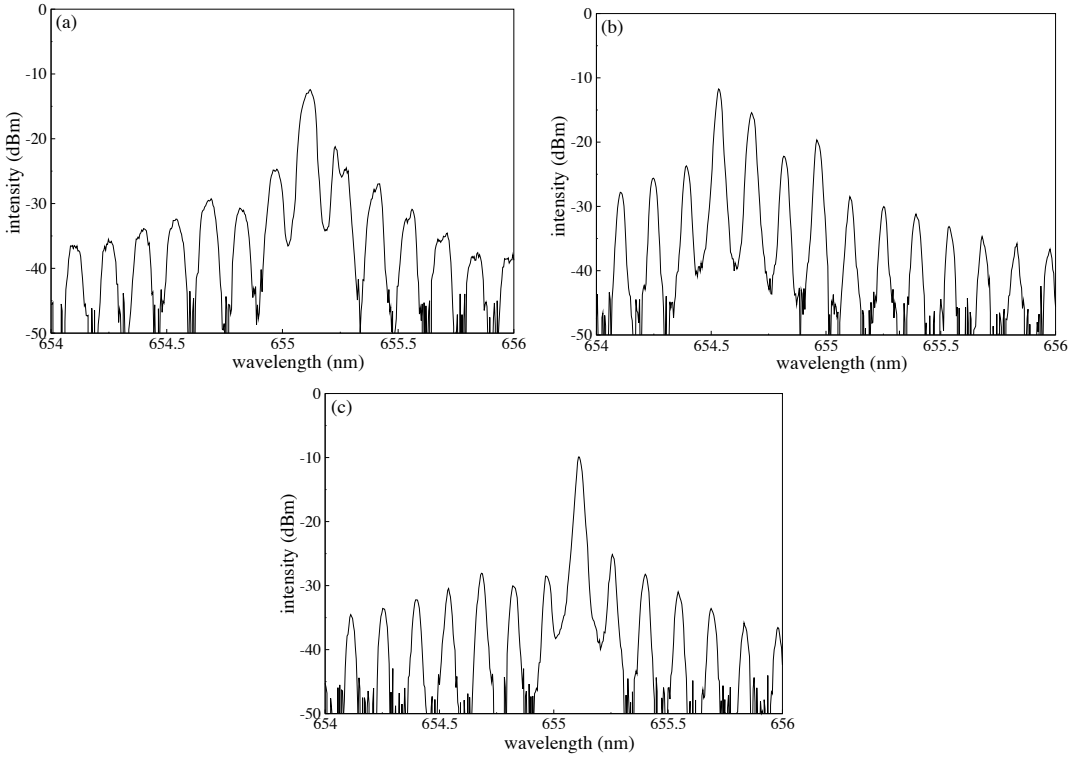

Figure 3.2: *(a) Optical spectrum of LD1, (b) optical spectrum of LD2, and (c) optical spectrum of LD2 injected by LD1.*

LD1 with thosse of LD2. The resulting combined peak appears about 2.5 GHz, and only arises when the RO frequency of the injection laser is near or identical to that of the injected one. Thus, as a consequence of the optical spectrum matching, we have an enhancement of the RO frequency peak of the injected laser. From this unidirectional situation we increase the light injected back in LD1 from LD2, approaching the situation of mutual coupling. When the injection received by LD1 has a relative power of 0.10% with respect to the other direction, a combined peak of the two RO frequencies appears, at the same place than that of unidirectional situation [Fig. 3.3(b)]. For higher values of the back-injection we observe a transition

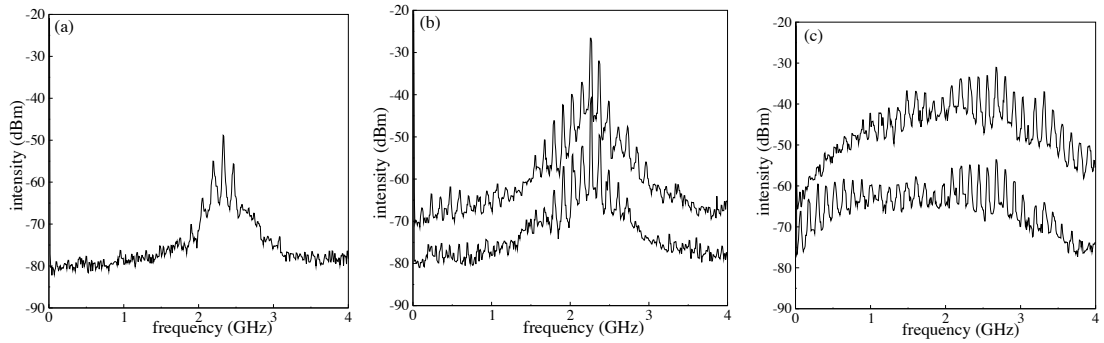

Figure 3.3: *Power RF spectra for increasing back-injection: (a) pure unidirectional coupling (RF spectrum for LD2), (b) strongly asymmetric coupling, and (c) weakly asymmetric (almost bidirectional) coupling. In (b, c) the top (bottom) trace corresponds to LD1 (LD2). The spectra are vertical displaced for clarity*

to a broad-band chaotic power spectrum [Fig. 3.3(c)]. The transition takes place at a relative power of the LD2 to LD1 coupling equal to 9.54% with respect to the direct path. In that case, the power spectra of the two lasers exhibit peaks separated at distances of ~ 120 MHz. This frequency corresponds to the sum of the two external cavities (8 ns) involved in the system.

Corresponding with this qualitative change in the power spectra, a transition to chaos can be observed in the output intensities of the two lasers. At Fig. 3.4 (left) we can see the output intensities corresponding to the injected powers considered above, LD1 at top and LD2 at bottom. The corresponding cross-correlation function at Fig. 3.4 (right) shows the characteristics of the transition to a chaotic output. Figures 3.4(a,b) plot the output intensities of the two lasers and the respective cross-correlation function for purely unidirectional injection, which has its highest peak at $-\tau_{1,2}$ (note that the horizontal scale is in units of $\tau_{1,2}$). Figure 3.4(d) displays the cross-correlation function of the output intensities of LD1 and LD2 with higher mutual coupling [shown in Fig. 3.4(c)], and reveals a quasi-periodic state for this

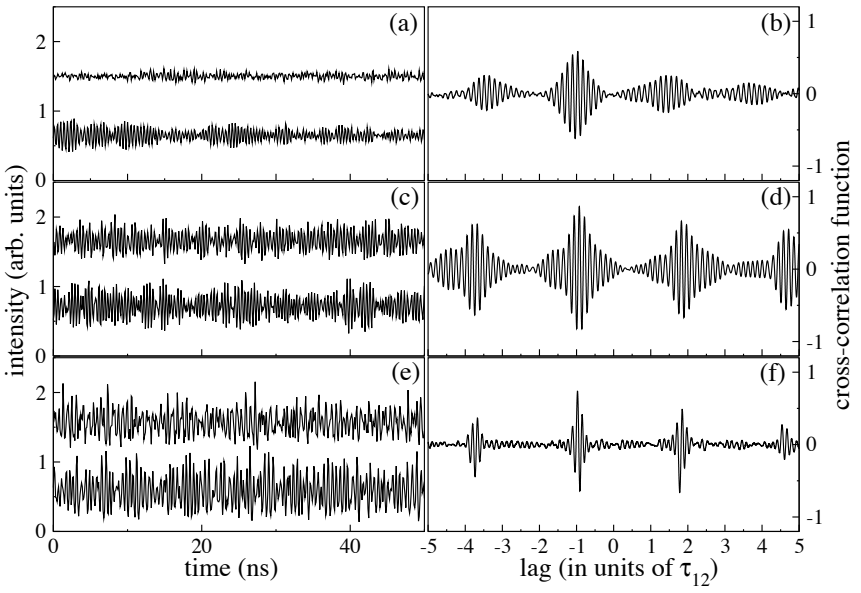

Figure 3.4: *Output intensities of LD1 (top) and LD2 (bottom) for different values of back injection from LD2 (left column), and respective cross-correlation function. For changing relative powers in LD2 to LD1 direction: (a,b)* 0%*, (c,d)* 0.10%*, and (e,f)* 9.54%*.*

very high asymmetry in the couplings. The highest peak appears at $-\tau_{1,2}$, but several higher harmonics occur at intervals $\tau_{1,2} + \tau_{2,1}$. Quasi-periodicity is revealed by growing peaks at those intervals in the cross-correlation function. The chaotic dynamics typical of symmetric coupling is observed in the weakly assymmetric coupling case [9.54% in Fig. 3.4(e)], and is characterized by a quick decrease to zero of the cross-correlation function away from its maximum, as shown in Fig. 3.4(f). The difference in the rates at which the envelope of the cross-correlation peak decay characterizes the transition from a quasi-periodic to a chaotic behavior.

These results show that the symmetry-breaking behavior underlying the leader-laggard dynamics (Heil *et al*, 2001) emerges from a quasi-periodic state that later transforms int a chaotic state with a well defined leader in the dynamics. The

quasi-periodic state is characterized by out-of-phase synchronized outputs, with a cross-correlation function exhibiting a clear maximum at $-\tau_{1,2}$ and secondary peaks at a distance equal to the sum of the external cavities, while in the chaotic case the secondary peaks suffer a loss of correlation.

3.2 Numerical results

In order to examine in a controlled way the route to chaos presented above, we now turn to numerical modeling of the system. Our model is based on the Lang-Kobayashi description of a single semiconductor laser with optical feedback (Lang and Kobayashi, 1980), generalized to account for bidirectional coupling (Mulet *et al*, 2002), and explained at Sec. 2.1.2 of the Introduction. To consider two bidirectionally coupled lasers without feedback we must take $\kappa_{j,j} = 0$ in the model from Eq. (2.3).

We have chosen values of the parameters that reproduce the experimental conditions. In particular the coupling times are $\tau_{1,2} = 3$ ns and $\tau_{2,1} = 5$ ns, and pump currents are chosen to be $I_{\mathrm{LD1}} = 1.2 \times I^{\mathrm{th}}_{\mathrm{LD1}}$ and $I_{\mathrm{LD2}} = 1.1 \times I^{\mathrm{th}}_{\mathrm{LD2}}$. We take a value $\alpha = 3$, and the individual wavelengths are $\lambda_1 = 655.1$ nm and $\lambda_1 = 654.5$ nm. Other parameters are given in Table A.1 of Appendix A. To establish a value for the detuning, we have to take into account that the lasers express several modes, and that the two coupled modes can be different from the maximum gain modes of each solitary laser. If we observe the experimental optical spectra of the solitary lasers, and the optical spectrum of the injected locked laser (see Fig. 3.2), the excited mode of the injected laser is a lateral mode of the solitary laser. We thus measure

the detuning as the frequency difference between the corresponding modes, which is approximately 2 GHz. With this consideration in mind, we can use the single-mode model for the simulations, obtaining results very similar to the experiment.

Following the same protocol as in the experiment, we start from unidirectionally coupled lasers, and perturbing this situation with injected light coming from the other path, we study the transition to chaos in our system.

To determine the value of the fixed $\kappa_{1,2}$, we first study the behavior of a unidirectionally injected semiconductor laser, when the injection level is slowly increased from zero. Figure 3.5 shows the output intensity of LD2 for increasing strength ($\kappa_{1,2}$) of the light injected from LD1 (for $\kappa_{2,1}$=0). At very low injection levels there is a steady state, with an optical power close to that of the solitary laser [Fig. 3.5(a)].

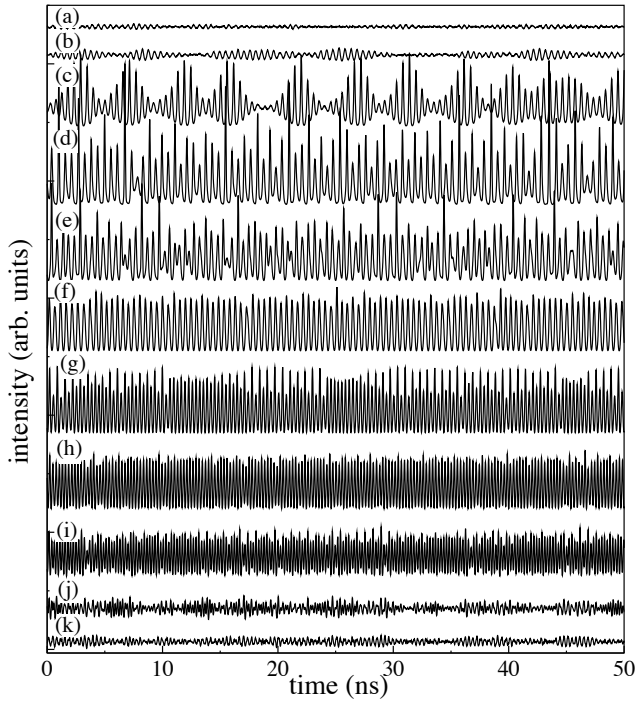

Figure 3.5: *Output intensity of LD2 for different values of injection from LD1 (intensities are shifted vertically for clarity). From top to bottom the different values of* $\kappa_{1,2}$*: (a) 0* ns^{-1}*, (b) 0.5* ns^{-1}*, (c) 1* ns^{-1}*, (d) 2* ns^{-1}*, (e) 4* ns^{-1}*, (f) 5* ns^{-1}*, (g) 10* ns^{-1}*, (h) 15* ns^{-1}*, (i) 20* ns^{-1}*, (j) 25* ns^{-1}*, and (k) 40* ns^{-1}*.*

For increasing values of $\kappa_{1,2}$ we can see how the output intensity of LD1 destabilizes LD2. For higher values of injection [Fig. 3.5(b) and (c)] a quasiperiodic state arises. Then a periodic behavior appears for increasing injection level [Fig. 3.5(f)] that is destabilized for higher values of $\kappa_{1,2}$, leading to chaotic behavior [Fig. 3.5(i)]. Finally for stronger injection levels a steady state appears again [Fig. 3.5(j) and (k)] (see Annovazzi-Lodi *et al* (1994) for more details).

In the simulations below we will consider a fixed value for the injection from LD1 to LD2 corresponding to the situation from Fig. 3.5(j) with $\kappa_{1,2}$= 25 ns^{-1}, for which the lasers show stable output behavior. Once we establish the value for $\kappa_{1,2}$, and with the pump currents and other parameters from Table A.1 of Appendix A, we calculate the relaxation oscillation frequencies of the lasers from the numerical optical spectrum, obtained from a standard Fourier transform of the optical field. The optical spectrum shows side peaks, which are associated with the relaxation oscillations of the laser. Vahala *et al* (1983) observed that the sidebands around the central frequency of the optical spectrum of a single mode semiconductor laser are due to the presence of relaxation oscillations, which results from the interplay between the intracavity optical intensity and the population inversion (Henning and Collins, 1983; Petermann, 1988). The coupling between the amplitude and phase fluctuations of the electric field, described by the α parameter, leads to an asymmetry between the sidebands, such that the low frequency sideband is higher than the high frequency one. When the laser is optically injected these sidebands are enhanced and their asymmetry grows. The injection changes the frequencies of those side peaks that are related to a competition between the relaxation oscillations of the laser and the external cavity resonances (see Homar *et al* (1993) for a detailed discussion).

From the experimental measurements it is possible to see a combination peak of the relaxation oscillation frequencies of both lasers due to the injection from LD1 to LD2 [∼2.5 GHz in Fig. 3.3(a)]. This experimental value can be used to validate the parameter values used in our simulations. Figure 3.6 represents the two side peaks corresponding to the relaxation oscillation (RO) frequencies of our two lasers. With our parameters, the values of the RO frequencies of the isolated lasers

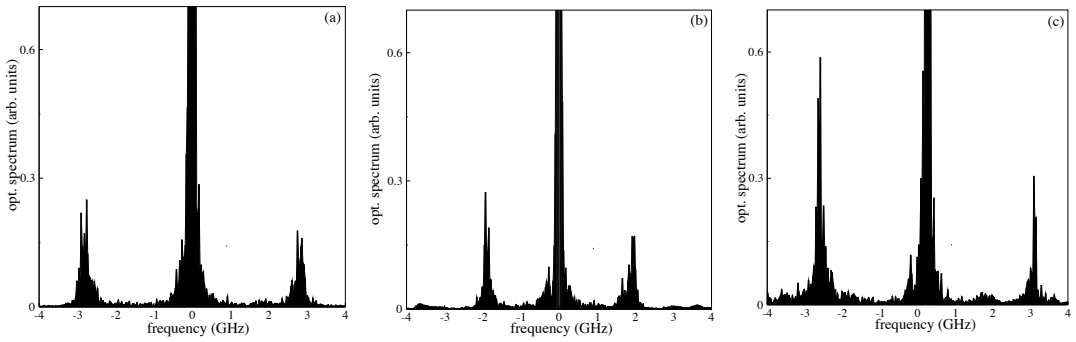

Figure 3.6: *Numerical optical spectrum for the solitary LD1 (a) and LD2 (b) lasers, and for LD2 injected by LD1 (c).*

are $f_1 \simeq 3$ GHz and $f_2 \simeq 2$ GHz [Fig. 3.6(a,b)]. When LD2 is injected by LD1 [Fig. 3.6(c)] its relaxation oscillations are enhanced and two strong asymmetrical side peaks appear at the optical spectrum. Due to the injection, the peaks of LD2 are displaced to higher frequencies, and occur at approximately f_1.

To compare with the experimental results of Fig. 3.2 we generate the output intensities for both lasers for a fixed value of $\kappa_{1,2}$ =25 ns^{-1} and for increasing $\kappa_{2,1}$. We start with a stable state and we destabilize LD1 with a small perturbation coming from LD2. Figure 3.7 plots the output intensities in the left column (top for LD1, bottom for LD2) and the respective cross-correlation functions in the right column, for increasing values of $\kappa_{2,1}$. Figure 3.7(a,b) corresponds to the case of unidirectional

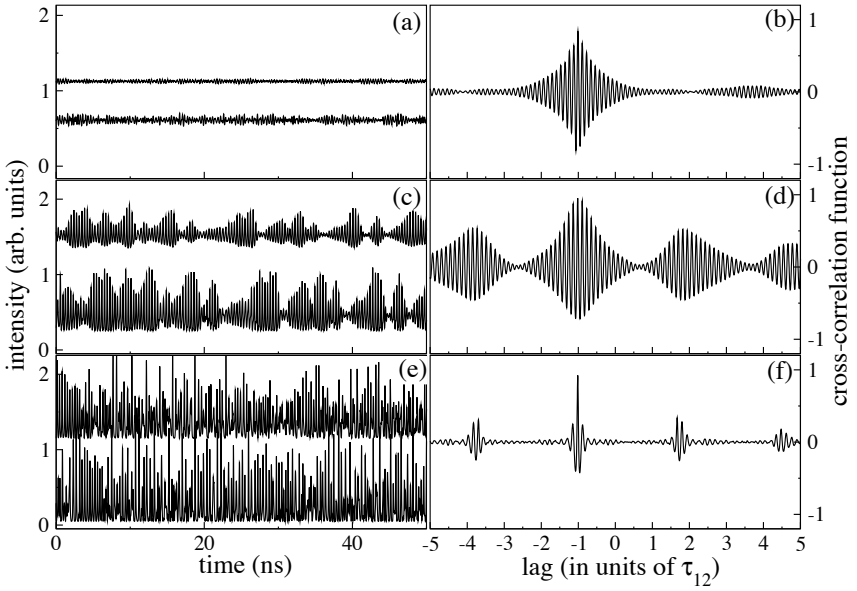

Figure 3.7: *Numerical output intensities of LD1 (top) and LD2 (bottom) for different values of injection from LD2 (left column), and respective cross-correlation function. For* $\kappa_{1,2}$*=25 ns*$^{-1}$ *and (a)(b)* $\kappa_{2,1}$*=0 ns*$^{-1}$*, (c)(d)* $\kappa_{2,1}$*=1.3 ns*$^{-1}$*, and (e)(f)* $\kappa_{2,1}$*=10 ns*$^{-1}$*.*

coupling. In the corresponding cross-correlation function, a peak at lag time equal to $-\tau_{1,2} = -3$ ns appears, corresponding to the flight time of the light from LD1 to LD2. As we increase $\kappa_{2,1}$, keeping $\kappa_{1,2}$ constant, a quasi-periodic state arises in Fig. 3.7(c,d), with $\kappa_{2,1} = 1.3$ ns^{-1}. The corresponding cross-correlation function in (d) shows again a maximum peak at $-\tau_{1,2} = -3$ ns, and secondary harmonics at a distance $\tau_{2,1} + \tau_{2,1} = 8$ ns. The decreasing behavior of the cross-correlation would not correspond to an ideal quasiperiodic state, but the introduction of internal white noise moves the cross-correlation function away from the ideal situation. For larger injection, $\kappa_{2,1} = 10$ ns^{-1}, a fully developed chaotic state appears with a cross-correlation revealing the typical lag time between both signals at a distance $-\tau_{1,2}$ [Fig. 3.7(e,f)].

Chapter 4

Controlling the leader-laggard dynamics in delay-synchronized lasers

The collective dynamics of networks is usually studied under the assumption that coupling between the network elements is instantaneous. But in networks of dynamical elements (Boccaletti *et al*, 2006), coupling signals take a finite time to travel from one node to another. When this coupling time is comparable to, or longer than, the characteristic time of the network elements, simultaneous synchronization of the dynamics (Boccaletti *et al*, 2002) is usually not possible [except in particular network architectures, see e.g. Sivaprakasam *et al* (2003); Fischer *et al* (2006); Lee *et al* (2006)], and lag synchronization arises (Rosenblum *et al*, 1997; Shahverdiev *et al*, 2002). In that situation, even if the network elements synchronize their dynamics, a lag time appears. This means that, in a given pair of elements, one of

them leads the dynamics and the other one lags behind (see Chapter 2).

Under these conditions, it is important to determine which elements are leading the dynamics and which ones are lagging behind. An important factor is whether the links between the elements are directed (unidirectional) or not (bidirectional). In the case of two oscillators coupled via a directed link, the element "emitting" the coupling signal is usually the leader [with the exception of certain coupling setups including delayed feedback loops, leading to anticipated synchronization, as explained at Sec. 2.1.1 of Introduction, (Voss, 2000; Masoller, 2001; Ciszak *et al*, 2003)]. If the link is undirected, any of the two elements can lead the dynamics depending on the asymmetries between them; if the elements are similar enough, the roles of leader and laggard switch randomly in time (Heil *et al*, 2001).

As we have seen in the Introduction of this Thesis, when the output of a semiconductor laser with feedback, operating in the LFF regime, is introduced into a second laser, power dropouts are also induced in the latter, provided the two lasers are similar enough in their physical properties. The dropouts are synchronized between the two lasers and, in general, the emitter laser leads the dynamics (i.e. the dropouts occur earlier) with a time lag equal to the coupling time. This synchronization state is, nevertheless much less common and more difficult to reach than the usual lag synchronization state (Locquet *et al*, 2002,a) discussed here. We note, however, that if the coupling and feedback strengths are tuned such that the total injection (feedback + coupling) is equal for the two lasers, and if the feedback time is larger than the coupling delay, the receiver laser can anticipate the emitter (Masoller, 2001).

Interestingly, a similar dynamics is observed in the case of two bidirectionally coupled lasers, even in the absence of an external mirror: coupling destabilizes the lasers

and produces a low-frequency dynamics consisting of synchronized dropouts (Heil *et al*, 2001).

In this chapter, we examine the transition between the two coupling schemes described above. Specifically, we vary in a controlled way the directionality of the coupling, ranging from pure unidirectional injection of the light emitted by one laser (which has an external mirror) into the other one (which does not have a mirror), to symmetrical bidirectional coupling by common light injection. To that end, we vary the amount of light being injected from the solitary laser back into the laser with external mirror. As we will see below, this allows us to control which laser leads the dynamics. Numerical simulations also indicate that the dynamical behavior can be qualitatively different between these two coupling setups.

4.1 Alternating the leader and laggard roles

We have an asymmetrical system consisting in two bidirectionally coupled lasers, one of them with feedback. One of the lasers thus receives two different injections, one from its own light and another coming from the other laser. With the aim of understanding how the coupling affects the choice of the leader, we start studying a unidirectional coupling configuration in which the laser with feedback transmits its dynamics to the solitary one. In this synchronized situation, in which the solitary laser locks its optical frequency to the transmitted one, we increase the back injection. As the bidirectional coupling increases, the leader role switches between the lasers due to the decrease of the optical frequency of the laser with feedback.

4.1.1 Experimental setup

Our experimental setup, shown in Fig. 4.1, consists of two parameter-matched AlGaInP index guided and multi-quantum well semiconductor lasers (Sharp GHO 6510B2A), coupled by mutual optical injection through two independent unidirectional paths. One of the lasers (LD1) is subject to optical feedback from an external mirror (M).

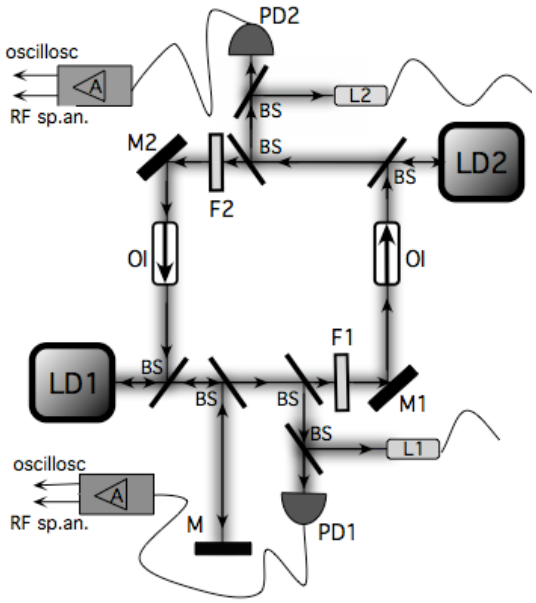

Figure 4.1: *Experimental arrangement of two semiconductor lasers coupled via two independent unidirectional paths. Laser LD1 receives optical feedback from mirror M. BS, beam splitters; F1 (fixed at 44% transmittivity) and F2 (variable), neutral density filters; M1 and M2, mirrors; OI, optical isolators; PD1 and PD2, photodiodes; L1 and L2, collimation lenses to send the light to the optical spectrum analyzer; A, amplifiers.*

Both lasers operate with a nominal wavelength of $\lambda_n = 654$ nm. The temperature and pump current of the lasers are controlled with an accuracy of $\pm 0.01^{\circ}$C and ± 0.1 mA, respectively. The laser outputs are split in order to simultaneously record the intensity and the optical spectra. For each laser, half of the light is collimated

and directly sent to an optical spectrum analyzer (Anritsu MS9710C) and the other is monitored by a fast photodetector of 1 GHz bandwidth (Thorlabs DET210). This received intensity is sent simultaneously via an amplifier (2 GHz bandwidth, Femto high-speed amplifier) to a 1 GHz oscilloscope (Agilent DS06104A), and to a RF spectrum analyzer (Anritsu MS2651B). We note that the 1 GHz bandwidth of the detectors smoothes out most of the fast pulsing dynamics, resulting in the measurement of only the slower dropout envelopes, which are used as low-frequency markers of the dynamics.

Optical isolators (Electro-Optics Technology, Inc.), labeled OI in Fig. 4.1, are placed in the two injection paths in order to have unidirectional coupling in each path. The amount of light injected into each laser is controlled by two neutral density filters (F1 and F2). For temperatures $T_{\mathrm{LD1}} = 21.03^{\mathrm{o}}\mathrm{C}$ and $T_{\mathrm{LD2}} = 20.34^{\mathrm{o}}\mathrm{C}$, the threshold currents of the solitary lasers are, respectively, $I^{\mathrm{th}}_{\mathrm{LD1}} = 31.80$ mA and $I^{\mathrm{th}}_{\mathrm{LD2}} = 32.55$ mA.

The temperatures and pump currents are adjusted such that the optical frequencies of LD1 (with its feedback) and LD2 (in isolation) are as similar as possible to each other. With $T_{\mathrm{LD1}} = 21.03^{\mathrm{o}}\mathrm{C}$ and $T_{\mathrm{LD2}} = 20.34^{\mathrm{o}}\mathrm{C}$ we adjust their intensities at I_{LD1}=33.51 mA and I_{LD2}=33.28 mA. The two coupling paths are $L_{12} = L_{21}$=1.02 m, corresponding to coupling times $\tau_{1,2} = \tau_{2,1} = \tau_c = 3.4$ ns. The external mirror M, that provides feedback to LD1, is also positioned in such way that the feedback time τ_f is equal to the coupling time, τ_c. The reduction of the threshold current of LD1 due to its feedback is 3.5%. When both lasers are turned on, their threshold currents are also decreased due to the injection. In the absence of the filters F1 and F2 (maximum mutual injection), the threshold reduction of LD1 is 2.6% with respect

to its threshold with feedback, and the reduction of LD2 is 2.1% with respect to its free-running threshold. Departing from this common injection, we place a fixed neutral density filter F1 (44% transmittivity) in the LD1 to LD2 injection path. A second variable neutral density filter F2 controls the relative injection between the two lasers.

4.1.2 Results

In the absence of injection in any of the two coupling paths, laser LD2 is stable while laser LD1 (the one with optical feedback) operates in the LFF regime, and thus undergoes power dropouts at irregular times. When a sufficient amount of light from LD1 is injected into LD2 (in an unidirectional configuration), the second laser exhibits power dropouts as well, following those of LD1 with a natural time lag equal to the coupling time τ_c. This behavior is shown in Fig. 4.2(a). The time lag can be determined by comparing the times at which synchronized power dropouts occur in the two lasers. A histogram of the time differences between synchronized power dropouts corresponding to this regime is shown in Fig. 4.2(b). The lag is calculated as the difference between the dropout time in LD1 and the one in LD2, therefore a negative value corresponds to an *advance* of LD1 over LD2, as expected and evident in Fig. 4.2(a). Intuitively, this lag is produced by the time needed by the light of one laser to affect the dynamics of the other one. The histogram of time differences was computed for $\sim$1000 synchronized dropouts. We note that another synchronized state is possible in this setup, in which the lasers are synchronized at zero-lag (provided the feedback and coupling times are equal) (Uchida *et al*, 2005), but this requires a very careful tuning to make the coupling and feedback strengths

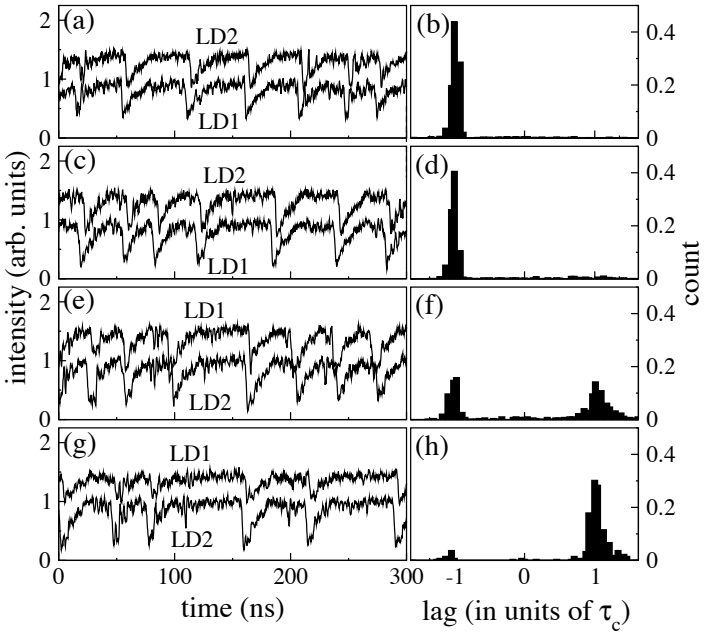

Figure 4.2: *Experimental output intensities (left column) and the corresponding histogram of time differences between synchronized dropouts in the two lasers (right column) for increasing transmittance of filter F2: (a,b) 0%, (c,d) 40%, (e,f) 63%, (g,h) 100%. The time traces have been shifted vertically for clarity.*

equal, and extremely similar lasers (Locquet *et al*, 2002); we have not considered that regime here.

We now allow for the light emitted from LD2 to reach LD1 and, varying the transmittivity of filter F2, control the strength of that coupling, which we will call backward coupling, while keeping the amount of light injected from LD1 into LD2 constant. Figure 4.2 shows that for transmittivities up to 40% (plots c,d) the situation does not change much with respect to the purely unidirectional case (LD1 leads the dynamics with a time $\sim \tau_c$), even though a substantial amount of light from LD2 is already entering LD1. At a transmittivity of around 60%, however [Fig. 4.2(e,f)] laser LD2 begins to have a noticeable influence and takes over the

leader role frequently. The situation resembles that of two mutually coupled lasers without mirrors and with equal frequencies (Heil *et al*, 2001), even though the system in that case is perfectly symmetrical and the present one is not, since here one of the lasers (LD1) is subject to feedback and the other one is not. Finally, if we keep increasing the amount of light being coupled back from LD2 into LD1 until the coupling is purely bidirectional [Fig. 4.2(g,h)], laser LD2 takes over the leader role permanently, and its dropouts precede almost always those of LD1, again a time $\sim \tau_c$.

Although there seem to be no differences between the histograms of the purely unidirectional case and low backward coupling (the distribution of time differences between dropouts are equal), differences exists in the output intensities and the optical spectra. Figure 4.3 shows the change in the experimental optical spectra of LD1 and LD2 for different transmittivity of the neutral density filter F2. Spectra (a) correspond to Fig. 4.2(a,b), and spectra (b) correspond to Fig. 4.2(c,d). Initially, unidirectional coupling leads to an increase in the wavelength of LD2 due to the injection and a substantial overlap in the spectra is observed. As we increase the backward coupling strength, the influence of LD1 on LD2 decreases, and finally the latter no longer shifts its intrinsic wavelength due to LD1 [Fig. 4.3(b)]. The wavelength shift between Fig. 4.3(a) (0% transmittivity) and Fig. 4.3(b) (40% transmittivity) is 0.2 nm. This is the limit in our system beyond which the role of leader changes. The laser with a positive drift in wavelength respect to its solitary value is the laggard of the dynamics (Martínez-Avila *et al*, 2007).

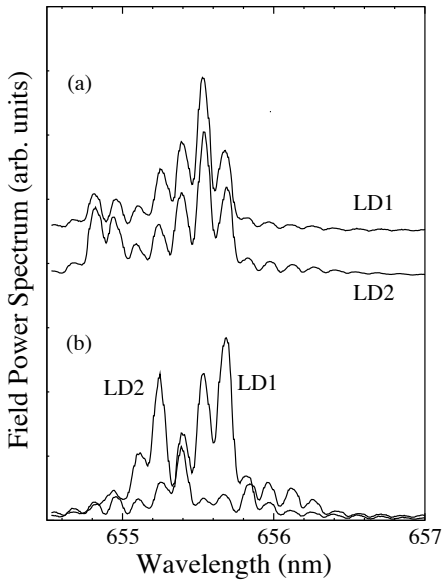

Figure 4.3: *Optical spectra for LD1 and LD2 for different values of transmittivity of F2: (a)* 0% *or unidirectional coupling, and (b)* 40%.

4.1.3 Numerical simulations

As mentioned above, the dynamical behavior shown in Fig. 4.2 is the envelope of a much faster underlying dynamics (Fischer *et al*, 1996), which cannot be detected by our bandwidth-limited monitoring equipment. In order to determine whether the leader-laggard dynamics described above also holds at these higher frequencies, we resort to numerical simulations of the system.

We take the Lang-Kobayashi description of a single semiconductor laser with optical feedback (Lang and Kobayashi, 1980), generalized to account for bidirectional coupling (Mulet *et al*, 2002), and described in Eqs. (2.3) and (2.4) of the Introduction. To take into account that the optical feedback is only present in LD1 we must add in the feedback term of the field equation a Kronecker delta as: $\delta_{j1}\kappa_{j,j}E_j(t-\tau_{j,j})e^{-i\omega_j\tau_{j,j}}$.

We have chosen typical values of the parameters to reproduce the experimental conditions. We have chosen the pump currents to be $I_{\mathrm{LD1}} = 1.03 \times I_{\mathrm{LD1}}^{\mathrm{th}}$ and $I_{\mathrm{LD2}} = 1.03 \times I_{\mathrm{LD2}}^{\mathrm{th}}$. The coupling times are $\tau_{1,2} = \tau_{2,1} = \tau_c = 3.4$ ns, and equal to the feedback time τ_f. The linewidth enhancement factor is $\alpha = 4.0$ and the spontaneous emission rates are $\beta_j = 0.5 \times 10^{-9}$ ps^{-1} for both lasers. Other parameters are given in Table A.1 of Appendix A. For this parameter set, the laser with feedback operates in the LFF regime, and we begin with this case in order to compare with the experimental results given above.

Mimicking the experimental procedure described above, we now introduce different values of $\kappa_{2,1}$ for constant values of $\kappa_{1,2}$ and κ_f. Figure 4.4 shows the output intensities of each laser and the corresponding histograms of the time difference between dropouts for increasing values of the backward coupling strength $\kappa_{2,1}$. The numerically computed time series have been filtered (with a low-pass 4th-order Butterworth filter and a frequency cutoff of 100 MHz) in order to reproduce the limited bandwidth of our experimental equipment.

In the case of purely unidirectional coupling, i.e. when no light from LD2 is injected back into LD1 [Fig. 4.4(a,b)], LD1 leads the dynamics with a time lag equal to the coupling time τ_c. The inset of (a) displays a detail of 100 ns of the time series, that clearly shows the leadership of LD1. For increasing coupling from LD2 to LD1, a transition occurs, and at a critical value of that coupling a symmetric situation arises, where the leader and laggard roles alternate randomly in time [Fig. 4.4(e,f)]. Beyond that critical point LD2 dominates the dynamics. In particular, when the amount of light injected from LD2 to LD1 is higher than in the opposite direction [Fig. 4.4(g,h)], LD2 clearly leads the dynamics, again with a time lag equal to the

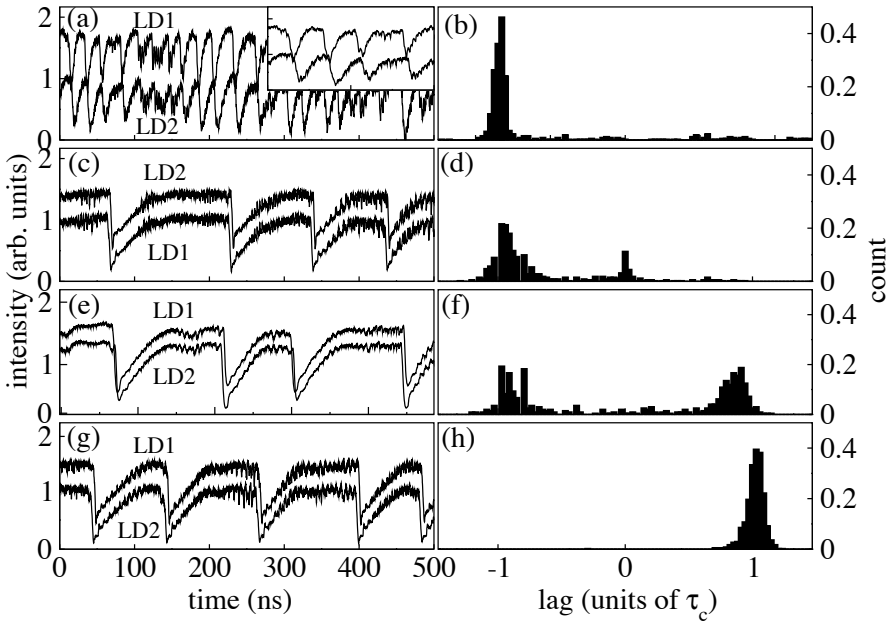

Figure 4.4: *Numerical output intensities (left column) and the corresponding histogram of time differences (right column) for increasing strengths of the injection received by LD1 from LD2, $\kappa_{2,1}$. The forward coupling strength from LD1 to LD2, is fixed to $\kappa_{1,2} = 80\ ns^{-1}$, and the feedback strength to $\kappa_f = 10\ ns^{-1}$. The values of $\kappa_{2,1}$ are: (a,b) 0 ns^{-1}, (c,d) 70 ns^{-1}, (e,f) 75 ns^{-1}, and (g,h) 90 ns^{-1}. Other parameters are given in Table A.1 of Appendix A.*

coupling time τ_c. These results are in agreement with the experimental observations shown in Fig. 4.2.

In order to quantify the synchronization level and time lag between the intensity signals for fast time scales (i.e. without filtering), we calculate the cross-correlation function between the two time series (Buldú *et al*, 2005):

$$C(\Delta t) = \frac{\langle (P_1(t) - \langle P_1 \rangle)(P_2(t+\Delta t) - \langle P_2 \rangle) \rangle}{\sqrt{\langle (P_1(t) - \langle P_1 \rangle)^2 \rangle \langle (P_2(t) - \langle P_2 \rangle)^2 \rangle}}\,, \tag{4.1}$$

where the angular brackets denote temporal averages. According to this definition

a maximum correlation at a positive time lag Δt indicates that LD2 is leading the synchronized dynamics with that time lag, and vice versa (see Appendix B).

Figure 4.5 represents the unfiltered time series of the lasers in the LFF regime (left column), with its corresponding cross-correlation function (right column) for two limit cases. In the unidirectional case [Fig. 4.5(a,b)], the fast dynamics is synchronized, and the cross correlation function shows that laser LD1 leads the dynamics, as expected from the results given above. In the presence of sufficiently large

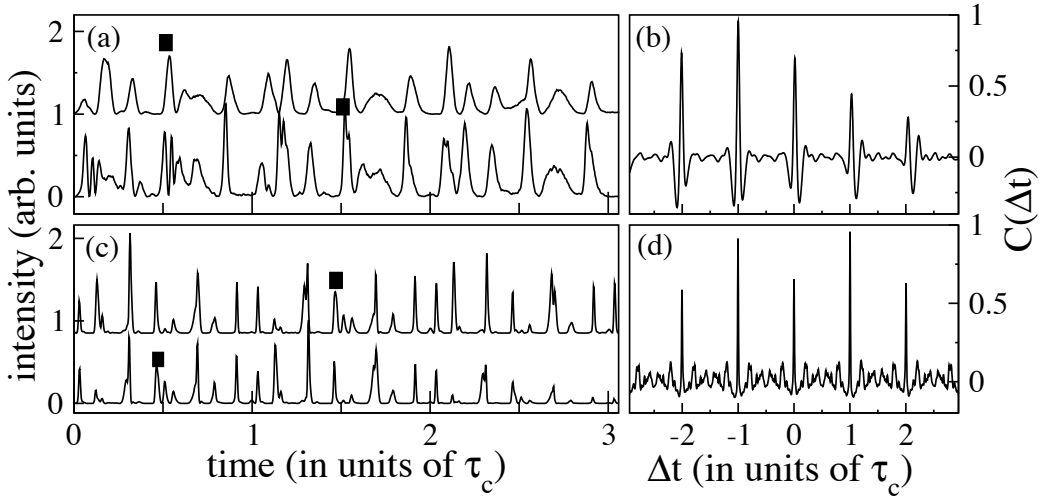

Figure 4.5: *Time series (a,c) and cross-correlation functions (b,d) for* $\kappa_{1,2} = 80\ ns^{-1}$ *and* $\kappa_f = 10\ ns^{-1}$ *for: (a,b)* $\kappa_{2,1} = 0\ ns^{-1}$ *and (c,d)* $\kappa_{2,1} = 90\ ns^{-1}$*. Black boxes denote the same dynamical instant in both time series.*

injection from LD2 back into LD1 [Fig. 4.5(c,d)], the leader and laggard roles switch and now LD2 is the leader. This behavior coincides with the dynamics of the signal envelopes (Fig. 4.2).

When the leader role alternates between the two lasers, the change reveals itself also in the fast dynamics. Figures 4.6(a) and (b) show a detail of LD1 and LD2

leading the dynamics respectively. Plot (c) represents the cross-correlation function for this intermediate state, showing two equally high peaks at $\pm\tau_c$. The switch of the leader is produced when the lasers turn off during the dropout events.

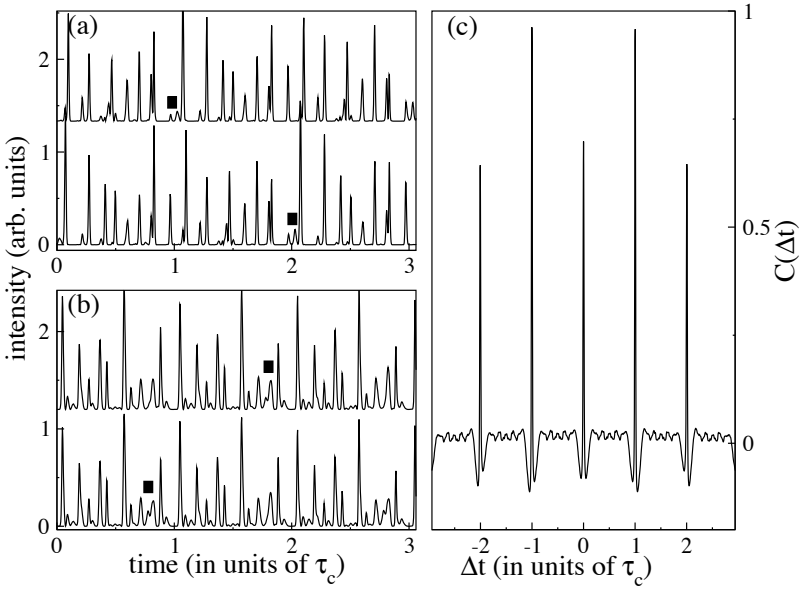

Figure 4.6: *Unfiltered time series (left plots) for LD1 (top traces) and LD2 (bottom traces) and the correspondent cross-correlation function (right plot) for* $\kappa_{1,2} = 80\ ns^{-1}$, $\kappa_{2,1} = 70\ ns^{-1}$ *and* $\kappa_f = 10\ ns^{-1}$. *Plots (a) and (b) show a stretch of time series in which LD1 and LD2 lead the dynamics, respectively. Black boxes denote the same dynamical instant in both time series.*

We have seen so far that our model reproduces satisfactorily the experimental observations, and shows that the leader-laggard dynamics holds at smaller time scales. We now turn our attention to other dynamical regimes exhibited by this system. When the pump current is higher than the ones considered previously, it is known that the lasers exhibit a fully chaotic dynamics, a regime known as coherence collapse (Mirasso, 2000; Heil *et al*, 1998).

We have examined whether the leader-laggard dynamics is maintained in that

regime, and if the roles can be made to switch by controlling the directionality of the coupling, as in the LFF case. Figure 4.7 compares the time traces and the corresponding cross-correlation functions in the two limiting cases of unidirectional and bidirectional coupling. The data show that the leader and laggard roles are reversed, as in the previous case.

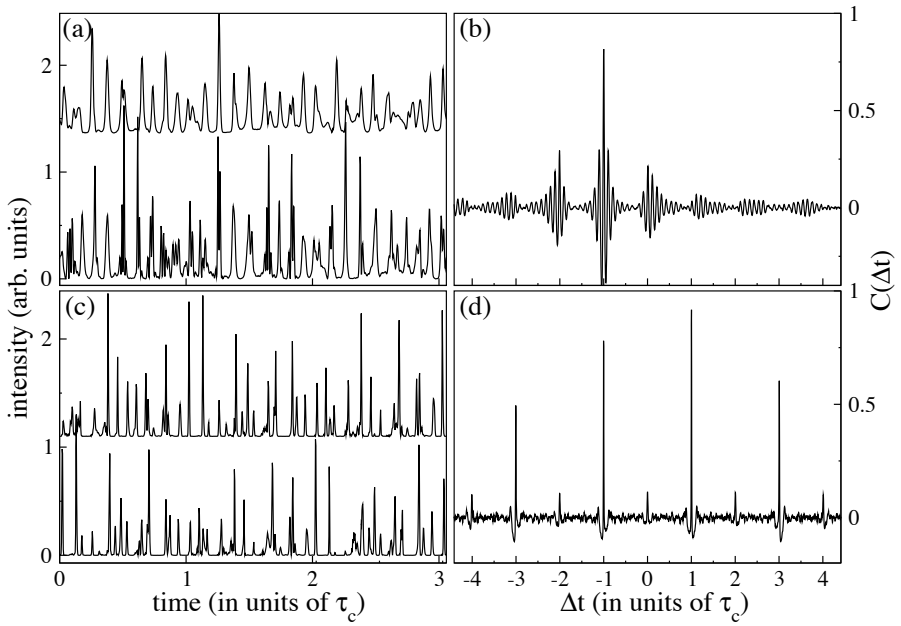

Figure 4.7: *Numerical output intensities of the lasers in the coherence collapse regime (left column) and the corresponding cross-correlation functions (right column) for* $\kappa_{1,2} = 80\ ns^{-1}$ *and* $\kappa_f = 10\ ns^{-1}$ *and two different backward coupling. In (a, b)* $\kappa_{2,1} = 0\ ns^{-1}$ *and in (c, d)* $\kappa_{2,1} = 90\ ns^{-1}$*. Other parameters are listed in Table A.1 of Appendix A except* $I_{LDj} = 1.2 \times I_{thj}$*,* $\alpha = 5$*, and* $\beta_j = 2 \times 10^{-9}\ ps^{-1}$*.*

With the aim of determining the boundaries of the dynamical behavior described above, we have also examined numerically, in a systematic way, whether a change in the coupling strength produces a variation in the type of dynamics exhibited by the coupled system. Our results indicate that, without varying other parameters, even

under large variations in the coupling from LD2 into LD1, $\kappa_{2,1}$, the system does not change its dynamical behavior. Only when the feedback strength κ_f varies, the dynamics of the lasers are modified.

Figure 4.8 shows the consequences of varying the feedback strength, when the coupling strengths in the two directions are non-zero. Starting from a synchronized

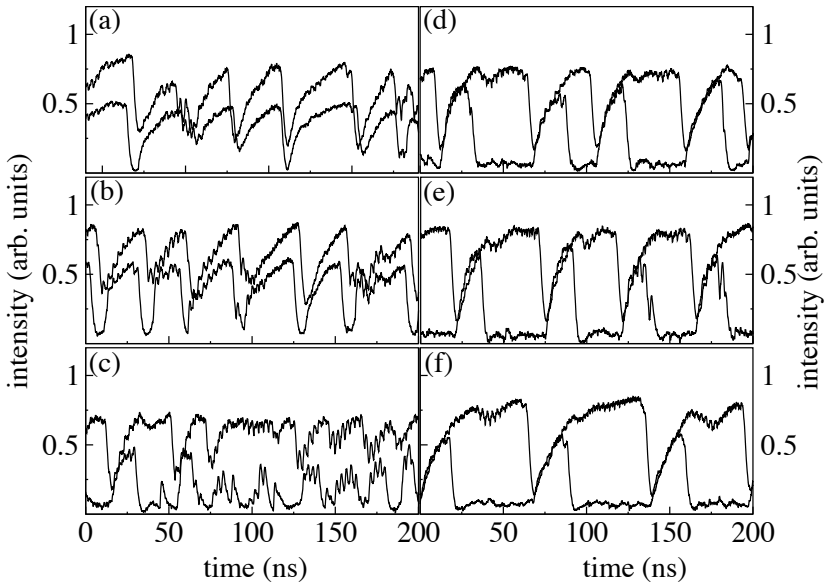

Figure 4.8: *Numerically determined laser output intensities for fixed values of coupling, $\kappa_{2,1} = 15\ ns^{-1}$ and $\kappa_{1,2} = 25\ ns^{-1}$, and different amounts of feedback on LD1. The time traces of LD1 have been shifted vertically upwards for clarity. (a) $\kappa_f = 15\ ns^{-1}$, (b) $\kappa_f = 20\ ns^{-1}$, (c) $\kappa_f = 30\ ns^{-1}$, (d) $\kappa_f = 35\ ns^{-1}$, (e) $\kappa_f = 40\ ns^{-1}$, and (f) $\kappa_f = 45\ ns^{-1}$.*

dropout regime, for fixed values of $\kappa_{2,1} = 15$ ns^{-1} and $\kappa_{1,2} = 25$ ns^{-1}, and for increasing values of the amount of feedback acting upon LD1, the figure shows a substantial change in the dynamics of LD2, while LD1 remains in the LFF regime, without loss of synchronization. Specifically, for large feedback strengths, laser LD2 undergoes power jump-ups synchronized with the dropouts of LD1, which have

been recently associated with a mechanism of episodic synchronization (Buldú *et al*, 2006). In this case the detuning induced in the receiving laser was the responsible for the occurrence of these jump-ups. The jump-ups are mediated by the frequency shift due to the feedback. For most of the time in the LFF regime, the dynamical trajectories of the lasers separate from each other and only coincide during these jump-ups, leading to an episodic synchronization.

4.2 Message transmission capabilities

Many studies have examined the viability of message transmission between two coupled chaotic lasers. Most of them have been devoted to unidirectional transmission schemes (Uchida *et al*, 2005; Argyris *et al*, 2005), but the possibility of transmitting information bidirectionally through the same channel is beginning to attract attention (Vicente *et al*, 2007). This type of communication obviously requires bidirectional coupling between the lasers, and therefore it is natural to ask whether the relatively simple setup considered in this chapter, namely two semiconductors lasers coupled face-to-face, is useful for bidirectional communications. Chaotic communications rely in what is known as chaos-pass filtering (Fischer *et al*, 2000). Through this mechanism, a message inserted into a chaotic carrier can be decoded by a receiver laser (which must be parameter-matched to the emitter) that filters out the message from the carrier. When synchronization between the lasers occurs with a time lag, as in the case presented in this chapter, it is known that only the laggard laser can act as a chaos-pass filter (Heil *et al*, 2001). This seems to prevent the use of the setup discussed here as a bidirectional communication system. However, we have shown above that we can control which laser leads the dynamics by acting

upon the coupling architecture of the system. One could thus envision a protocol that would allow one to switch the leader and laggard roles so that the laser required to act as emitter at any given time is made to lead the dynamics during that time.

4.2.1 Experimental results

Figure 4.9 shows the experimental setup used to investigate this issue by introducing the message, first in LD1 and then in LD2, in order to check experimentally that switching the leader and laggard roles of the lasers produces also a switching of their chaos-pass filtering characteristics.

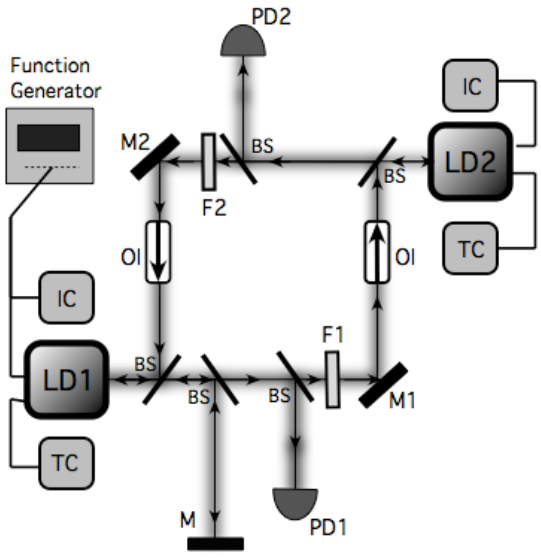

Figure 4.9: *Experimental arrangement of message introduction in two semiconductor lasers coupled via two independent unidirectional paths. Laser LD1 receives optical feedback from mirror M. BS, beam splitters; F1 (fixed at 44% transmittivity) and F2 (variable), neutral density filters; M1 and M2, mirrors; OI, optical isolators; PD1 and PD2, photodiodes.*

Departing from a chaotic state of laser LD1 (due to its feedback) we synchronize the two lasers without the neutral density filters F1 and F2. With $T_{\mathrm{LD1}} = 20.48^{\mathrm{o}}\mathrm{C}$ and $T_{\mathrm{LD2}} = 21.08^{\mathrm{o}}\mathrm{C}$ we adjust their intensities at I_{LD1}=33.02 mA and I_{LD2}=33.35 mA, to have the optical spectra of LD1 (with its feedback) as similar

as possible to that of LD2. It is necessary to have very similar optical frequencies to minimize the coupling strength to reach synchronization when we increase the backward injection. If coupling is too large, one laser would force too much the other one, destroying the filtering capability of the receiver. In that case only a passive amplification of the transmitted signal takes place.

After that, we place a filter F1 in the LD1 to LD2 path, to control the leadership of the dynamics through the neutral density filter F2, as in the previous experiment. We made a first rough approximation to limit the range of values for the introduced frequency (by modulating the pump current of the laser), looking to the RF spectra for the two lasers. It is necessary to introduce a frequency that can be detected at the RF-spectrum of the transmitter. If we consider a frequency smaller than that of the average LFF frequency the filtering process does not work. If it is similar to the average LFF frequency, a high amplitude is necessary to see the message in the transmitter, and consequently the filtering does not work in the receiver. Therefore, appropriate frequencies are those slightly higher than the average LFF frequency. For the unidirectional case, in which no backward injection from LD2 is received by LD1, we apply a 46-MHz modulation (with a waveform generator, Agilent 33250A), with 10mV of amplitude, to the pump current of the emitter laser LD1. The chaotic signal of LD2 synchronizes with the chaotic part of the signal transmitted from LD1 and its periodic part is suppressed (i.e. filtered) by the receiver. Figure 4.10 (a), top trace, shows the chaos-pass filtering in the RF spectrum of LD2. A clear peak appears at the RF-spectrum of LD1 at the introduced frequency, which is filtered out in the spectrum of the receiver laser, LD2 [Fig. 4.10 (a), bottom trace]. The amplitude of the introduced signal is such that it is not observed in the output intensity of the transmitter laser [Fig. 4.10(b)].

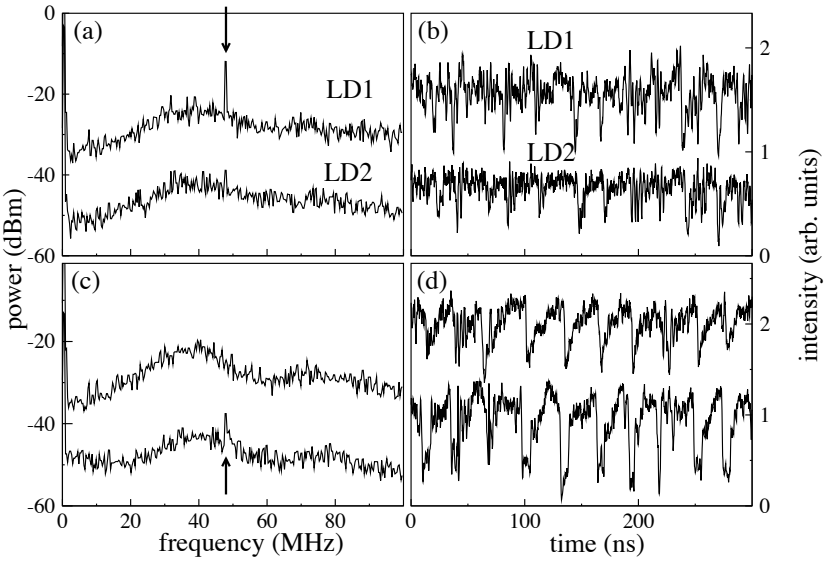

Figure 4.10: *Experimental analysis of the chaos-pass filtering capabilities of the system for unidirectional (a,b) and bidirectional (c,d) coupling. (a,c) RF power spectra, (b,d) corresponding time series. The traces of LD1 have been shifted vertically for clarity in all plots. The vertical arrows in (a,c) indicate the input modulation in each case. The transmittivity of filter F2 in (c,d) is 63%. Other parameters are those of Sec. 5.1.1.*

When the backward injection received by LD1 is increased, and LD2 leads the dynamics, we modulate the pump current of LD2 and the filtering characteristics reappear in LD1 RF-spectrum [Fig. 4.10(c,d)]. We have to note that it was less difficult to "hide" the introduced signal in this last case. The amplitude of the introduced signal was 10 mV but it was possible to reach 20 mV and still have a correct mask in the time series and a good filtering from LD1.

Applying the modulation in the opposite direction, i.e. on the laggard, the modulation peak is maintained in the leader (Heil *et al*, 2001), i.e. chaos filtering does not occur.

4.2.2 Numerical simulations

The previous results constitute further experimental confirmation of the leader-laggard switch, and hint at the possibility that this system can be used for bidirectional communication by controlling the backward coupling strength $\kappa_{2,1}$. We have explored this possibility numerically, by introducing a binary message into the pump current of the lasers. Following the situation of Fig. 4.10, we first transmitted the message from LD1 to LD2, under conditions where LD1 is the leader, and then transmission was realized from LD2 to LD1, varying the amount of coupling $\kappa_{2,1}$ in order to make LD2 the leader. The message is decoded by subtracting the light emitted by the two lasers, taking into account the delay between the signals. The bit message is introduced with an amplitude equal to 3% of the pumping current, and the subtracted signal is filtered with a 4th-order Butterworth low-pass filter and 400 MHz of cut-off.

Figure 4.11 compares the two situations of the experiment. Figure 4.11 (left) shows the time traces of emitter and receiver, and the message extraction is shown in the right panels, for the cases where the message is introduced in LD1 and recovered by LD2 [Fig. 4.11(a,b), LD1 is the leader], and the message is encoded by LD2 and recovered by LD1 [Fig. 4.11(c,d), LD2 is the leader]. In the left plots, the upper time trace (shifted vertically for convenience) represents LD1 and the lower time trace corresponds to LD2. In the right plots, the upper trace is the input message and the lower trace is the recovered message. The results show that message recovery is better in the unidirectional than in the bidirectional case.

The differences in the effectivity of message recovery indicate that the synchronization quality is not the same in the two regimes considered. Since the cross-correlation

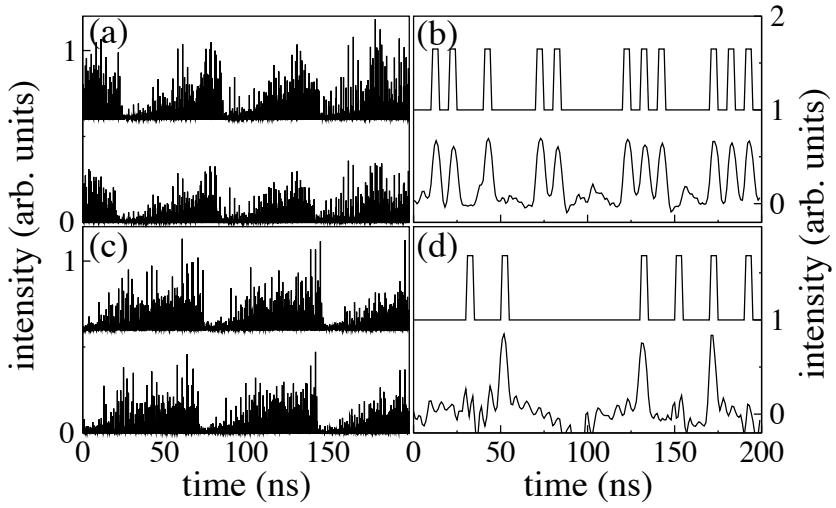

Figure 4.11: *In (a,b) the message is encoded by LD1 with* $\kappa_{1,2} = 80\ ns^{-1}$ *and* $\kappa_{2,1} = 0\ ns^{-1}$*, and in (c,d) the message is encoded by LD2 with* $\kappa_{2,1} = 90\ ns^{-1}$ *and* $\kappa_{1,2} = 80\ ns^{-1}$*. The feedback strength is* $\kappa_f = 30\ ns^{-1}$*, other parameters as in Sec. 4.1.*

function (shown in Fig. 4.7 above to be relatively high) is only an averaged quantity, it does not provide information on potential dynamical deviations from perfect synchronization. In order to quantify such deviations, we computed the sliding correlation coefficient, defined as the maximum of the cross-correlation function, computed with temporal averages over a moving time window of width 3.4 ns (see Appendix B).

Figure 4.12 compares this sliding correlation coefficient with the standard cross-correlation function for the two conditions considered in Fig. 4.11.

The figure shows that even though in the unidirectional case the synchronization is only instantaneously lost during the dropouts, thus it is possible to recover the message. In the bidirectional situation, synchronization loss is widespread, which leads to a poor message recovery when the direction of information transmission is

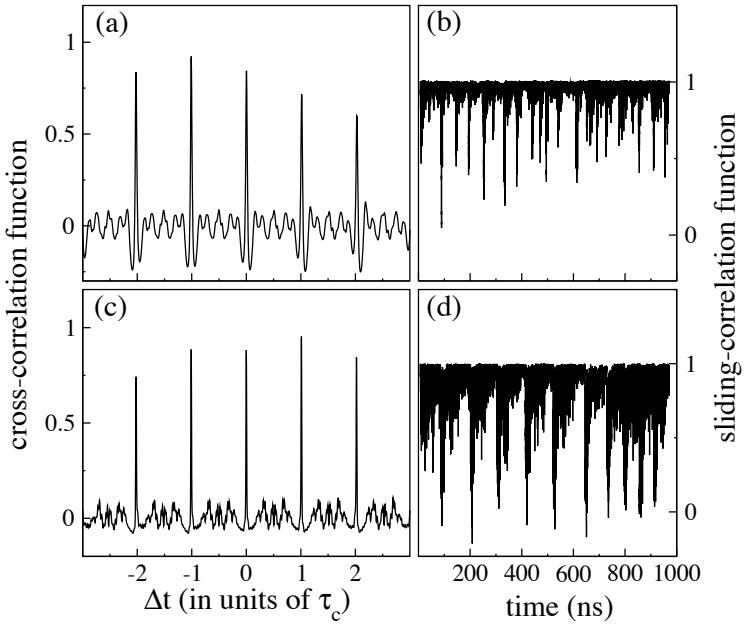

Figure 4.12: *Cross-correlation (left) and sliding-correlation (right) functions for* $\kappa_f = 30\ ns^{-1}$ *and different coupling strengths. (a,b)* $\kappa_{2,1} = 0\ ns^{-1}$ *and* $\kappa_{1,2} = 80\ ns^{-1}$*; (c,d)* $\kappa_{2,1} = 90\ ns^{-1}$ *and* $\kappa_{1,2} = 80\ ns^{-1}$*.*

from LD2 to LD1.

Chapter 5

Processing distributed inputs in coupled lasers

Many information-processing systems, such as the brain or telecommunication networks, are composed of multiple dynamical elements coupled to each other, which receive multiple signals of different frequencies at diverse input locations. It is therefore a matter of interest to determine the effects that the coupling between the dynamical nodes of a processing network has on the integration of distributed signals.

In the phenomenon of ghost resonance (GR), an excitable system subject to two different periodic signals exhibits a resonance at a frequency not present in the input driving (Chialvo *et al*, 2002). This phenomenon, invoked to explain the missing fundamental illusion arising in the perception of complex sounds (Chialvo, 2003), has been shown to be produced by the interplay between noise and periodic forcing in a non-dynamical threshold device (Chialvo *et al*, 2002), but it can also be caused by the

application of periodic perturbations to a chaotic system. The latter effect has been experimentally observed in a semiconductor laser with optical feedback operating in the low-frequency fluctuation regime (Buldú *et al*, 2003) and in the polarization response of VCSEL's (van der Sande *et al*, 2005). In those cases, the interplay between the external modulation and the complex dynamical threshold of the system shows a response similar to the effect of a combined periodic-noisy external signal on a simpler excitable system with a well defined excitation threshold (Chialvo *et al*, 2002).

Here we introduce two different periodical signals, modulating each of the laser's pump currents, and we study the response of two coupled lasers to this distributed signal. In this chapter, we compare experimentally the relatively simple case of distributed signal processing by two mutually coupled excitable elements, specifically two semiconductor lasers in two different cases: when the excitable dynamics is induced by coupling, and when the lasers are independently excitable systems. The first case are two semiconductor lasers coupled face-to-face. The second case consists in two semiconductor lasers mutually coupled but with optical feedback in each one. This second architecture is common in neuronal systems. Sensory neurons, for instance, do not usually operate in isolation (Keener and Snyder, 1998) and recent studies in neuronal systems, both theoretical (Balenzuela and García-Ojalvo, 2005) and experimental (Manjarrez *et al*, 2006), show that coupling is able to mediate the processing of distributed inputs in networks of neurons (which possess independent dynamics even in the absence of coupling). We study both situations using semiconductor laser as highly controllable excitable systems.

5.1 Mutually coupled semiconductor lasers without feedback

As we explain in the Introduction, in two lasers mutually coupled through their respective optical fields in a bidirectionally face-to-face configuration, the dynamics is only produced by the coupling. Each laser is stable in absence of the mutual optical injection. This coupled system has been shown to have a pulsated output (Heil *et al*, 2001), similar to that observed in a single semiconductor laser with optical feedback in the low-frequency fluctuation regime. In that case, previous experimental studies have shown that the response of the system to a periodic forcing of the pump current is strongly enhanced by the coupling (Buldú *et al*, 2002). We will show that coupling induces entrainment to a frequency not present at the input of any of the two lasers. The introduced signals are processed by the total system as a whole.

5.1.1 Experimental arrangement

Our experimental system consists of two AlGaInP index-guided and multi-quantum well semiconductor lasers (Roithner RLT6305MG), LD1 and LD2 in what follows, mutually injected as shown in Fig. 5.1. Both lasers have a nominal wavelength of $\lambda_n = 635$ nm.

The temperature and pump current of the lasers are controlled with an accuracy of $\pm 0.01\,^{\circ}$C and ± 0.1 mA, respectively. For temperatures $T_{LD1} = 19.80\,^{\circ}$C and $T_{LD2} = 17.98\,^{\circ}$C, their threshold currents (in isolation) are respectively $I^{th}_{LD1} = 18.3$ mA and $I^{th}_{LD2} = 18.0$ mA. The operating currents are set to $I_{LD1} = 18.9$ mA and $I_{LD2} = 19.4$ mA. To quantify the effect of the facet of the opposite laser as a

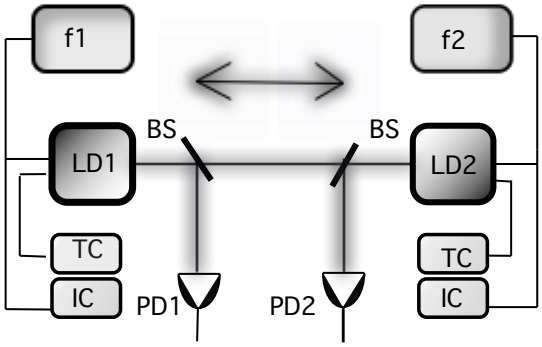

Figure 5.1: *Schematic setup: LD1 and LD2 are the laser diodes; TC and IC are the temperature and current controllers, respectively; f1 and f2 are the frequencies of the external periodic signals; BS are beamsplitters; PD1 and PD2 are photodetectors.*

source of external optical feedback, we estimated the threshold reduction of each laser when the opposite laser is turned off, obtaining a reduction of 3.79% for LD1 and 1.20% for LD2. When both lasers are turned on, the threshold current also decreases, but due to the interaction between the fields the threshold reduction is in that case 4.50% for LD1 and 5.70% for LD2. Two beamsplitters in the coupling branch allowed the detection of the laser outputs by fast photodetectors of 1 GHz bandwidth (Thorlabs DET210). The received signal is sent to a 5 GS/s acquisition card (Gage 85G). The external periodic signals are introduced by modulating the pump current of the lasers with two Agilent 33250A signal generators.

In the conditions of our particular experiment, the lasers remain stable in the absence of external perturbations (Chialvo *et al*, 2002), but when external sinusoidal signals are introduced through their pump currents, synchronized intensity dropouts appear. The dropouts are synchronized with a time delay $\tau_c = 3.43$ ns between the lasers (time that the light takes to travel the distance between them). In other words, the dropouts of one laser advance those of the other a time interval τ_c. In

the absence of frequency difference between the lasers, they randomly alternate the leading role in the dynamics as we saw in the previous chapter. To avoid this effect, which makes difficult to estimate the correlation between both output intensities, a slight frequency detuning is introduced by tuning the operating temperatures, since the laser with higher optical frequency is known to lead the dynamics (Heil *et al*, 2001).

5.1.2 Signal processing mediated by coupling

We applied two distributed inputs, in the form of pump current modulations of different frequencies to each laser (f_1 in LD1, and f_2 in LD2). The external modulations were introduced in the pump current of the lasers with two function generators (Agilent 33250A).

First we choose two harmonics of a common fundamental frequency f_0, defined by $f_1 = kf_0$ and $f_2 = (k+1)f_0$ with $k > 1$.

The behavior of the system for $k = 2$ and $f_0 = 5$ MHz is shown in Fig. 5.2 for increasing amplitudes of the modulation, chosen equal for both signals.

The figure shows the time trace of the intensity of LD1 on the left, and the probability distribution function (PDF, which associates a probability to each value of a discrete random variable) of the interval between dropouts on the right (the results are basically identical for LD2, since both lasers are synchronized). The PDF is computed from a collection of 1000 dropouts in each case. For a small modulation amplitude (top row in Fig. 5.2) the dropouts occur infrequently at different periods. As the amplitude grows (middle row), most inter-pulse intervals occur at a definite period corresponding to the fundamental frequency $f_0 = 5$ MHz ($T_0 = 200$ ns),

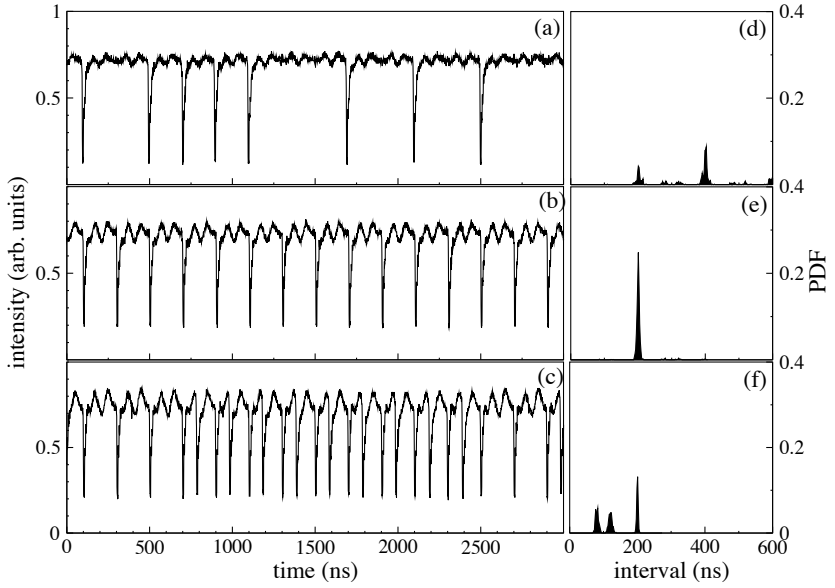

Figure 5.2: *Output intensity of LD1 (left column) and the corresponding probability distribution functions of the time difference between dropouts (right column) for increasing values of the modulation amplitude (A_1 for LD1 and A_2 for LD2): (a,d) $A_1 = A_2 = 0.191$ mA , (b,e)$A_1 = A_2 = 0.409$ mA and (c,f) $A_1 = A_2 = 0.575$ mA.*

which is not present in either of the input signals. For larger amplitudes (bottom row), the input signals take over and dropouts begin to occur at the (larger) input frequencies, reducing the response of the system at the missing fundamental frequency. Therefore, a resonant behavior is observed with respect to the modulation strength: for an intermediate modulation amplitude, the system optimally processes the distributed inputs.

In order to ensure that a resonance occurs at $f_r = 5$ MHz, we statistically analyze the output times series for different modulation amplitudes, evaluating the average and the relative standard deviation of the inter-dropout intervals at each amplitude. Figure 5.3 shows that the standard deviation is minimal for an average inter-dropout

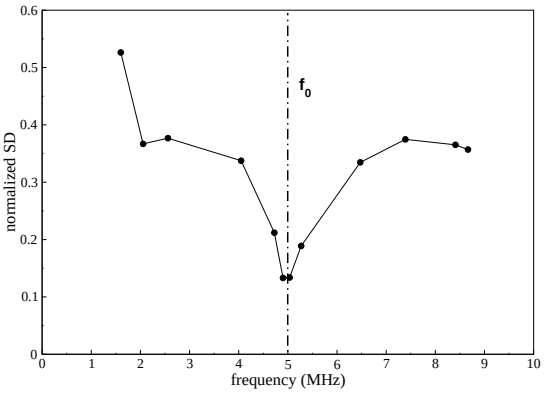

Figure 5.3: *Standard deviation of the interval between dropouts (normalized to the mean interval) versus the mean inter-dropout frequency (inverse of the mean interval between dropouts).*

frequency (*i.e.* the inverse of the mean interval between dropouts) equal to $f_r = 5$ MHz, which indicates that the periodicity is maximal at that output frequency.

5.1.3 Inharmonic response

The results shown above do not correspond to a trivial resonance at the frequency difference $f_2 - f_1$. To demonstrate this, we introduce a frequency shift, Δf, in the input frequencies:

$$f_1 = kf_0 + \Delta f\,, \qquad f_2 = (k+1)f_0 + \Delta f \tag{5.1}$$

Such detuning renders the two input frequencies incommensurate and no longer harmonics of f_0.

We kept the modulation amplitudes constant at $A_1 = A_2 = 0.409$ mA, and varied the frequency of laser LD1 from $2f_0 = 10$ MHz to $3f_0 = 15$ MHz in steps of 0.5 MHz, while changing at the same time the frequency of laser LD2 from $3f_0 = 15$ MHz to

$4f_0 = 20$ MHz, keeping $f_2 = f_1 + f_0$.

Figure 5.4 shows that in this case the response frequency, defined as the inverse of the interval between two consecutive dropouts, increases linearly with the detuning,

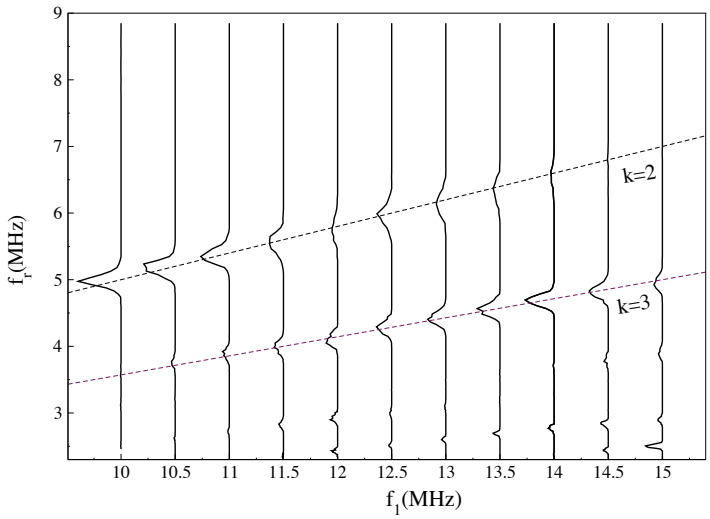

Figure 5.4: *Experimental PDFs of the response frequency f_r (the inverse of the dropout interval) for increasing values of f_1 (and therefore Δf). The dashed lines correspond to the theoretical resonance frequencies given by Eq. (5.2).*

even though the difference between the input frequencies remains equal to f_0. The maxima of the response frequency distribution obey the following simple relation,

$$f_r = f_0 + \frac{\Delta f}{k + 1/2}\,, \tag{5.2}$$

which was obtained by Chialvo *et al* (2002) from a straightforward analysis of the maxima of the linear superposition of two sinusoidal functions with frequencies given by Eq. (5.1).

5.1.4 Comparison with numerical simulations

The experimental results described above can be numerically reproduced by means of the system of delay-coupled rate equations described at Sec. 2.1.2 of the Introduction, taking the feedback term as zero ($\kappa_{j,j} = 0$). As we explained before, the common light path for both directions of coupling allows us to use the simplified notation $\kappa_{12} = \kappa_{21} = \kappa_c$.

In the simulations that follow we have set $\alpha = 3.0$, $\beta = 0.5 \times 10^{-9}$ ps^{-1}, and $\kappa_c = 30$ ns^{-1}. The rest of the laser parameters have been chosen to reproduce the experimental conditions, including the threshold currents $I^{th}_{LD-1} = 18.30$ mA and $I^{th}_{LD-2} = 18.02$ mA, and the coupling time $\tau_c = 3.43$ ns. The rest of parameter values are displayed in Table A.1 of Appendix A. The pump currents take the form $I_{1,2} = I_{DC1,DC2}[1 + A_{1,2}\sin(2\pi f_{1,2}t)]$, where $I_{DC1,DC2}$ are the DC pump currents, $A_{1,2}$ the modulation amplitudes and $f_{1,2}$ their corresponding frequencies, chosen again following Eq. (5.1). The DC levels are chosen to be $I_{DC1} = 1.032 \times I^{th}_{LD1}$ and $I_{DC2} = 1.076 \times I^{th}_{LD2}$.

In order to reproduce the experimental results presented in Fig. 5.2 for the case $\Delta f = 0$, we fix the input frequencies to $f_1 = 10$ MHz and $f_2 = 15$ MHz, increasing the amplitude of both modulations simultaneously. The results can be seen in Fig. 5.5, where the ghost resonance at the frequency $f_r = 5$ MHz is observed for intermediate values of the modulation amplitudes (note the qualitative resemblance with Fig. 5.2). Finally we analyze the effect on f_r of a detuning Δf introduced in both modulation frequencies, following Eq. (5.1). Increasing Δf from 0 MHz up to 5 MHz in steps of 0.001 MHz, we compute the response frequencies (*i.e.* the inverse of the time interval between consecutive dropouts) of 25 dropouts for each

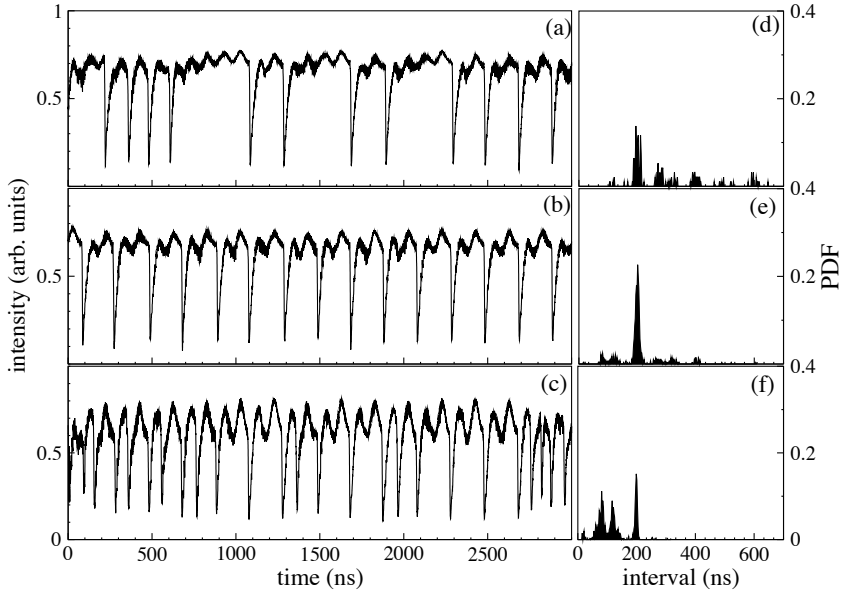

Figure 5.5: *Numerically computed output intensity of LD1 (left column) and the corresponding probability distribution functions of the inter-dropout intervals (right column) for increasing values of the modulation amplitude: (a,d)* $A_1 = A_2 = 0.013$ *, (b,e)* $A_1 = A_2 = 0.020$*, and (c,f)* $A_1 = A_2 = 0.045$*.*

Δf. Figure 5.6 shows the response frequency f_{res} as a function of f_1, and also the comparison with the theoretical predictions of Eq. (5.2) (dashed lines). We can observe how, as f_1 increases, the maximum response frequencies (resonance frequencies) jump between values of f_r to a value of f_r corresponding to higher k parameters. This is in agreement with the experimental PDFs represented in Fig. 5.4, where the PDF maxima jump from the $k = 2$ to $k = 3$ line when f_1 is increased. This dependence of f_r with Δf indicates that the ghost resonance is a nontrivial resonance.

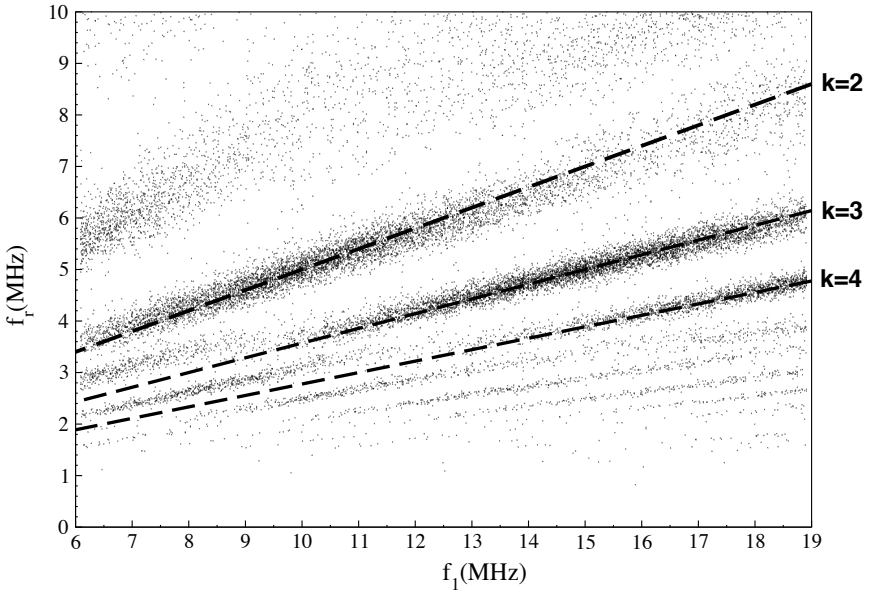

Figure 5.6: *Numerically determined response dropouts frequency f_r as a function of f_1. Dashed lines correspond to theoretical predictions given by Eq. (5.2) for $k = 2 \ldots 4$.*

5.2 Mutually coupled semiconductor lasers with optical feedback

We now consider two mutually coupled semiconductor lasers each one with optical feedback. In this case the lasers have independent dynamics even in the absence of coupling. As explained at Sec. 1.3.3 of the Introduction a laser with optical feedback, in the low-frequency-fluctuation regime, has been shown to have excitable properties (Giudici *et al*, 1997; Mulet and Mirasso, 1999), responding with intensity dropouts to pump perturbations only when the perturbation amplitude surpasses a certain threshold. Nevertheless, and due to the complexity of this particular system (Sano, 1994; van Tartwijk *et al*, 1995), such excitation threshold is not a

well defined constant value. In any case, in this second configuration we have two independently excitable units (two semiconductor lasers with optical feedback), that are mutually coupled through their output fields. We will show how the coupling between these two independent units also induces entrainment to a frequency not present at the input of any of the two lasers.

5.2.1 Experimental setup

Our experimental setup is represented in Fig. 5.7. Two semiconductor lasers, LD1 and LD2, are mutually injected and subject to their own optical feedback from the external mirrors M. The coupling between the lasers can be controlled through a neutral density filter (NDF). The two AlGaInP index-guided and multi-quantum

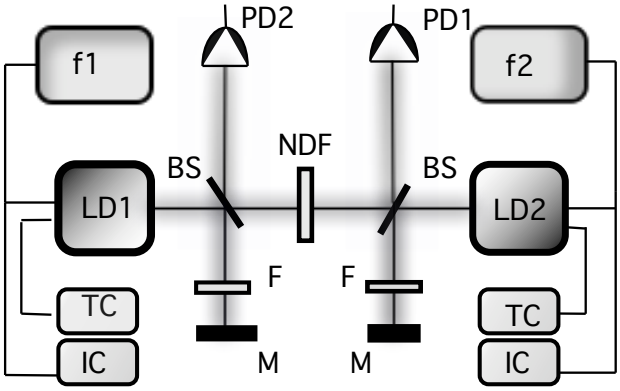

Figure 5.7: *Schematic setup. LD1 and LD2: laser diodes, TC and IC: temperature and current controllers, F1,F2: frequencies of the external signals, BS: beamsplitters, PD1 and PD2: photodetectors, M: mirrors, F: feedback filters, NDF: coupling filter.*

well semiconductor lasers (Roithner RLT6505MG) operate at a nominal wavelength $\lambda = 650$ nm. Their temperature and pump current are controlled with an accuracy of $\pm 0.01^{\circ}$C and ± 0.1 mA, respectively. At temperatures $T_{\mathrm{LD1}} = 18.68\ ^{o}$C and $T_{\mathrm{LD2}} =$

18.26^oC, the threshold currents of the lasers (in isolation) are, respectively, $I^{\text{th}}_{\text{LD1}} =$ 17.1 mA and $I^{\text{th}}_{\text{LD2}} = 16.6$ mA. The operating currents are set to $I_{\text{LD1}} = 17.9$ mA and $I_{\text{LD2}} = 18.1$ mA. The relative pump currents, with respect to the threshold, are slightly different for both lasers, but this small asymmetry does not have an important influence in the results that follow. Antireflection-coated objectives are used to collimate the light emitted by the two lasers. The external mirrors M are placed 51 cm away from each laser, introducing a feedback delay time τ_f equal to the coupling time $\tau_c = 3.4$ ns. Filters F in front of each mirror diminish the quantity of reinjected light.

We position the external mirrors for optimum alignment, minimizing the laser's current threshold in the presence of optical feedback. This reduction is of 3.3% for LD1 and 2.4% for LD2. To quantify the effect of the opposite laser as a source of additional feedback we estimate the threshold reduction when the opposite laser is turned off, obtaining a reduction of 1.2% for LD1 and 1.1% for LD2 with respect to the thresholds in isolation. When both lasers are turned on, the threshold reductions are 4.8% for LD1 and 4.2% for LD2. The laser outputs are monitored by two fast photodetectors PD1 and PD2 of 1 GHz bandwidth (Thorlabs DET210). The received signal is sent to a 5 GS/s acquisition card (Gage 85G), and to an spectrum analyzer (Anritsu MS2650B) via two amplifiers (2 GHz bandwidth, Femto high-speed amplifier).

5.2.2 Dynamics in the absence of coupling

As mentioned above, in isolation and for moderate feedback strengths, semiconductor lasers with optical feedback are known to have excitable properties, whereby

small perturbations in the pump current produce large and brief dropouts in the emitted intensity (Giudici *et al*, 1997; Mulet and Mirasso, 1999). An example of the dynamics of the two lasers in the absence of coupling is shown in Fig. 5.8(a). The plots show that the lasers undergo power dropouts at irregular times, driven by the underlying complex dynamics of the delayed system (Sano, 1994), which can

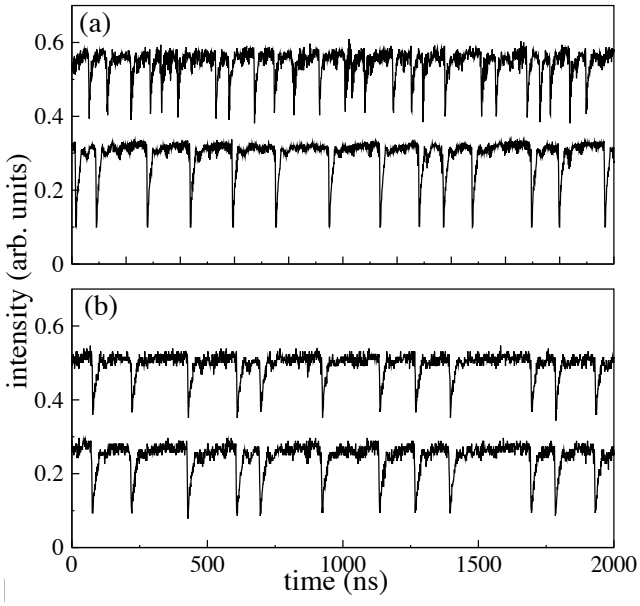

Figure 5.8: *Output intensity of LD1 (top traces) and LD2 (bottom traces) without (a) and with (b) coupling. In (a) the output intensities are independent; in (b), the lasers are synchronized.*

be considered effectively as a noise source. Note that the 1 GHz bandwidth of the detectors smoothes out the fast pulsing dynamics (Fischer *et al*, 1996), resulting in a measurement of only the slower dropout envelope, which is the signal used in this study. When we start coupling the lasers by increasing the transmittivity of the neutral density filter, correlations between the power dropouts arise, until for the maximum coupling strength attainable in our experimental setup (when the NDF

is removed) the lasers are fully synchronized [Fig. 5.8(b)]. In the results that follow, the lasers will be located in this regime. Synchronized dynamics in this experimental setup has been previously reported by Klein *et al* (2006).

5.2.3 Signal processing mediated by coupling.

As we have seen, an isolated laser with feedback undergoes pulsed dynamics in the form of an irregular train of power dropouts. Applying a harmonic modulation to the laser's pump current allows to control this irregular behavior, leading to a periodic train of dropouts at the frequency of the input signal (Sukow and Gauthier, 2000). This effect is most pronounced when the modulation frequencies are on the order of tens of MHz, even though the typical characteristic frequencies of the laser are higher (the relaxation oscillation frequency without feedback is of the order of tens of GHz, and the frequency difference of the external cavity modes are of the order of hundreds of MHz). As we explained at the Introduction an external periodic signal can enhance the probability of produce a dropout event when the external frequency is equal to the mode-antimode difference frequency [see Sukow and Gauthier (2000) and Sano (1994) for details].

With two lasers individually entrained at the input frequencies f_1 and f_2, we remove the coupling filter NDF and observe how the ghost resonance frequency arises in the synchronized dynamics of the system. To that end we gradually increase the amplitude of the input signals and calculate the probability density function (PDF) of the inter-dropout time interval of the output intensity series.

Figure 5.9 shows the output intensity of LD1 (a-c) and their corresponding probability distribution function of the time interval between consecutive dropouts (d-f)

for increasing values of the modulation amplitude (which is the same for both sinusoidal signals). The dynamics of LD2, not shown, is identical to that of LD1, since the two lasers are synchronized. The results of Fig. 5.9 show that for low values of the modulation amplitude [Fig. 5.9(a,d)] the output intensity exhibits dropouts, but

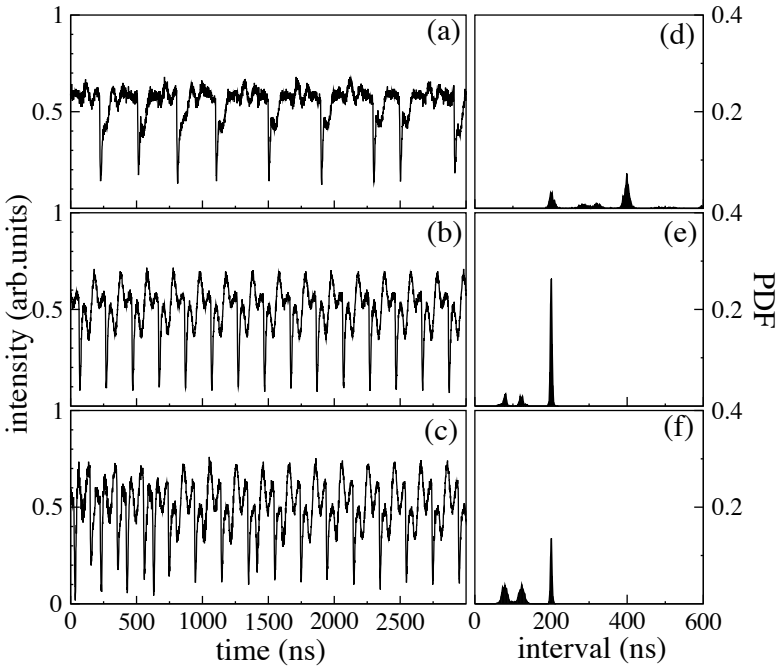

Figure 5.9: *Experimental output intensity of LD1 (left column) and the corresponding probability distribution functions of the time intervals between consecutive dropouts (right column) for increasing values of the modulation amplitude: (a,d)* $A_1 = A_2 = 0.285$ *mA; (b,e)* $A_1 = A_2 = 0.643$ *mA; (c,f)* $A_1 = A_2 = 0.750$ *mA. The input frequencies are* $f_1 = 10$ *MHz and* $f_2 = 15$ *MHz, corresponding to inter-pulse periods* $T_1 = 100$ *ns and* $T_2 = 66.7$ *ns. The ghost frequency is* $f_0 = 5$ *MHz, corresponding to a period* $T_0 = 200$ *ns.*

they are not distributed regularly; the corresponding PDF of the inter-dropout intervals exhibits several peaks. For intermediate values of the modulation amplitude [Fig. 5.9(b,e)], the system shows a well-defined resonance at the ghost frequency, characterized by a single sharp peak of the PDF at the interval $T_r = 200$ ns.

When the modulation amplitude is further increased [Fig. 5.9(c,f)], the peak at the ghost resonance period diminishes and the system shows intensity dropouts at the input frequencies f_1 and f_2. As in the experiment of the previous section the system optimally processes the distributed inputs, for an intermediate modulation amplitude. In that case, the resonance arose exclusively from the interplay between the direct electrical modulation of the pump current and the indirect optical driving coming from the other laser. On the other hand, the ghost resonance arises from the combination of the entrainments of the individual lasers to their respective input frequencies.

In the experimental conditions used, the lasers are detuned such that one of them consistently leads the dynamics, with a time lag equal to the coupling time (Heil *et al*, 2001). The behavior of the system does not change if the input modulations are switched between the leader and laggard lasers. It is remarkable that the distributed signals are processed irrespective of this underlying asymmetry in the coupled dynamics.

The subharmonic resonance presented above can also be observed at the level of the RF-spectrum of the lasers' outputs, as shown in Fig. 5.10. Peaks of the three frequencies involved, the two (higher) input frequencies $f_1 = 10$ MHz and $f_2 = 15$ MHz and the fundamental frequency $f_0 = 5$ MHz, are clearly observed in the spectrum. The height of the peaks at f_1 and f_2 increases monotonically with the modulation amplitude (from top to bottom), while the peak at f_0 is highest at an intermediate amplitude, which is a clear indicator of a resonance occurring at the missing fundamental frequency (Chialvo, 2003).

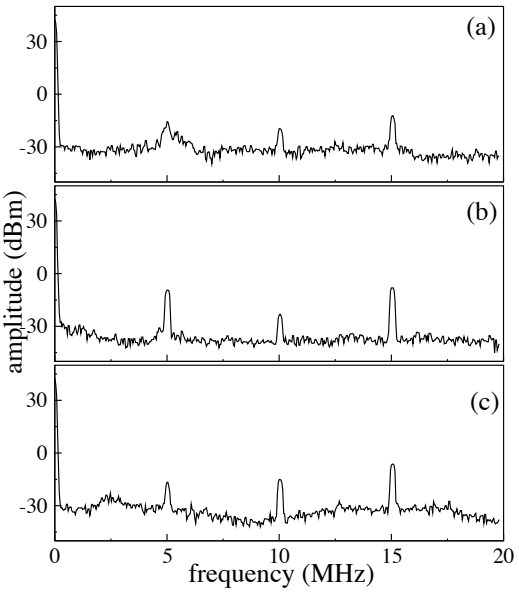

Figure 5.10: *Experimental RF-spectrum of the output intensity of LD1 for increasing values of the modulation amplitude (from top to bottom).*

5.2.4 Inharmonic response

To demonstrate that the previous results do not correspond to a trivial resonance at the difference between f_1 and f_2, we introduce a frequency detuning Δf in both input frequencies, as in previous section. The prediction of Eq. (5.2) indicates again that in this case the resonance frequency increases linearly with the detuning, even though the difference between the input frequencies is still f_0. Experimentally, the detuning is increased from 0.5 MHz to 5 MHz in steps of 0.5 MHz, while the modulation amplitudes are kept constant at $A_1 = A_2 = 0.464$ mA.

Figure 5.11 shows the resulting probability density function or PDF for increasing values of Δf, and the theoretical resonance frequencies predicted by Eq. (5.2), in dashed lines. The PDFs are plotted vertically versus the response frequency f_r (*i.e.*

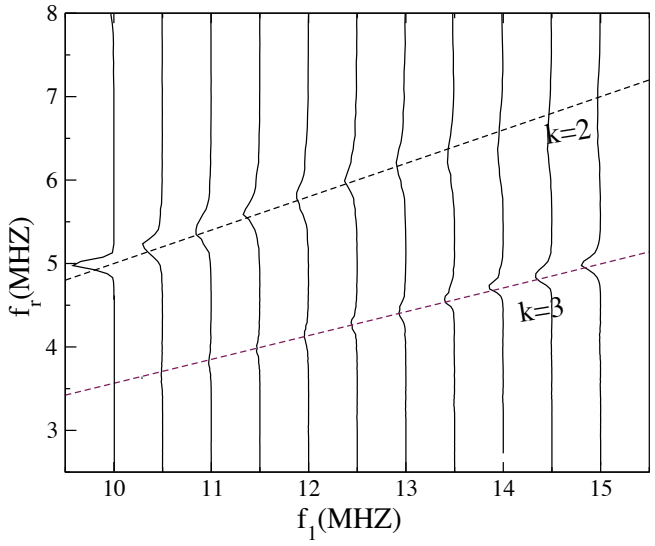

Figure 5.11: *Experimental distribution of response frequencies f_r (vertically) versus the input frequency f_1 (and therefore Δf). The dashed lines correspond to the theoretical resonance frequencies given by Eq. (A.5).*

inverse of the dropout interval), and they are lined up horizontally with respect to the frequency f_1 at which they were obtained. We can observe how the maxima of the experimental PDF, which corresponds to the resonance frequency f_r, shifts with Δf according to the theoretical prediction of Eq. (5.2), therefore demonstrating the existence of a nontrivial ghost resonance.

5.2.5 Numerical simulations

We modeled the phenomena described above with the rate equations given at Sec. 2.1.2. The difference in that model is the addition of a term that accounts for the feedback on each laser:
$\kappa_{j,j}e^{-i\omega_j\tau_{j,j}}E_j(t-\tau_{j,j})$. The feedback term of the field equation is described by two

parameters: the feedback strength $\kappa_{j,j}$ and the external round-trip time $\tau_{j,j}$, which are also assumed equal for the two lasers, and we will use from now one the simplified notation: $\kappa_{1,1} = \kappa_{2,2} = \kappa_f$, and $\tau_{1,1} = \tau_{2,2} = \tau_f$.

We chose parameter values that reproduce the experimental conditions. In particular, the pump currents are $I_{1,2} = I_{1,2}^{\mathrm{DC}}\left[1 + A_{1,2}\sin\left(2\pi f_{1,2}t\right)\right]$, where $I_{1,2}^{\mathrm{DC}}$ are the DC pump currents, $A_{1,2}$ are the modulation amplitudes and $f_{1,2}$ their corresponding frequencies, chosen again following Eq. (5.1). The DC levels are taken to be $I_1^{\mathrm{DC}} = 1.058 \times I_{LD1}^{\mathrm{th}}, I_2^{\mathrm{DC}} = 1.076 \times I_{LD2}^{\mathrm{th}}$.

Figure 5.12 shows the results obtained numerically in the harmonic ($\Delta f = 0$) case, with $f_1 = 10$ MHz and $f_2 = 15$ MHz. For low amplitudes the dropouts are not entrained, while for intermediate amplitudes the response at the missing fundamental frequency increases. For even higher modulation amplitudes, the peak at f_0 diminishes again.

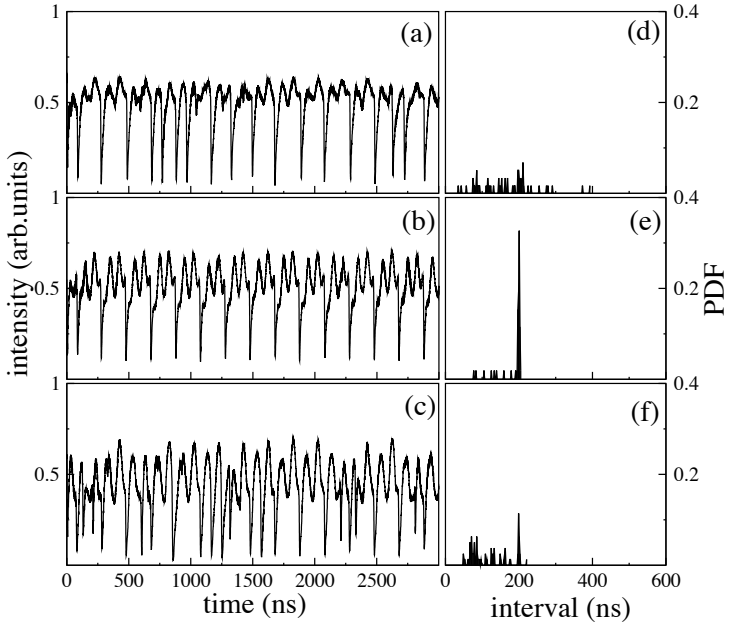

Figure 5.12: *Numerical output intensity of LD1 (left column) and the corresponding probability distribution functions (right column) for increasing values of the modulation amplitude: (a,d)* $A_1 = A_2 = 0.004$*, (b,e)* $A_1 = A_2 = 0.006$ *and (c,f)* $A_1 = A_2 = 0.008$*. The parameters are the same as in the Fig. 5.5 except:* $\kappa_c = 20\ ns^{-1}$*,* $\kappa_f = 10\ ns^{-1}$*, and* $\tau_c = \tau_f = 3.43\ ns$*.*

To emphasize the fact that the response at the missing fundamental frequency is mediated by coupling, we compare in Fig. 5.13 the response of the system with and without coupling. With coupling both lasers are synchronized (panel (a), only one of the lasers is shown), and the system responds at the fundamental period (200 ns). On the other hand, when the lasers are isolated from each other (middle

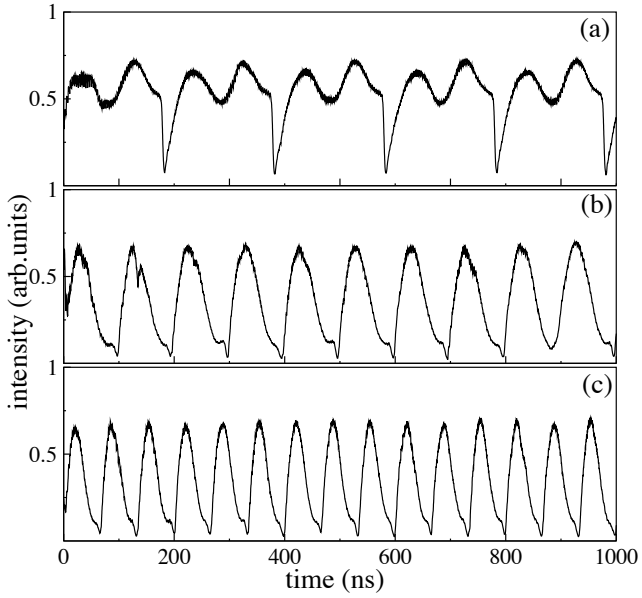

Figure 5.13: *Response of the coupled lasers to the complex harmonic signal (a) compared with the individual responses in the absence of coupling (b,c). Parameters are those of Fig. 5.12(b,e), with $\kappa_c = 0$ in panels (b) and (c).*

and bottom rows) only the corresponding periods of the individual modulations (100 ns and 66.6 ns) are detected. In that case, the external driving leads to a strong periodic component in the laser output, as shown in panels (b) and (c) of Fig. 5.13, which is strongly reduced in the coupled case [Fig. 5.13(a)].

5.2.6 Influence of coupling and feedback strengths

The fact that the lasers have excitable dynamics, even in the absence of coupling (see Sec. 5.2.2), allows us to study the effect of coupling on the signal processing

efficiency. To that end, we fix the amplitude of the input modulation to its optimal level, as obtained above, and maintain a constant level of feedback as well. The response of the system for increasing levels of coupling is shown numerically in Fig. 5.14.

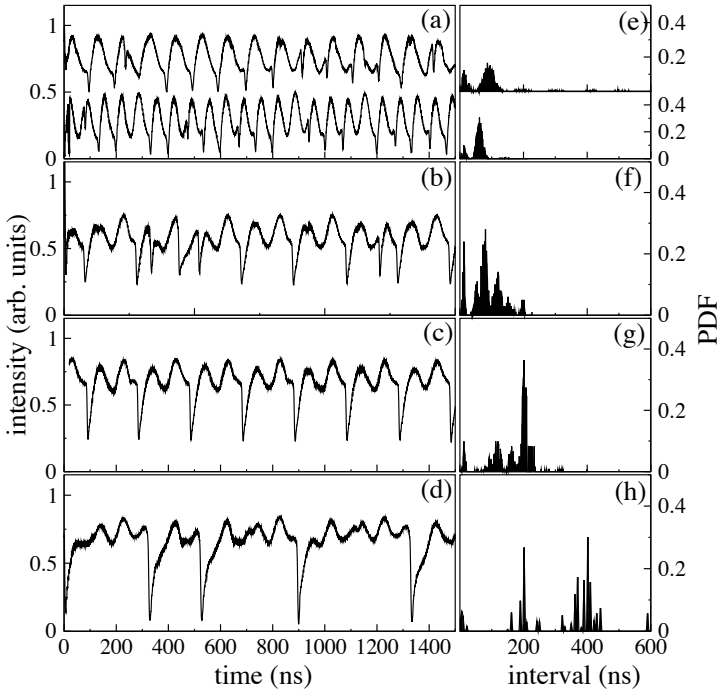

Figure 5.14: *Output intensities and probability distribution function of the time interval between dropouts for increasing coupling strengths: (a,e) $\kappa_c = 0$ ns^{-1}, (b,f) $\kappa_c = 10$ ns^{-1}, (c,g) $\kappa_c = 20$ ns^{-1}, (d,h) $\kappa_c = 40$ ns^{-1}. In panels (a,e) the results corresponding to both lasers are shown; the results for laser 1 (up) have been shifted vertically for clarity. In panels (b-d, f-h) only the output of only one laser is shown, since the lasers are synchronized. Other parameters are those of Fig. 5.12.*

In the absence of coupling the lasers exhibit independent dynamics, each responding to its own input frequency [Fig. 5.14(a)]. As the coupling is increased a response at the ghost frequency (corresponding again to a 200 ns interval between dropouts)

appears, becoming optimal for an intermediate coupling level [Fig. 5.14(c)].

Two features stand out from the results shown in Fig. 5.14. First, synchronization of the lasers is not sufficient to produce a response at the ghost frequency. This is shown, for instance, in Fig. 5.14(b,f), where coupling is strong enough to synchronize the lasers' outputs (and thus only one time trace is shown in the figure), but is not strong enough to produce a ghost response. Second, for very strong coupling the ghost response disappears again [Fig. 5.14(d,h)], because the two lasers behave essentially as a single unit subject to two input modulations (Buldú *et al*, 2003), and the system parameters have been chosen in such a way that the ghost response is not present for a single laser. This leads to a non-monotonic behavior of the system's response with respect to coupling strength, and a need to optimize that parameter in order to observe the phenomenon.

We also analyzed numerically the influence of the feedback strength on the system response, for a coupling strength fixed to the optimal level determined in the previous paragraphs. As shown in Fig. 5.15, the feedback strength also needs to be optimized in order to obtain a response of the system at the ghost frequency. For low feedback levels [Fig. 5.15(a,d)], both lasers respond preferentially to the two input frequencies. It is worth noting that the lasers have already synchronized their dynamics at this point, but nevertheless they cannot process the input signals adequately. As the feedback level increases (identically for the two lasers), a joint response arises at the ghost frequency (corresponding again to a time interval between dropouts of 200 ns). The response is lost once more at high feedback levels, revealing another resonant response of the system, this time with respect to the feedback strength. This non-monotonic behavior is due to the fact that the feedback strength affects the response

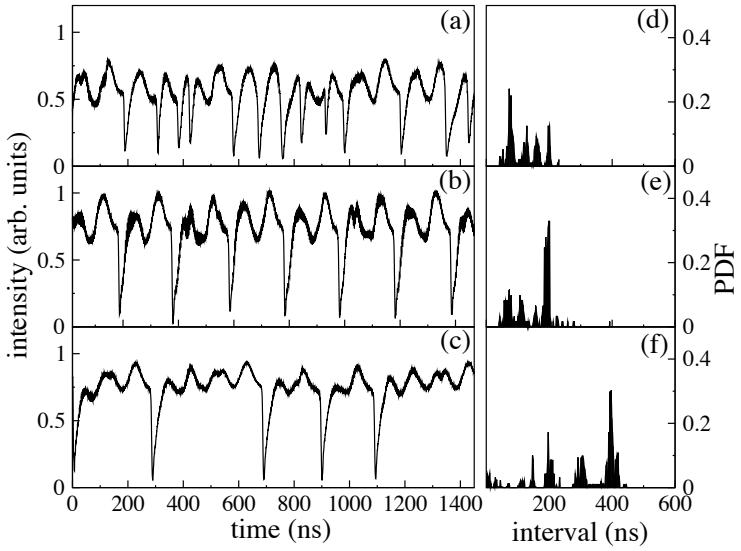

Figure 5.15: *Output intensities and probability distribution function of time interval between dropouts for increasing feedback levels: (a,d) $\kappa_f = 5\ ns^{-1}$, (b,e) $\kappa_f = 10\ ns^{-1}$, (c,f) $\kappa_f = 30\ ns^{-1}$. The lasers are synchronized, so only one time trace is shown. The coupling strength is $\kappa_c = 20\ ns^{-1}$. Other parameters are those of Fig. 5.12.*

of each laser to the external modulation (Sukow and Gauthier, 2000), in such a way that tuning the feedback level varies the sensibility of each laser to a given input frequency range. A ghost response can only arise when the feedback levels are tuned such that the two lasers respond preferentially to the ghost frequency.

Chapter 6

Noise-induced zero-lag synchronization in mutually coupled lasers

Over the last decades, much attention has been paid in the field of the stochastic processes, to the question of how the noise can lead to order (Horsthemke and Lefever, 1984; García-Ojalvo and Sancho, 1999; Lindner *et al*, 2004). In a seminal work, Bryant and Segundo (1976) showed that the introduction of white noise in a neuron model produced an invariance in the firing times. In that study, repeating stimulations of the neuron with the same segment of Gaussian-white noise current was seen to elicit a reproducible inter-spike time response. Another study of the reliability of spike generation in neocortical neurons of rats was made by Mainen and Sejnowski (1995). They showed that for constant stimuli the spike trains were imprecise, whereas the introduction of fluctuations in the stimuli, resembling synaptic

activity, produced spike trains with reproducible timing. In lasers, a good example of the regularity introduced by noise was given by Uchida *et al* (2004), which showed the reproducibility of a laser's response to a noisy drive signal. Specifically, a noisy signal was sent repeatedly to a Nd:YAG microchip laser and after a transient, the system was capable to produce identical response outputs. For small amplitude of the added noise, the outputs are not identical because the internal-noise-driven relaxation oscillations are dominant in the laser output. There is an optimal amplitude of the noise for which the consecutive outputs are identical, because the simultaneous noise-driven signal overcomes the internal noise. For higher amplitudes the outputs lose the ability of produce identical responses.

Another consequence of the introduction of an adequate amplitude of noise is the synchronization of coupled systems. This topic has been studied by Maritan and Banavar (1994), and Toral *et al* (2001) in theoretical works on chaotic systems, Neiman *et al* (1999) in FitzHugh-Nagumo-type neurons, Sánchez *et al* (1997) in chaotic circuits and Zhou and Kurths (2002) in chaotic oscillators. The common feature in all these works is that when a certain amount of noise is introduced in coupled systems, the independent copies are driven to collapse onto the same trajectory.

As we explained in Sec. 2.1.2 of Chapter 2, the isochronal or zero lag synchronous state (without delay) of two mutually coupled semiconductor lasers is unstable. In any case, there are several methods to obtain zero-lag synchronization in coupled lasers. Recently, zero-lag synchronization was found in two mutually delay-coupled semiconductor lasers, adding to each laser self-feedback matched to the coupling delay time (Klein *et al*, 2006). Fischer *et al* achieved isochronous synchronization between two delay-coupled semiconductor lasers by relaying the dynamics via a third

mediator laser (Fischer *et al*, 2006) or a mirror (Vicente *et al*, 2007). Roy *et al* made a numerical study to achieve stable isochronal synchrony between two mutually delay-coupled oscillators through the use of a third dynamical system (Zhou and Roy, 2007). Here we study the possibility of achieving the isochronal solution in a symmetrical bidirectionally coupled semiconductor laser system, by applying a common source of external noise to the pump current of both lasers. Departing from the synchronized state of two mutually coupled lasers, with a well defined leader-laggard configuration, we introduce the same noise in the two lasers' pump currents. For large enough noise intensity, the system reaches a common output without lag between them, stabilizing the isochronal solution.

6.1 Experimental configuration

Our experimental setup consists of two parameter-matched AlGaInP index-guided and multi-quantum well semiconductor lasers (Sharp GHO6510B2A) mutually coupled in a symmetrical way (Fig. 6.1). Both lasers operate in a nominal wavelength

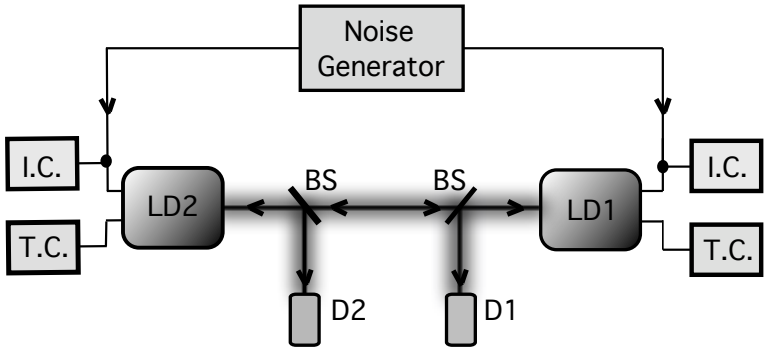

Figure 6.1: *Experimental setup. LD: laser diodes, BS: beamsplitters, D: detectors, and I.C, T.C: current and temperature controllers.*

$\lambda_n = 654$ nm. The temperature and pump current of the lasers are controlled with an accuracy of ± 0.001°C and ± 0.01 mA, respectively, and are adjusted such that the optical frequencies of LD1 and LD2 (in isolation) are as similar as possible to each other. For temperatures $T_{\mathrm{LD1}} = 21.961$°C and $T_{\mathrm{LD2}} = 25.840$°C, the threshold currents of the solitary lasers are, respectively, $I^{\mathrm{th}}_{\mathrm{LD1}} = 31.32$ mA and $I^{\mathrm{th}}_{\mathrm{LD2}} = 30.79$ mA.

The coupling path is $\tau_{1,2} = \tau_{2,1} = \tau_c = 3$ ns. The laser outputs are sent simultaneously to a 4 GHz oscilloscope (Tektronix CSA7404), and to an optical spectrum analyzer (Ando AQ6317B). We add external noise simultaneously to the pump currents of both lasers, with a variable intensity from -140 dBm/Hz to -110 dBm/Hz. The frequency bandwidth of the noise ranges from 50 to 400 MHz.

Symmetric mutual coupling was ensured by the injection of a well-controlled amount of the light emitted by each laser into the other. First we adjust the temperatures of the lasers to approach as much as possible their optical spectra [Fig. 6.2(a) and (b)], in order to optimize the mutual injection. With these values of temperature we optimize the pump currents and the bidirectional alignment by looking for the maximum enhancement of the output power for mutual injection when the lasers are near threshold. When each laser is near its own threshold, we observe an enhancement of 60% with respect to the solitary output power when the mutual injection takes place. We fix the pump currents to $I_1 = 1.05 I_{th_1}$ for LD1 and $I_1 = 1.02 I_{th_2}$ for LD2, where I_{th_1} and I_{th_2} are their respective solitary thresholds. Figure 6.2(c,d) shows the optical spectra in the presence of mutual coupling for LD1 and LD2. Both spectra have a strongly multimode behavior, typical of working close to threshold. In this condition, the lasers operate in the LFF regime. The reason to work on this regime is the easy observation and measurement of the isochrony

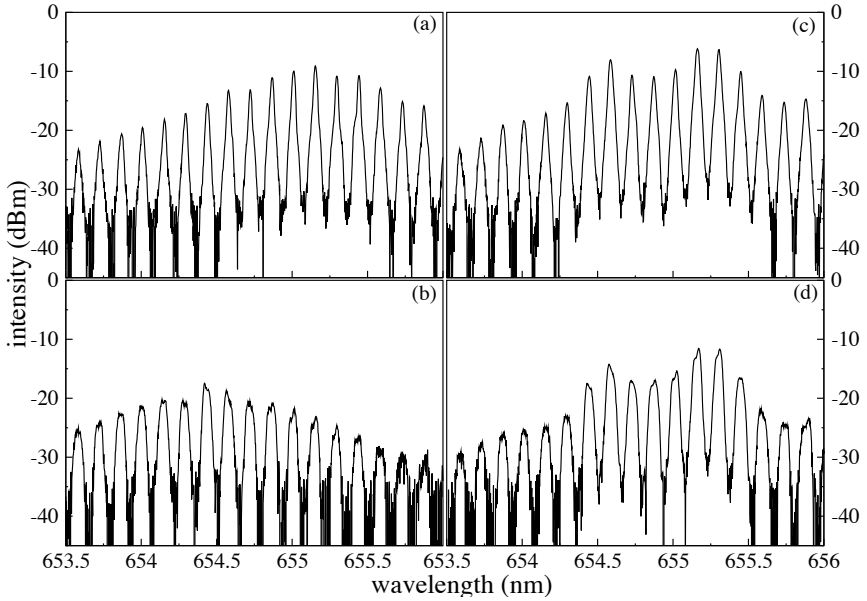

Figure 6.2: *Optical spectra for the solitary lasers: (a) LD1, (b) LD2, and (c,d) after mutual coupling for each laser respectively (in absence of external noise).*

during the experiments.

With the system symmetrically injected, we introduce the same noise source simultaneously to the pump current of the two lasers through the internal bias-T of the laser mounts. The noise is superimposed to the DC operating level set by the current controller. The mount has a low frequency cut-off around 200 KHz and a nominal high frequency cutoff at 500 MHz. From 500 MHz to 1 GHz the mount does not have a flat response in frequency. The response depends on the operation point and has a wavy profile. The specifications of the noise generator give a bandwidth of 400 MHz, but when we increase the amplitude of the noise it is possible to have an increased frequency range. We introduce the noise simultaneously to each mount and vary the amplitude of the noise from -140 dBm/Hz to -110 dBm/Hz, changing the amplitude in steps of -10 dBm/Hz. Figure 6.3 displays the output

intensities and the corresponding cross correlation functions for different values of

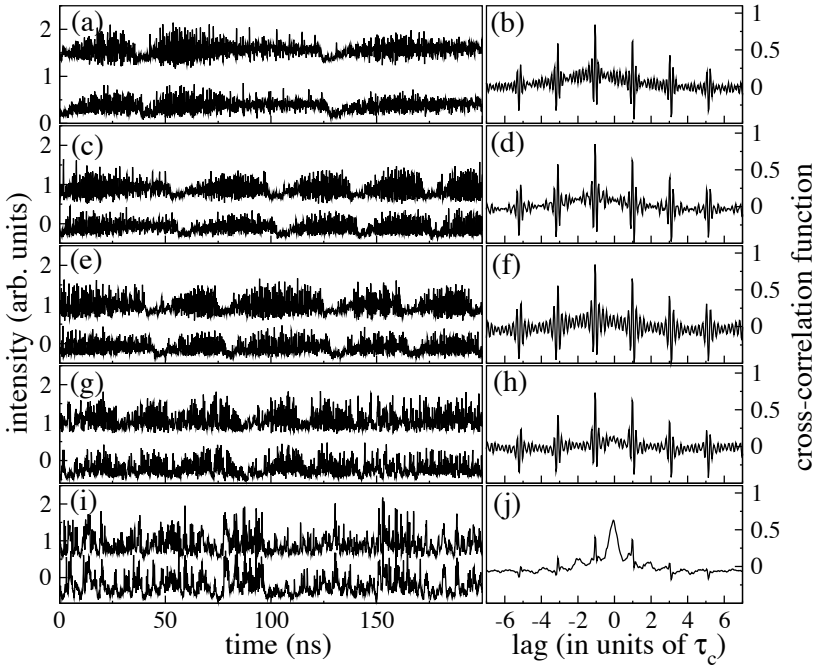

Figure 6.3: *Experimental output intensities and corresponding cross correlation functions for different values of injected noise level: (a,b)* 0 *dBm/Hz, (c,d)* -140 *dBm/Hz, (e,f)* -130 *dBm/Hz, (g,h)* -120 *dBm/Hz, (i,j)* -110 *dBm/Hz.*

the noise level. The output intensities are displaced vertically for clarity, with the top trace representing the output of LD1 and the bottom trace representing LD2. In Fig. 6.3(a) to (i) we can observe how the noise affects the synchronization level in the output intensities of the lasers. Without noise [Fig. 6.3(a,b)] LFF dynamics can be observed in the output intensities, and the correspondent cross-correlation function shows a maximum at $\tau_c = -3$ ns. The LFF dynamics starts to disappear in Fig. 6.3(g), but the cross-correlation still shows a maximum peak at τ_c. Finally for a noise level of -110 dBm/Hz [Fig. 6.3(j)] a correlation peak arises at zero lag. In this case, the cross-correlation of the signals shows a broadening of its maximum

peak due to the loss of fast dynamics in the output intensities (see Sec. 6.2). These results show that noise induces zero-lag synchronization in mutually coupled lasers.

6.2 Numerical simulations

In order to establish the nature of the broadening of the maximum correlation peak in the regime of noise-induced zero-lag synchronization [Fig. 6.3(i,j)], we perform a numerical modeling of the system. Our model is based on the Lang-Kobayashi description of a single semiconductor laser with optical feedback (Lang and Kobayashi, 1980), generalized to account for bidirectional coupling between two lasers (Mulet *et al*, 2002), as explained in Sec. 2.1.2. We take the feedback strengths as 0 to model two bidirectionally coupled lasers without feedback. We can simplify the notation because, in this case, we consider the coupling strength equal in both directions $\kappa_{1,2} = \kappa_{2,1} = \kappa_c$, and we have a unique optical path in the setup, so that $\tau_{1,2} = \tau_{2,1} = \tau_c$.

External noise, represented by the term $\xi(t)$, is added to the first term of the carrier density equation [Eq. (2.4)] as: $C_j[1 + \xi(t)]$ which is taken to be a time-correlated noise of the Ornstein-Uhlenbeck type, Gaussianly distributed with zero mean and correlation:

$$\langle \xi(t)\xi(t') \rangle = \frac{D}{t_c} e^{-(t-t')/t_c} \tag{6.1}$$

with D being the strength of the noise and t_c its correlation time. The variance of the noise is given by D/t_c, and hence we will measure its amplitude as:

$$\sigma = \sqrt{D/t_c} \tag{6.2}$$

We set $\alpha = 3.5$, $\tau_c = 3$ ns, $\Delta\omega_{12} = -2.8$ GHz, and $t_c = 800$ ps. The rest of the parameter values are given in Table A.1 of Appendix A. The correlation time of the noise is fixed to the frequency cut-off of the laser mount (500 MHz). White noise is not a good assumption in this case. The reason is that the carrier dynamics can not follow the fast frequencies of the external noise, and the noise intensity of a white noise needs to be very large in order to have some influence (Toral *et al*, 2001).

The effect of the external noise in the system can be understood by examining the mechanism of the power dropouts in the LFF regime, in the framework of the Lang-Kobayashi model. In this context, a fluctuation can take the system away from the basin of attraction of the stable fixed point and produce a dropout event. In the case of mutual coupling this occurs at different times for each laser, due to the time needed by the light to travel between them. The result is a synchronized state with two output intensities whose dropout events are displaced a time equal to τ_c in a leader-laggard dynamics.

The experiments described above show that common external noise stabilizes the isochronal synchronized state. As in the experiments, we chose mutual symmetrical coupling, and with a fixed noise correlation time, we vary the intensity of the added noise. In Fig. 6.4, left column, we show the numerical output intensities filtered at 1.5 GHz, with a low pass 4th order Butterworth filter, to simulate the experimental conditions. As in the experimental results, the output intensities are shifted vertically for clarity. The top traces show the output intensities for LD1 and the bottom traces those of LD2. Figure 6.4 (right) shows the corresponding cross-correlation function of this filtered series for different strengths of the noise. In Fig. 6.4(a,b) the synchronized system shows a correlation peak at $\tau_c = 3$ ns in the absence of noise,

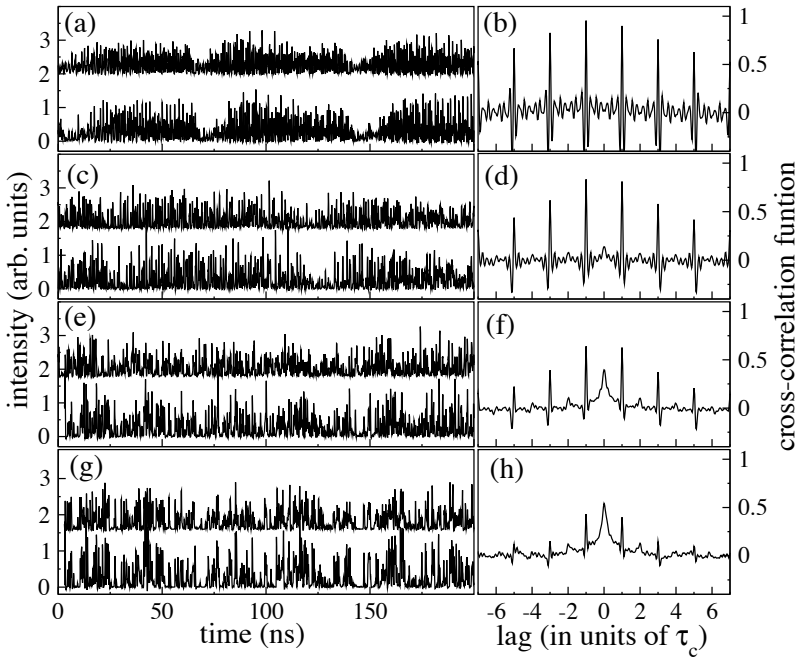

Figure 6.4: *Numerical output intensities and corresponding cross correlation functions for increasing values of the external-noise strength D: (a,b) 0 ps, (c,d) 1 ps, (e,f) 4 ps, and (g,h) 8 ps.*

with output intensities in LFF regime. As we increase the amplitude of the noise in Fig. 6.4(c,d) the dynamics changes but the cross correlation does not change the location of the peak. Only with an amplitude of 4 ps in Fig. 6.4(e,f), we can observe the appearance of a peak at 0 ns in the cross-correlation function, which becomes maximum at 8 ps [Fig. 6.4(g,h)].

To estimate the approximate value of the noise correlation time, we consider first the maximum value of the bandwidth specified by the datasheet of the laser mount (500 MHz). As we explained before, this value is higher than the specifications of the noise generator (note that there is an increase in the frequency cut-off of the noise generator due to the change of amplitude of the noise). For an Ornstein-

Uhlenbeck noise the correlation time is the inverse of the frequency cut-off. This value corresponds to an approximate correlation time of 2 ns. With that correlation time value fixed, we vary the noise strength to find the optimal amplitude of the noise ($\sigma = 0.1$). For this value we observe a peak of the cross-correlation showing the zero lag solution, but the shape is broader (with respect to the background) than the one observed experimentally. Once we find the value of the amplitude, we can vary the correlation time until the cross-correlation function matches the one obtained experimentally.

Figure 6.5 shows these results, plotting in the top trace the cross-correlation function observed experimentally. The bottom trace shows the calculated cross-correlation function for the maximum bandwidth of the mount (500 MHz according to the datasheet).

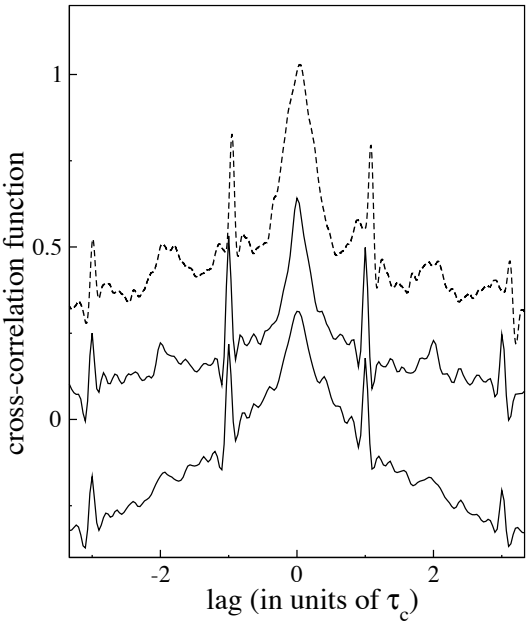

Figure 6.5: *Cross-correlation functions corresponding to experimental data (top), and numerical observations with $t_c = 0.8$ ns (center), and $t_c = 2$ ns (bottom).*

Taking this value for an ideal Lorenzian transform function we estimated the noise parameters as: $\sigma = 0.1$, $t_c = 2000$ ps, and $D = 20$ ps [Fig. 6.5 (bottom)]. Finally, the middle trace of Fig. 6.5 shows the cross-correlation that matches the experimental data (and corresponds to noise parameters $\sigma = 0.1$, $t_c = 800$ ps, and $D = 8$ ps). The optimal value of the correlation time corresponds to a 1.25 GHz of bandwidth, and thus we use this value ($t_c = 800$ ps) for the calculations.

We now inspect in detail the output intensities of Fig. 6.4(h), for which we obtain the drift to zero lag in the cross-correlation peak. To that end we generate numerically the filtered and unfiltered signals for the corresponding values of the noise amplitude ($\sigma = 0.1$, $t_c = 800$ ps, and $D = 8$ ps). Figure 6.6(a) represents the filtered signals and Fig. 6.6(b) shows the unfiltered signals.

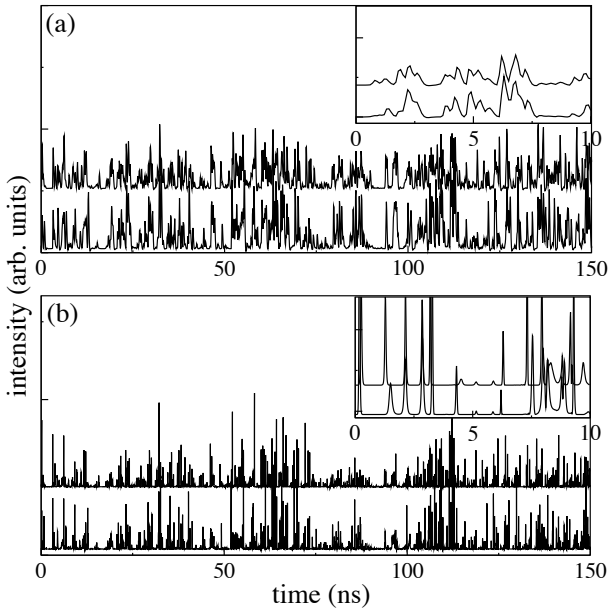

Figure 6.6: *(a) Numerical filtered and (b) unfiltered output intensities for both lasers for $D = 8$ ps and $t_c = 800$ ps. The insets shows a detail of the series.*

The figure shows that although the filtered time series exhibits synchronization at zero lag (see inset), isochrony is absent in the unfiltered time series.

This difference is clear if we represent the cross-correlation functions for both kind of signals, filtered (Fig. 6.7, top traces) and unfiltered (Fig. 6.7, bottom traces), changing the noise strength, but keeping constant the correlation time. For low noise levels ($D = 0$ ps and $D = 1$ ps) the cross-correlation for unfiltered signals shows a peak at τ_c, as the filtered one [Fig. 6.7(a,b)], denoting the existence of a well-defined leader in the dynamics. As we increase the noise level [Fig. 6.7(c),

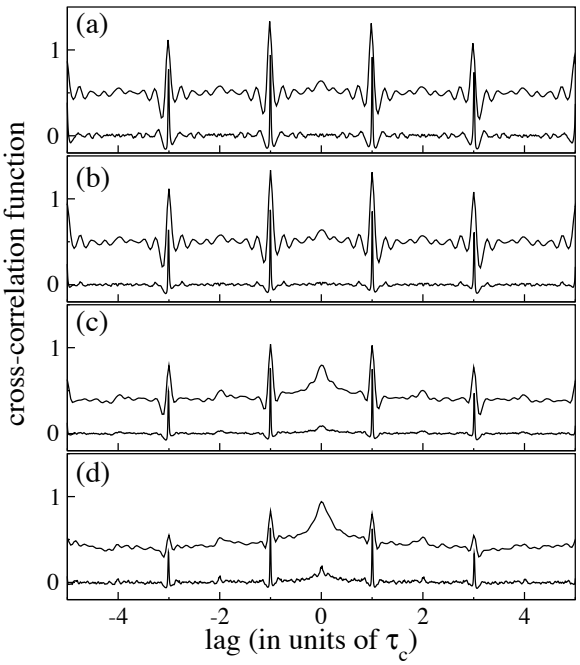

Figure 6.7: *Cross-correlation functions corresponding to output numerical intensities with different noise strengths D, for filtered (top) and unfiltered (bottom) signals. (a) 0 ps (b) 1 ps (c) 4 ps, and (d) 8 ps (t_c=800 ps).*

$D = 4$ ps] differences between the two cross-correlation functions become stronger. The one corresponding to filtered signals shows a growing peak at 0 ns, denoting the emergence of the isochronal solution, but the cross-correlation corresponding to

unfiltered signals does not show this peak [Fig. 6.7(d), $D = 8$ ps].

The difference between both types of correlations shows that the noise acts only in the slow dynamics of the system for these values of the parameters. The correlation time of the noise plays an important role on the dynamics of chaotic lasers (Buldú *et al*, 2001). If we ignore bandwidth limitations in our experimental system, we can simulate the output intensities for different noise correlation times and compare the cross-correlation functions for filtered and unfiltered signals, to find a value that shows isochrony for both kinds of signals. Figure 6.8 displays both cross-correlation functions for changing correlation times at constant amplitude of the

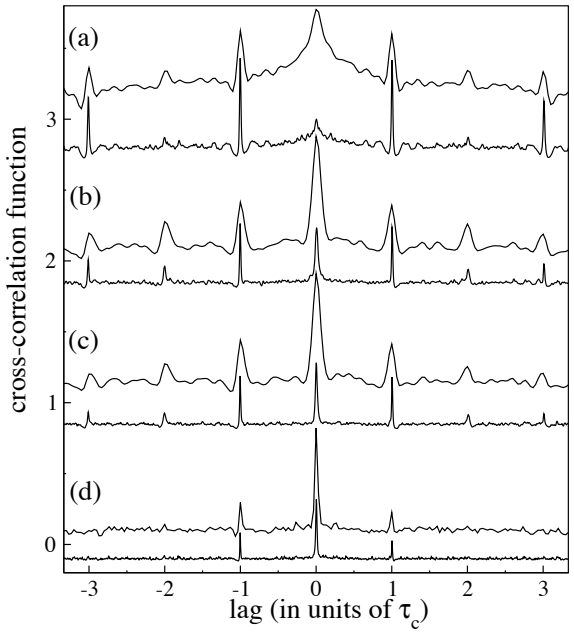

Figure 6.8: *Cross-correlations functions for filtered (top) and unfiltered (bottom) signals for $D = 8$ ps for different values of noise correlation time: (a) $t_c = 800$ ps, (b) $t_c = 100$ ps, (c) $t_c = 10$ ps, and (d) $t_c = 0.01$ ps.*

introduced noise. The top traces show the cross-correlation function for filtered

signals, and the bottom traces the corresponding function for the unfiltered signals. Figure 6.8(a) shows again the results for $t_c = 800$ ps, for which there is a large difference between the filtered and unfiltered cross-correlation, but with a good match with the experimental results. Figure 6.8(b) represents the cross-correlation function for $t_c = 100$ ps. For even smaller t_c, [Fig. 6.8(c)], both cross-correlation functions have some similarities, but it is in Fig. 6.8(d), with $t_c = 0.01$ ps, *i.e.* an almost white noise, that both cross-correlations show the same behavior. This confirms that the non-zero correlation time of the noise is the cause of the differences between both types of cross-correlations. For high correlation time of the noise, the system only reacts to the fluctuations in its slow dynamics, whereas in the limit of very low noise correlation time both dynamics can respond, for the same noise strength.

Chapter 7

Synchronization via clustering in a small delay-coupled laser network

It is important to understand how a system of coupled oscillators synchronizes when the delays in the interactions are different for the different oscillators. Non-uniform, distributed time delays arise naturally in coupled systems, and several authors have reported that they can have a stabilizing effect (Atay, 2003; Huber and Tsimring, 2005; Eurich *et al*, 2005; Masoller and Marti, 2005). Here we study the influence of non-uniform coupling strengths and non-uniform delay times on the onset of synchronization in an experimental system consisting of three semiconductor lasers mutually coupled through an external mirror. Our results show that synchronization arises via the formation of two-laser clusters. This observation is in good agreement with a simple theoretical model. Clustering has been studied theoretically (Nakamura *et al*, 1994; Manrubia and Mikhailov, 1999; Park *et al*, 1999) and experimentally (Wang *et al*, 2000; Otsuka *et al*, 2003; Tanguy *et al*, 2006) in large ensembles of

coupled oscillators. Recently, Rogister and Roy (Rogister and Roy, 2007) studied a square array of lasers (50×50) with homogeneous local coupling, finding that the synchronization of the lasers of the array resulted in localized excitations, wandering along well-defined trajectories. The experimental system presented here could allow for a systematic analysis of the emergence of such behavior in a simpler small array.

7.1 Experimental setup

A schematic diagram of the experimental setup is displayed in Fig. 7.1. Three semiconductor lasers (LD1, LD2, and LD3, AlGaInP index-guided and multi-quantum well devices, Sharp GHO65010B2A) are mutually coupled through their lasing fields via an external mirror (M), which supplies optical feedback to each laser.

The lasers have a nominal wavelength of 654 nm when operating in isolation. The temperature and pump current of the lasers are controlled with an accuracy of $\pm 0.01^{\circ}$C and ± 0.1 mA, respectively. At temperatures $T_{\mathrm{LD1}} = 19.76^{\circ}$C, $T_{\mathrm{LD2}} = 18.53^{\circ}C$, and $T_{\mathrm{LD3}} = 18.32^{\circ}$C, the threshold currents of the lasers (when isolated) are $I^{\mathrm{th}}_{\mathrm{LD1}} = 31.96$ mA, $I^{\mathrm{th}}_{\mathrm{LD2}} = 29.87$ mA, and $I^{\mathrm{th}}_{\mathrm{LD3}} = 31.10$ mA. The operating currents are set to $I_{\mathrm{LD1}} = 32.77$ mA, $I_{\mathrm{LD2}} = 30.00$ mA, and $I_{\mathrm{LD3}} = 32.10$ mA. The operating conditions are slightly different because the temperature and the injection currents of the lasers are adjusted to match their optical frequencies as closely as possible, in order to have the strongest mutual optical coupling.

The detection of the laser outputs is achieved by fast photodetectors of 1 GHz bandwidth (Thorlabs DET210).The received signal is sent simultaneously to a 1 GHz oscilloscope (DS06104A Agilent), and to an spectrum analyzer (Anritsu MS2651B)

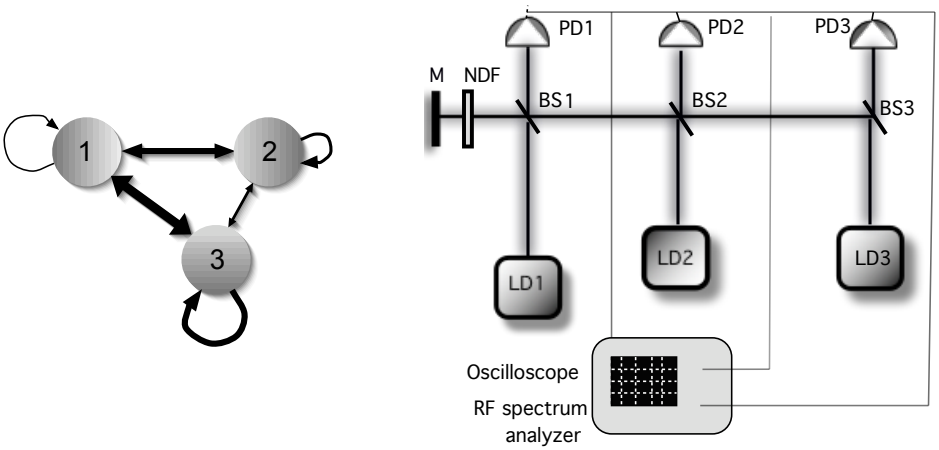

Figure 7.1: *Left, scheme of the network studied. Note the different length and weight of the links. Right, experimental setup: LD, laser diodes; BS, beamsplitters; M, mirror; NDF, neutral density filter; PD, photodetectors.*

via two amplifiers (2 GHz, Femto high-speed amplifier). We note that the two input channels of the oscilloscope allow the detection of only two laser outputs simultaneously.

We study how the synchronization is lost as coupling through the neutral density filter (NDF) decreases. In order to characterize the system, we first examine the individual dynamics of each laser. In a second part we study the effect of a the decrease of the injection in each pair of mutually coupled lasers. Finally, we study how the synchronization is lost in the total array.

Three beam splitters with 50% transmittance (BS1, BS2 and BS3) couple the lasers to each other through the common reflected light of the external mirror. This external mirror also supplies the feedback of each laser. Figure 7.2 shows the detail of the feedback path of the light for each laser diode. The feedback conditions are different, due to the heterogeneous geometry of the setup. It can be noticed that the

light fed back into laser LD1 passes only one beam-splitter (BS1), while the light

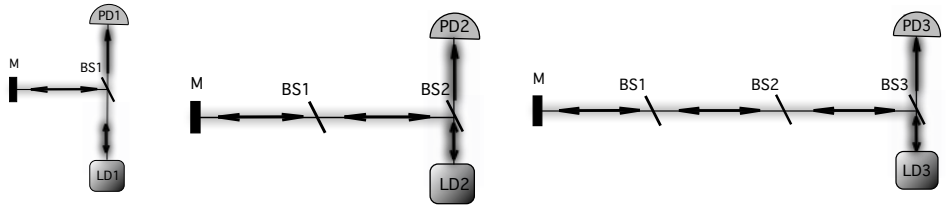

Figure 7.2: *Detailed feedback path for: LD1, left, LD2, center, and LD3, right.*

fed back into laser LD2 (LD3) passes two (three) beam splitters.

The feedback delay times are different for each laser as well, and we note that the laser with the strongest feedback is LD1 while the laser with larger feedback time is LD3. In this geometrical arrangement the feedback delay times are $\tau_{1,1} = 5.43$ ns, $\tau_{2,2} = 4.8$ ns, and $\tau_{3,3} = 7.3$ ns.

To quantify the effect of feedback in each laser due to the interaction between the fields, we calculate the threshold reduction for each one, in the absence of NDF and coupling. The reduction is 4.90% for LD1, 4.5% for LD2 and 3.90% for LD3. Each laser operates, in the absence of coupling with the other two, in the low-frequency fluctuation (LFF) regime, induced by its own optical feedback from the external mirror. The laser intensities and the RF spectra are displayed in Fig. 7.3. The mean time interval between dropouts is approximately $T_{LD1} \sim 170$ ns, $T_{LD2} \sim 65$ ns and $T_{LD3} \sim 85$ ns for LD1, LD2 and LD3 respectively. The frequency of the dropouts is different for each laser, because their operating and feedback conditions vary among the three lasers.

If we consider the laser diodes coupled by pairs in the setup of Fig 7.1, blocking in each case the third laser, we have two bidirectionally coupled lasers, both with

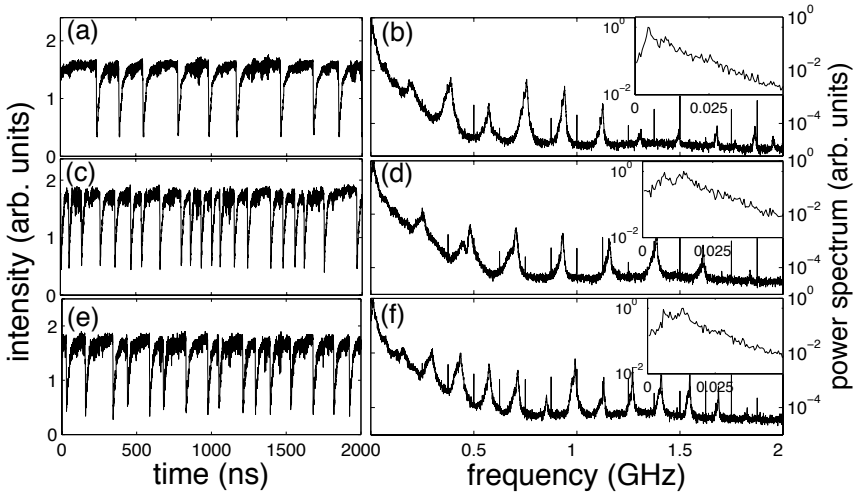

Figure 7.3: *LFF dynamics in the absence of coupling: LD1 (a,b), LD2 (c,d) and LD3 (e,f). Left column: experimentally observed intensities; right column: experimental RF-spectra. The insets display the low-frequency peak.*

feedback. Figure 7.4 shows how the mirror provides mutual coupling between two of the lasers. We take LD1 coupled with LD2 to explain how the light coming from each laser is divided by the two beamsplitters. One part of the light emitted by LD1 is fed back again to the laser and another part is injected to LD2 through the

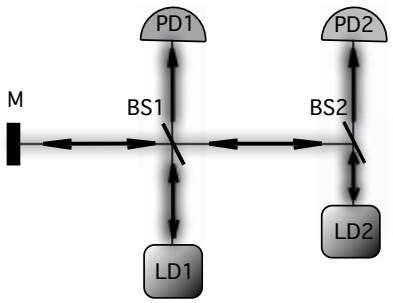

Figure 7.4: *Detailed path of the light in the mutual injection of two of the lasers of the array.*

reflection in the mirror, and vice-versa. It can be noticed that the delay times for the feedback are different in both lasers, whereas the flight times between the two lasers are equal. The flight times (coupling times) between the laser pairs are: $\tau_{1,2}$ = 5.06 ns, $\tau_{1,3}$ = 6.4 ns, and $\tau_{2,3}$ = 6.03 ns.

Blocking the light coming from one of the three lasers of the array, we can consider the other two lasers mutually coupled as in Fig. 7.4, and observe the mutual coupling between only those two lasers. To quantify the effect of the mutual coupling in each laser pair, we calculate the threshold reduction for each one, in the absence of NDF, due to injection of the light coming from the other laser and its own feedback. For the pair corresponding to LD1 mutually coupled with LD2, both with feedbacks, we have a threshold reduction of 3.5% for LD1 and a 3.8% for LD2. For the LD1-LD3 pair we have a threshold reduction of 3.1% for LD1 and a 3.3% for LD3. And finally, for the LD2-LD3 pair we have a reduction of 2.8% for LD2 and a 3% for LD3.

Decreasing the total injected light coming from the mirror, we observe a loss of synchronization. Synchronous behavior will be defined in terms of the mutual occurrence of power dropouts, which act as low-frequency markers of the lasers' dynamics.

Figure 7.5 compares the dynamics of each pair of mutually coupled lasers. The left column of each plot represents the output intensities for a decreasing amount of total injected light (from top to bottom), and the right column shows the respective histograms of inter-dropout intervals. The top left plot represents LD1 and LD2 under mutual coupling, the top right represents LD1 and LD3, and the bottom plot shows the dynamics of LD2 and LD3. In all cases both lasers have optical feedback. From the synchronized state of each of the laser pairs, represented at the first row of

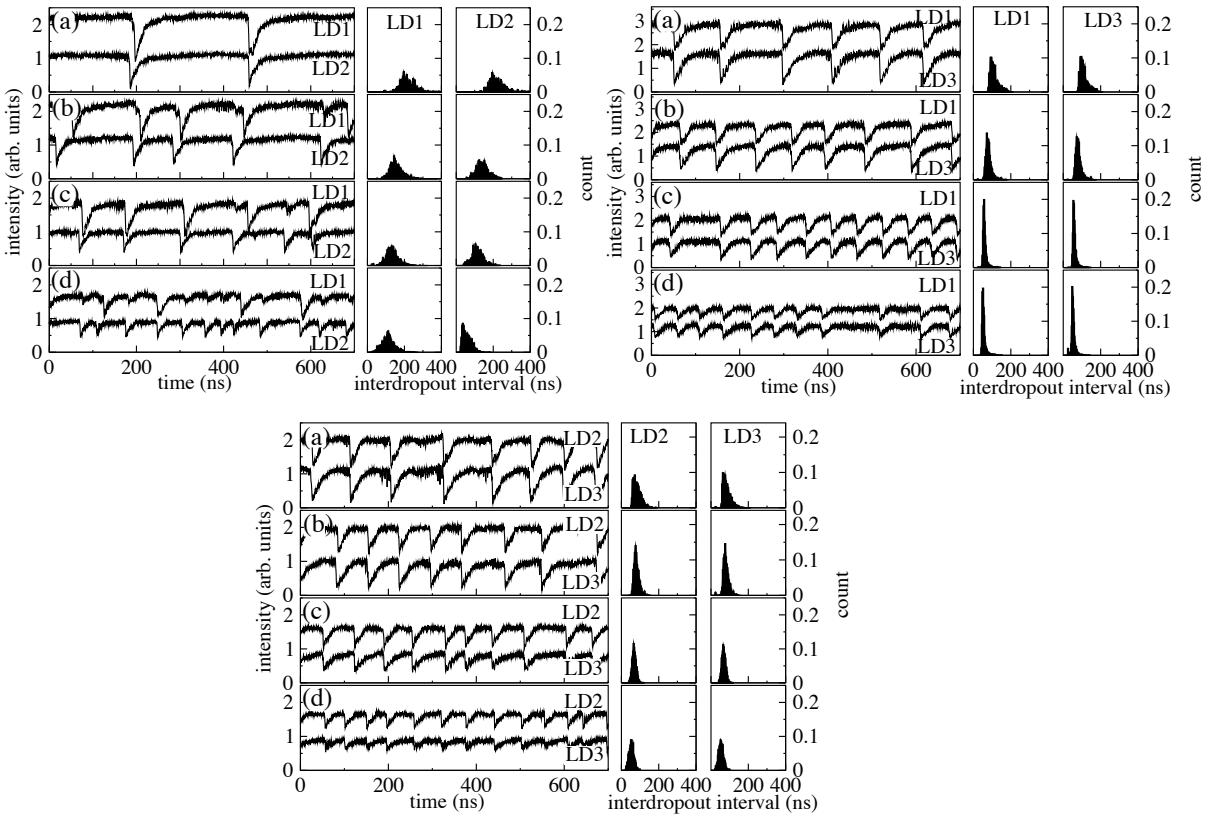

Figure 7.5: *Output intensities for lasers mutually coupled in pairs (left panels), and inter-dropout time interval histograms (right panels), for decreasing values of total light injection (transmittivity of NDF). Signals have been displaced vertically for clarity. Values in each plot: (a) 100%, (b) 70%, (c) 63%, and (d) 50% of transmittivity.*

each plot, we decrease the injected light by changing the transmittivity of the neutral density filter. It is clearly shown that LD1 and LD2 lose their synchronization when we decrease the total injected light at 50% of its initial level. If we compare the loss of synchronization of LD1-LD2 pair with the LD1-LD3 pair, in the latter we do not observe any loss of synchronization for these values of decreasing transmittivity (Fig. 7.5 top right). The same situation is observed when we consider the LD2-LD3 pair: the decrease of the total injected light does not destroy the synchronization of

that laser pair. In all three cases a decrease in the injected light produces a decrease in the mean time period of the dropouts, due to the reduction of the coupling and feedback strengths. These results show that the LD1-LD2 synchronized state is less strong than the other two pairs, when we consider each pair separately.

When a third laser is added to the system, we have three globally coupled semiconductor lasers with feedback. We now examine how synchronization is lost in this system as the optical coupling between the lasers decreases. When the three lasers are coupled, the threshold current of each one is decreased due to the injection light of the other two by 3% for LD1, 3.90% for LD2 and 3.70% for LD3.

The coupling strength is controlled by the neutral density filter located in front of the mirror. In the absence of the NFD the system is synchronized, and all three lasers adjust their dynamics to drop out together [Fig. 7.6, left plot]. When we decrease the transmitted light through the neutral density filter, a clustering dynamics arises, in which only two of the lasers synchronize their dropouts, while the third laser drops independently of the other two [Fig. 7.6, right plot]. It has to be reminded that the output intensity of the three lasers must be recorded in pairs due to constraints in the number of simultaneous channels of the oscilloscope. The left columns of the two plots in Fig. 7.6 show the output intensities for each pair of lasers and the right columns show the corresponding detailed RF spectrum at low frequencies, which reveals the mean period of the dropout events. When the filter absorbs 40% of the incident light [Fig. 7.6, right plot], the coupling is weaker and a clustering state arises: LD1 and LD3, synchronize their dropouts (second row), while laser LD2 drops independently of the other two (first and third row).

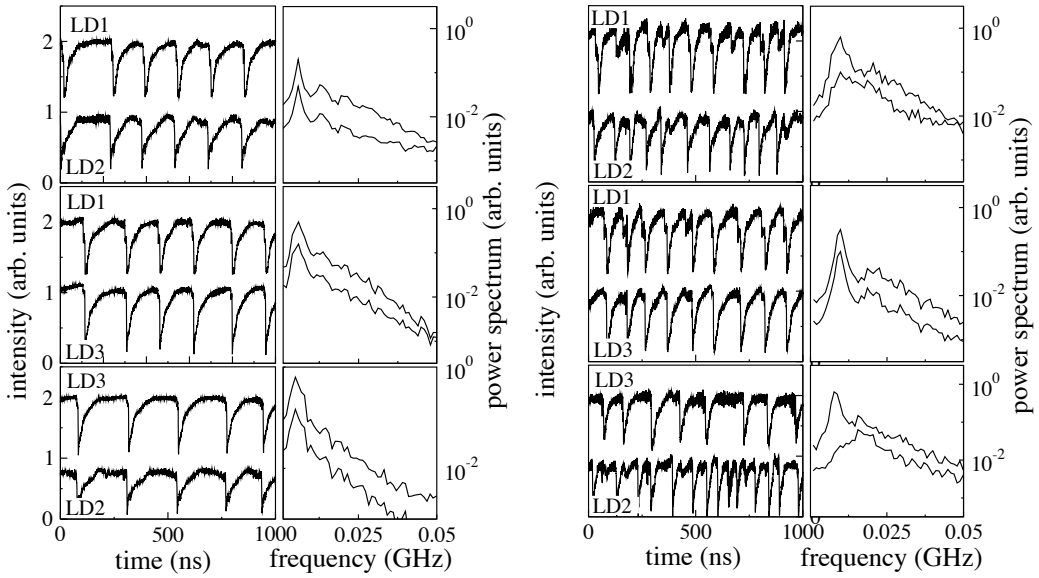

Figure 7.6: *Dynamics in the synchronized (left plot) and clustering (right plot) regimes. In each plot the left column shows the experimentally observed intensities; and the right column shows a detail of the corresponding power spectrum for LD1 and LD2 (top), LD1 and LD3 (center) and LD2 and LD3 (bottom). The different laser pairs are not monitored simultaneously.*

Figure 7.7 provides insight into how synchronization develops in the frequency domain, by depicting the RF-spectra of the synchronization (left column) and clustered states (right column). The synchronized lasers show a substantial overlap in the whole RF-frequency spectrum, not only at low frequencies (inset). In Fig. 7.7(a,c,e) one can see the coincidence of almost all the higher harmonic peaks of the spectrum. Figure 7.7(b,d,f) represents the clustered state for lower coupling. Figure 7.7(d) shows the locking of almost all frequency peaks in their spectra, specially the lowest frequency peak corresponding to the low-frequency fluctuations (figure inset). Clearly, the clustered pair is formed by LD1 and LD3. This contrasts with what happens with LD2 [Fig. 7.7(b,f)], where the overlapping is very poor, particularly

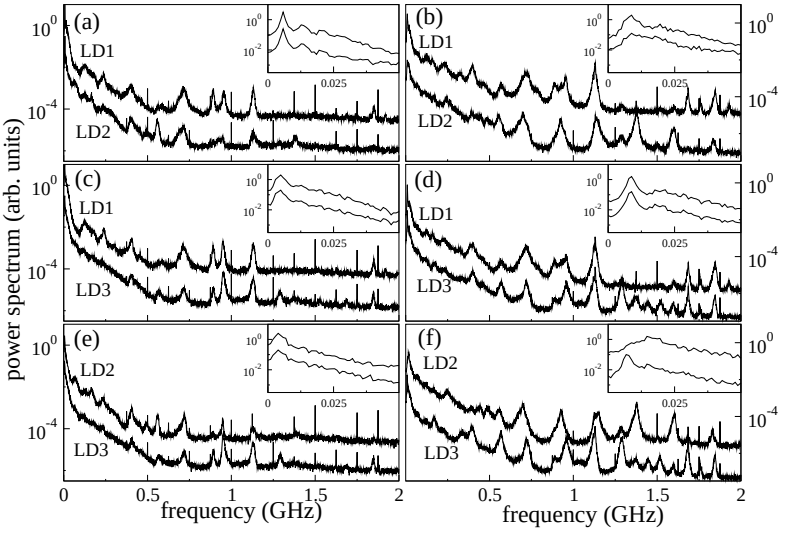

Figure 7.7: *Experimental RF-spectra in the synchronized state (left column) and in the clustered state (right column). (a,b) LD1 and LD2; (c,d) LD1 and LD3; (e,f) LD2 and LD3. The insets display the low-frequency peak.*

at the LFF peak (inset).

The choice of lasers integrating the cluster depends on the coupling strengths in the network. In another experiment (with different working temperatures and intensities), with the same setup (same distances) but with an additional fixed neutral density filter (NDF2: 70% of transmittivity) located between LD1 and BS1, diminishing the injection and feedback strengths of LD1, the cluster was formed by LD1 and LD2.

With this new setup (Fig. 7.8) we proceed in the same way as in the last experiment. Under temperatures of $T_{LD1} = 19.76^o$C, $T_{LD2} = 18.29^oC$, and $T_{LD3} =$

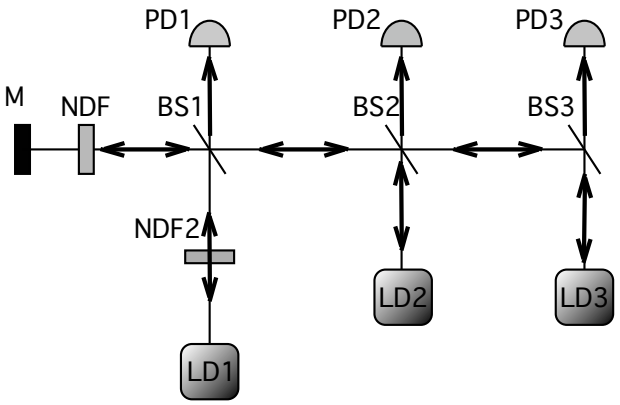

Figure 7.8: *Experimental setup with different strengths. LD: laser diodes; PD: photodiodes; BS: beamsplitters; M: mirror; NDF: variable neutral density filter; NDF2: fixed neutral density filter (70% transmittivity)*

18.17^{o}C, the threshold currents of the solitary lasers are respectively, $I^{th}_{LD1} = 31.7$ mA, $I^{th}_{LD2} = 28.79$ mA, and $I^{th}_{LD3} = 31.25$ mA. The operating currents are set to $I_{LD1} = 32.81$ mA, $I_{LD2} = 30.23$ mA, and $I_{LD3} = 32.08$ mA. The threshold reduction for each one, in absence of NDF (due to the feedback) are 1.6% for LD1, 3.40% for LD2 and 2.7% for LD3.

The output intensities of the lasers have similar average period with $T_{LD2} \sim$57 ns and $T_{LD3} \sim$64 ns, and now the average period of LD1 is $T_{LD1} \sim$37 ns (in the previous experiment the higher similarity was also between LD2 and LD3).

Considering the lasers coupled by pairs (blocking the third laser), we decrease the total injected light with the NDF placed in front of the mirror. The LD1-LD3 pair is in this case the pair that loses synchronization first.

Figure 7.9 displays the output intensities for mutually coupled lasers in pairs when the total light injection decreases (varying the transmittivity of NDF). The top left

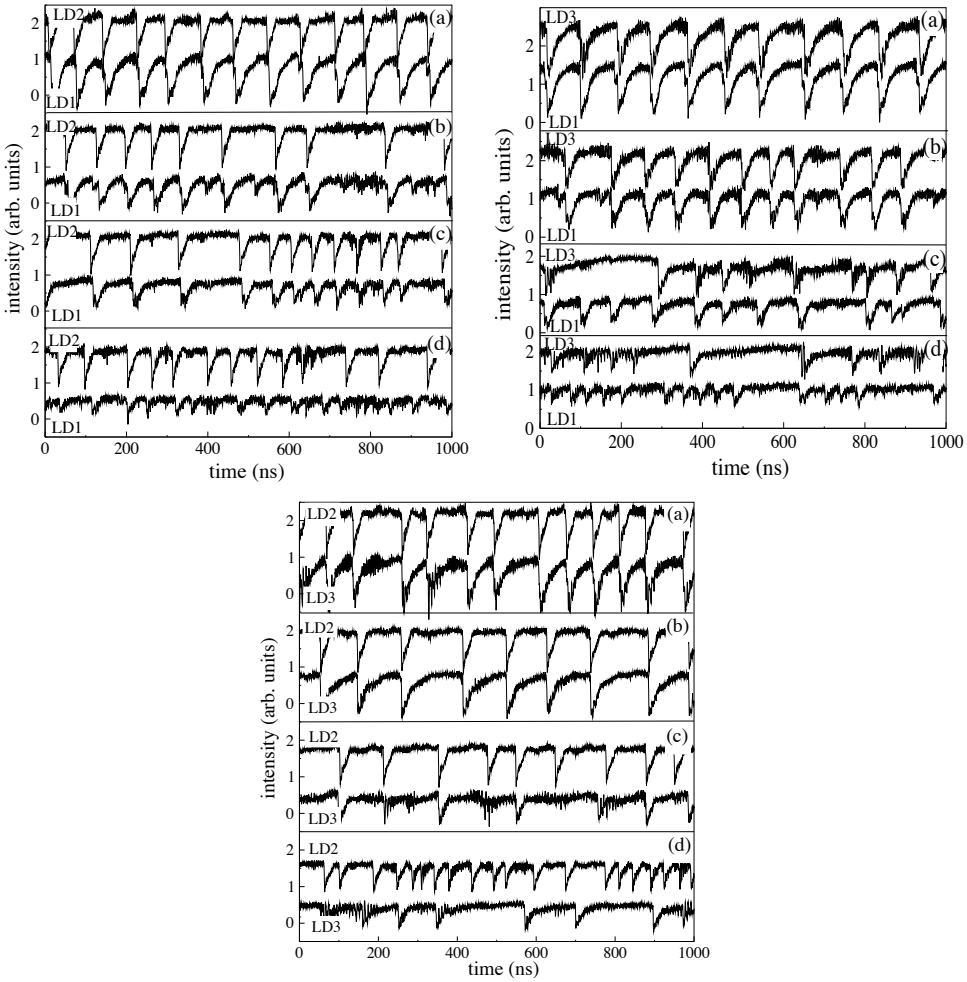

Figure 7.9: *Output intensities for lasers mutually coupled in pairs for decreasing values of total light injection (transmittivity of NDF). Signals have been displaced vertically for clarity. Values in each plot: (a) 100%, (b) 70%, (c) 63%, and (d) 50% of transmittivity.*

panel shows the intensity behavior of the LD1-LD2 pair. The mutual injection is sufficiently strong to maintain the synchronization until the total injected light decreases a 50% [Fig. 7.9, top left, panel (d)]. The top right plot shows the intensity behavior for LD1-LD3 pair when the transmittivity of NDF decreases. The synchronized behavior is maintained only at Fig. 7.9, top right, panels (a,b), and it

is lost when the transmittivity of the NDF is reduced below the 63% of the total injected light. Finally, the bottom plot shows the respective output intensities for LD2 and LD3. Although this pair of lasers seems not to have as strong synchronization behavior as LD1 and LD2 pair (it starts to lose synchronization in panel (c)), the synchronization is completely lost at Fig. 7.9, bottom, panel (d), for 50% of decreased transmittivity.

When we couple the lasers with 100% of light injection, the threshold current of each laser is decreased due to the light injected from the other two by 1.2% for LD1, 2.8% for LD2 and 2% for LD3. It is evident from the threshold reduction that LD2 is more affected than the other two. Figure 7.10(left) shows the dynamics in this case: clearly, the low frequency peaks in the different lasers occur simultaneously, and the output intensities are synchronized.

When we decrease the amount of coupling, the lasers that remain synchronized (making a cluster) are LD1 and LD2, as we can see in Fig. 7.10(right).

The fact that in the two experiments described above the geometry of the setup was the same (the lasers were placed at the same distances) and the their internal parameters did not change (the same lasers were used) shows that the choice of the lasers forming the cluster has a high dependence on the coupling strengths which vary experimentally depending on the alignment between the lasers.

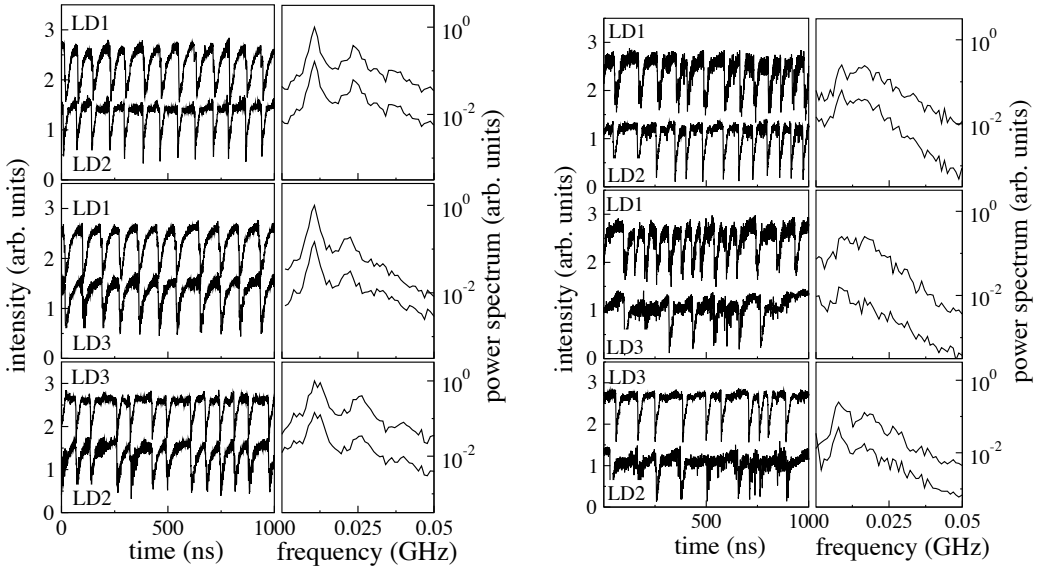

Figure 7.10: *Dynamics in the synchronized (left plot) and clustering (right plot) states. On each figure in the left column shows experimentally observed intensities; and the right column shows a detail of the corresponding power spectrum for LD1 and LD2 (top), LD1 and LD3 (center) and LD2 and LD3 (bottom). The different laser pairs are not monitored simultaneously.*

7.2 Numerical simulations

In order to establish what is the effect of coupling on the choice of lasers in a cluster, we have performed simulations based on a model that takes into account the effects of optical feedback and mutual optical injection (García-Ojalvo *et al*, 1999; Kozyreff *et al*, 2000). Extensive simulations unveil a rich variety of dynamical regimes and demonstrate that the clustered and the synchronized behaviors also occur when there are parameter mismatches between the lasers. For the sake of simplicity, we describe the dynamics of the array assuming that the laser parameters are identical. The equations for the slowly-varying complex amplitude, $\mathcal{E}_i$, and the carrier density,

$\mathcal{N}_i$, in the $i-$th laser read:

$$\begin{aligned}\dot{\mathcal{E}}_i &= i\omega_i\mathcal{E}_i + \gamma(1+i\alpha)(\mathcal{N}_i - 1)\mathcal{E}_i + \sqrt{D}\xi_i(t) \\ &+ \sum_{j=1}^{3}\kappa_{i,j}\mathcal{E}_j(t-\tau_{i,j})\exp\left(-i\omega_0\tau_{i,j}\right), \qquad (7.1)\\ \dot{\mathcal{N}}_i &= \gamma_e(\mathcal{I} - \mathcal{N}_i - \mathcal{N}_i|\mathcal{E}_i|^2), \qquad (7.2)\end{aligned}$$

where ω_i is the solitary frequency (that is, in the absence of feedback or coupling) of the $i-$th laser, relative to a common reference frequency, ω_0. α is the linewidth enhancement factor, k is the cavity loss coefficient, γ_e is the carrier decay rate, $\kappa_{i,j}$ is the coupling coefficient between lasers LDi and LDj ($\kappa_{i,i}$ being the self-feedback coefficient), $\mathcal{I}$ is the pump parameter (the threshold being $\mathcal{I}_{\rm th} = 1$ in the absence of feedback and coupling), D is the spontaneous emission strength and ξ_i are uncorrelated Gaussian white noises with zero mean.

The pump parameter and the delay times are comparable to those used in the experiments: $\mathcal{I} = 1.037$, $\tau_{1,1} = 5.3$ ns, $\tau_{2,2}$= 4.3 ns, and $\tau_{3,3}$= 7.1 ns, $\tau_{1,2} = 4.8$ ns, $\tau_{1,3}$= 6.2 ns, and $\tau_{2,3} = 5.7$ ns. The internal laser parameters are $\gamma = 250$ ns^{-1}, $\alpha = 4$, $\gamma_e = 0.6$ ns^{-1}, $D = 10^{-5}$ ns^{-1}, and $\omega_0 = 2\pi c/\lambda_0$, where c is the speed of light in vacuum and $\lambda_0 = 654$ nm.

In the simulations we observe that a cluster usually develops before the three lasers synchronize, with the feedback strengths, the coupling strengths, and the relative detunings among the lasers determining which lasers integrate the cluster.

Figure 7.11 compares the experimental spectrum obtained in Fig. 7.3, with the numerical RF spectrum of each laser with its own feedback. The feedback coefficients $\kappa_{i,i}$ used in the simulations take into account the fact that laser LD1 (LD3) has the

strongest (weakest) feedback.

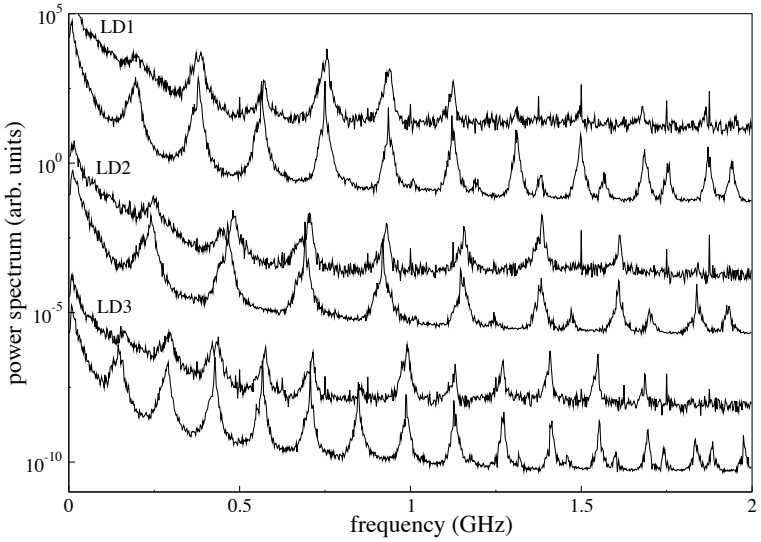

Figure 7.11: *RF spectrum for each laser with feedback experimentally (top) and numerically (bottom) obtained.*

Figure 7.12 shows the output intensities and the power spectrum for the synchronized state (left plot) and the clustered state (right plot). Figure 7.12(a,b) corresponds to LD1, (c,d) to LD2 and (e,f) to LD3. Figure 7.12(g) represents the displaced output intensities for the three lasers simultaneously, LD1 at top, LD3 at center and LD2 at bottom, shifted vertically for clarity. The intensities were filtered to simulate the bandwidth of the detectors, and normalized such that the amplitude of the dropouts of laser LD1 is 1. The coupling parameters (which are considered symmetric, $\kappa_{i,j} = \kappa_{j,i}$) take into account that lasers LD1-LD2 (LD2-LD3) have the strongest (weakest) coupling. It is worth noticing that in the experiment, different alignment quality can make the coupling strengths not only quite arbitrary but also asymmetric.

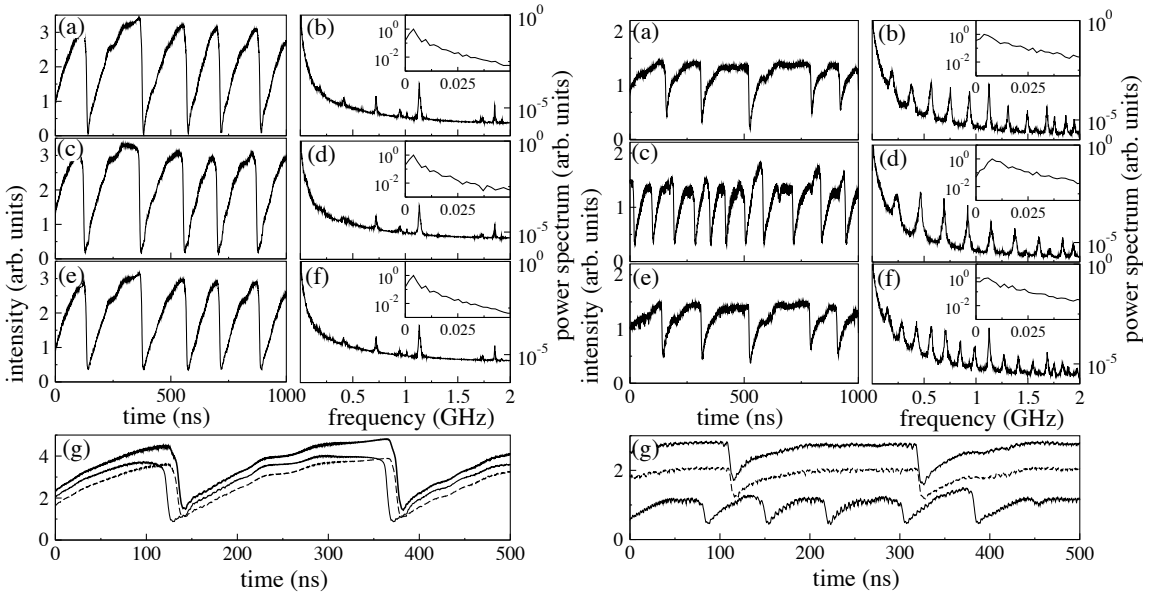

Figure 7.12: *Dynamics in the synchronized state (left) and in the clustering state (right). Each figure shows the output intensity at left and RF-spectrum at right for LD1 (a,b), LD2 (c,d), and LD3 (e,f). Panels (g) show the time traces of all three lasers. From top to bottom: LD1, LD2, LD3.*

For the choice of lasers integrating the cluster, two mechanisms seem to be relevant and compete. On the one hand, the lasers that have more similar optical injection (feedback and coupling) tend to cluster. In the absence of detunings, it is observed that as the coupling increases, LD2 and LD3, or LD1 and LD2, cluster before all three lasers synchronize (results not shown). On the other hand, if one of the lasers is weakly coupled to the other two, or if two lasers are more strongly coupled, often the strongly coupled lasers are the ones forming the cluster.

In the simulations, coupling among the lasers was adjusted by variations of the frequency detunings and the coupling coefficients, the latter depending on the optical alignment. As an example, Fig. 7.12 (right) displays a cluster formed by LD1 and

LD3, which arises when LD3 has negative detuning with respect to LD1. A simple interpretation of the observed cluster is the following: the external optical injection (feedback + coupling) modifies the lasers' optical frequencies, and roughly speaking, the frequencies shift towards negative values, with the shifts being proportional to the total injection strengths. Since LD1 is the laser that has *stronger* injection, its frequency shift is the strongest. Moreover, the beam splitters along the injection path decreases the mutual influence between LD2 and LD3, that is, their mutual coupling does not change too much their optical frequencies. The cluster is formed by LD1, which has higher relative coupling, and the laser with less change in its frequency after the coupling. Although LD2 and LD3 had similar outputs after coupling, when they were coupled together with LD1 the amount of received light their optical frequencies changed in a different manner. LD3 receives less injected light than LD2 and as consequence the optical frequency of LD3 changed less than that of LD2. Thus after coupling LD2 needs more injection strength to belong to the synchronized system. When the total injected light is decreased the first laser that loses the synchronization is in this case LD2.

In the intensity power spectra we can observe the synchronization mechanism in the frequency domain. Without mutual coupling (Fig. 7.11), the spectrum of each laser consists of a dominant peak at a low frequency (the inverse of this frequency is the average dropout period), and harmonics separated by the external cavity frequency, $1/\tau_{i,i}$. Since the average dropout period is different for the different lasers, the main peaks are at different frequencies. Moreover, since the delay times $\tau_{i,i}$ are also different, the harmonic peaks are located at different frequencies. When the lasers are coupled the spectra of the lasers synchronize at both low and high frequencies [Fig. 7.12 left, (b,d,f)]. For weaker feedback and coupling, the numerical

spectra show that the frequencies begin to adjust both in the low and high frequency ranges: some harmonics begin to disappear, while others "move" such that they overlap [Fig. 7.12 right, (b,d,f)]. The same process of frequency selection, where some peaks vanish and others "move" (in a sort of frequency pulling phenomenon occurring in the RF spectrum), is observed experimentally (Fig. 7.7).

Chapter 8

Summary, conclusions and future work

In this Thesis we have presented the results of a set of experimental investigations of the dynamics of delay-coupled semiconductor lasers. The characterization of these systems includes topics such as the processing of information by coupled lasers, the choice of a leader in their lag-synchronized dynamics, or how chaos arises in two coupled semiconductor lasers.

8.1 Summary and conclusions

We summarize all the results and conclusions presented in this Thesis as follows:

- The transition to chaos of a semiconductor laser through a quasiperiodic state was reported in the past adding an optical feedback (Mørk *et al*, 1990) or

through mutual coupling (Hohl *et al*, 1999). In Chapter 3 we studied the quasiperiodic route to chaos of two semiconductor lasers mutually coupled through two independent unidirectional paths. The transition from unidirectional to bidirectional coupling was implemented by increasing the coupling strength of one of the paths, while keeping the other constant. We have seen how the transition from stable unidirectional injection to chaos arises through a quasiperiodic state.

Adjusting the currents and temperatures of the lasers in a unidirectional configuration, we maximize the injection by choosing optical frequencies sufficiently close to each other. In this regime, the output intensity of the receiver laser is forced to oscillate at the relaxation oscillation frequency of the driver, with a delay time ($\tau_{1,2}$) introduced by the interaction. When the back injection is slightly increased, the external modes of the other cavity are excited and the laser output becomes quasiperiodic. This quasiperiodic behavior is produced by a competition between the external compound-cavity modes and the relaxation oscillation frequencies of both lasers. When the mutual coupling is sufficiently high the chaotic behavior appears.

- We have examined in Chapter 4 how a system of two coupled chaotic oscillators behaves under conditions of lag synchronization. Our experimental setup consists on two semiconductor lasers coupled via mutual injection of their emitted fields, and allows for the control of the coupling directionality. Our results show that the laser leading the dynamics changes depending on the coupling scenario. When one of the lasers has autonomous chaotic dynamics, in the form of irregularly spaced sudden power dropouts (low-frequency fluc-

tuations), and this dynamics is injected into a solitary laser (which is stable in the absence of injection), the injecting laser obviously leads the dynamics. Such role, however, can be transferred to the other laser by converting the coupling from unidirectional to bidirectional. The transition occurs via a state in which the two lasers alternate randomly the leader and laggard roles. This type of behavior is not only restricted to the low-frequency dynamics that we have studied experimentally, but also to fully developed chaotic dynamics (coherence collapse) that occurs for higher pump currents, as shown by numerical simulations. Our model also shows that the type of dynamics can be changed in a continuous way by acting upon the optical feedback strength affecting the laser with independent dynamics.

We have discussed the potential of this system for bidirectional chaotic communications. Our experimental results show that whenever one of the lasers leads the dynamics, the other laser (the laggard) is able to operate as a chaos-pass filter. However, we have not been able to send information bidirectionally in an effective way. Numerical simulations show that, even though the maximum cross-correlation is similar in both the unidirectional and bidirectional cases, sudden synchronization losses in the latter situation prevent the system from being used as a reliable setup for bidirectional chaotic communications.

- When two coupled nonlinear systems are perturbed by two independent periodical signals, it is possible to observe a resonance at their outputs at a third frequency not present in the input, what is known as a ghost resonance.

  In Chapter 5 we have given experimental and numerical evidence of the existence of such a ghost resonance in two mutually coupled semiconductor lasers.

The resonance is not trivial, since it persists in the case of incommensurate input frequencies, showing a behavior that agrees with theoretical predictions. Similar results have been obtained in simpler theoretical models (Chialvo *et al*, 2002) and in single semiconductor lasers with optical feedback (Buldú *et al*, 2003), but to our knowledge this was the first experimental observation in coupled systems.

In the second part of the chapter, we have shown experimentally that coupling between two excitable systems, specifically two semiconductor lasers with optical feedback, is able to mediate the processing of distributed inputs, applied in the form of pump current modulations of different frequencies. For large enough coupling strengths, the laser outputs have the form of synchronized trains of power dropouts which become entrained to a frequency that is not present in the input signals. When these signals are harmonics of a missing fundamental, as in the previous case, the response occurs at precisely the fundamental frequency. On the other hand, in the case where the two input frequencies are equally shifted from these harmonics, the system responds following a linear law, which arises from analyzing the linear summation of the two input modulations (Chialvo *et al*, 2002). The superposition law holds even though the two signals acting upon a given laser are clearly different, one of them being electrical (through direct pump current modulation) and the other optical (through injection from the other laser). This type of response to complex input signals has been reported in the human brain with psychophysical experiments (Schouten *et al*, 1962) and magnetoencephalographic recordings (Pantev *et al*, 1996), which highlights the importance of understanding the integration of distributed inputs by networks of information processing

elements.

- In Chapter 6 we have experimentally and numerically shown that the introduction of a global noise can stabilize the isochronal solution in two mutually coupled semiconductor lasers.

  Departing from a low frequency regime, in the synchronized state of the system with a well defined leader of the dynamics, we simultaneously added the same amount of colored noise to the pump current of the two lasers. For low amplitude, the noise is not capable of affecting the dynamics of the system, but for higher values of the amplitude the laser outputs synchronize without delay.

  A more detailed study showed that there is a threshold in the noise correlation time above which the fast dynamics of the system is not affected. The envelope of the dynamics (the dropout events) is affected by the colored noise for large enough noise intensity, but a cross-correlation study of the numerical output intensities shows a threshold in the correlation time above which the fast dynamics cannot synchronize with zero lag. For noise correlation times smaller than that threshold, and eventually in the white noise limit, the isochronal solution of the *total* dynamics of the system is stabilized.

- In Chapter 7 we have experimentally studied the route towards synchronization in a small network of three semiconductor lasers coupled with distributed delay times. Our results show that clusters emerge generically as the system goes towards synchronization for increasing coupling strength. A detailed study of the coupling between each pair of lasers showed that the cluster in the three laser system was formed by the pair of lasers with highest mutual coupling.

The lasers which have most affinity (least detuning, highest parameter mismatch, and as a consequence highest coupling) will maintain the synchronized behavior for decreased injected light, whereas the third laser needs more coupling to belong to the synchronized system. The overlap of some of the peaks in the RF spectrum in the clustering state, denotes that it is an intermediate stage before a complete loss of synchronization.

The experimental observations are satisfactorily reproduced by a rate equation model of the Lang-Kobayashi type. The model is valid for a laser emitting in a single longitudinal mode. The lasers in the experiments emit multiple longitudinal modes, and yet the agreement between the experiment and the model predictions is surprisingly good. This can be explained as due to the out of phase dynamics of the longitudinal modes. Because of the competition for the common carrier reservoir, the longitudinal modes oscillate in antiphase, such that the total output (that is, the sum of the modal intensities) is similar to that of a single-mode laser. The numerical simulations performed in this experiment helped us to understand which is the determining factor for the choice of lasers forming the cluster. We showed that the coupling determines which laser enters the cluster and which one loses the synchronization first.

8.2 Discussion and future work

The way to couple two lasers allows different working protocols, but in this Thesis we used the following steps:

First we changed the temperatures until the wavelengths of the lasers were as

similar as possible. With the temperatures fixed, the lasers were mutually (or unidirectionally) injected. Then, the alignment of the lasers was mechanically optimized (using the translation stage) by maximizing the increase of the receiver laser output power near its threshold, due the injection of transmitter laser. This increase can be measured introducing a power meter in the detection path. Finally, the pump currents were slightly changed to obtain the optimal locking of the injected laser, by matching their optical spectra.

Based upon the experience obtained from performing the experiments, the following recommendations are made for improving the design of future experimental designs:

- A fiber implementation of the couplings and feedbacks would be desirable in order to work with more stable and controllable experimental setups. A fiber pigtailed laser and all-fiber detections would be a good improvement for future studies.

- To study the lasers in depth, a future step would be to have a systematic experimental knowledge of the change in optical spectrum induced by the coupling. An in situ measurement of the absolute change in wavelength can be done with a fiber ring resonator (with much more resolution than conventional optical spectrum analyzers).

- An improvement of the modulation introduced into the pumping current of the lasers would consist on using a Bias-T of high bandwidth (1 GHz or more). The real bandwidth and behavior of the laser mounting tee is not well known and introduces a high uncertainty when used as modulation source. The pos-

sibility of studying optoelectronic feedback and coupling was impossible with the bandwidth exhibited by the mounting.

There are many open problems that require further study. One such problem is to provide a mathematical description of the real multimode behavior of these kind of lasers. The mono-mode approximation works for almost all the situations addressed in this Thesis, but a study in depth requires a multimode extension of the model.

Another problem that needs additional study is the relationship between the numerical value of the coupling and feedback strengths with its experimental value. For the moment we use comparative measures of the numerical and experimental value of the strength. We compare the relative level of coupling in the two coupling directions, or in the unidirectional scheme looking at the behavior of the output intensities. In our work we paid particular attention to the control of the mutually coupled systems, particularly referred to the prediction of the leader role and the emergence of chaotic synchronization. In these cases we check the output intensity characteristics using cross-correlation functions or using their Fourier transform (RF spectrum analyzer) and compared with the numerically calculated ones to infer the coupling or the feedback strengths.

Part III

APPENDICES

Appendix A

Semiconductor parameters

A.1 Semiconductor basics

Along this Thesis diverse parameters of the semiconductor material were used. A detailed understanding of the equations used in numerical simulations demands a knowledge of semiconductor materials. We first explain, in a very general way, the semiconductor physics and the different parameters that have dynamical relevance on the rate equations used in this Thesis.

In a semiconductor material, the allowed states of the electrons form continuous energy bands. The probability that an electronic state of energy ϵ can be occupied by an electron is given by the Fermi-Dirac distribution (Liu, 2005):

$$f(\epsilon) = \frac{1}{1 + e^{(\epsilon - \epsilon_F)/k_B T}} \ , \tag{A.1}$$

where ϵ_F is the Fermi level, the energy value for which the occupancy level is 1/2

(for an energy $\epsilon = \epsilon_F$ half of the states with this energy are occupied). k_B is the Bolzmann constant and T is the absolute temperature. In semiconductors, the Fermi energy is located between the valence band, which is completely occupied at T=0, and the conduction band, which is completely empty.

In a semiconductor material electronic transitions occur between the conduction and valence energy bands, in particular transitions leading to photon emission. In fact, the transitions that generate laser emission occur between lower energy levels of the conduction band and higher energy levels from the valence band. A semiconductor for which the minimum of the conduction band (the conduction-band edge ϵ_c) and the maximum of the valence band (valence-band edge, ϵ_v) do not occur at the same momentum value ($\overrightarrow{k}$), such as Si, is called an indirect-gap semiconductor.

These semiconductors cannot be used for light generation since the emitted photons would not be able to take away the extra momentum generated by the transition. Typical components of laser diodes such as GaAs have a direct bandgap. The bandgap is the difference between ϵ_c and ϵ_v (<4eV for a typical semiconductor) and normally decreases with temperature.

The most important semiconductor components for laser diodes are combinations from group III elements (Al, Ga, In) with group V elements (N, P, As, Sb). A compound of two, three or four elements forms a binary, ternary or quaternary alloy, respectively. Examples of binary compounds are GaAs, InP, AlAs and InSb. Ternary compounds are, for instance, $Al_xGa_{1-x}As$ and $GaAs_{1-x}P_x$. A quaternary example is $In_{1-x}Ga_xAs_{1-y}P_y$. A compound with small bandgap tends to be a direct-gap material, whereas one with a large bandgap tends to be an indirect-gap material.

When two crystals have the same structure and the same mesh constant they

are called lattice-matched. It is possible to construct a laser diode with arbitrarily thick layers of lattice-matched materials. For example in $Al_xGa_{1-x}As/GaAs$ structures, the ternary compound $Al_xGa_{1-x}As$ is closely lattice-matched to GaAs, and in $In_{1-x}Ga_xAs_yP_{1-y}/InP$, the correspondent quaternary compound is lattice-matched to InP. Some of our semiconductor laser diodes are AlGaInP structures grown in a GaAs substrate (Fig. A.1)

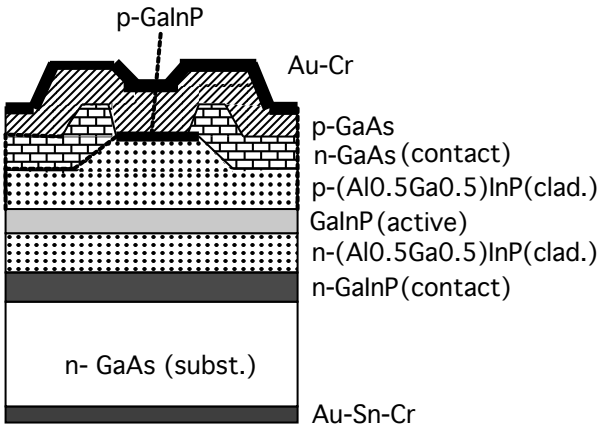

Figure A.1: *Schematic structure of a typical AlGaInP laser.*

The AlGaInP system offers a wide variety of energy gaps in the III-V alloys. It is a good system for fabricating light-emitting and laser diodes in the region below 700 nm. They have a very low threshold current (from 17 to 40 mA) and relatively high output power (10 mW).

When a semiconductor material is externally excited with a forward voltage bias during a period of time, the material can reach a quasi-equilibrium state in which electrons and holes are not characterized by a common Fermi level but characterized by two separate quasi-Fermi levels. The probability of occupancy in the conduction

and the valence bands are described by two separate Fermi-Dirac distributions:

$$f_c(\epsilon) = \frac{1}{1 + e^{(\epsilon - \epsilon_{Fc})/k_B T}} \tag{A.2}$$

$$f_v(\epsilon) = \frac{1}{1 + e^{(\epsilon - \epsilon_{Fv})/k_B T}} \ , \tag{A.3}$$

for the conduction and the valence bands respectively. ϵ_{Fc} and ϵ_{Fv} are the quasi-Fermi levels for the conduction and valence bands.

A.2 Parameters of numerical simulations.

Throughout this Thesis the numerical simulation model is based on the equations from Lang and Kobayashi (1980):

$$\begin{aligned} \frac{dE}{dt} &= \frac{(1+i\alpha)}{2}\left[G - \gamma\right] E + \kappa_f e^{-i\omega\tau_f} E(t-\tau_f) \\ &+ \sqrt{2\beta N}\,\xi(t) \end{aligned} \tag{A.4}$$

$$\frac{dN}{dt} = C - \gamma_e N - G|E|^2 \ , \tag{A.5}$$

that describe the optical field amplitude $[E(t)]$ and the population inversion $[N(t)]$ in a semiconductor laser with optical feedback. As we explain at the Introduction of this Thesis, optical feedback is possible due to the low reflectivity at the front facet of the laser. When we place a mirror in front of the laser we can re-introduce the outgoing light again into the laser cavity.

Along this Thesis we used an easy-to-use population inversion equation. To make a better comparison between numerical and experimental results we introduced the

bias current, $C_b = I_b/I_{th}$, the ratio between the pump and the threshold currents. The first term of Eq. (A.5) results on:

$$C = \frac{I}{e} = C_b \frac{I_{th}}{e} = C_b C_{th} \ , \tag{A.6}$$

where $C_{th} = \frac{I_{th}}{e}$ is the pump current at threshold. Taking in mind the inversion population expression at threshold ($N_{th} = C_{th}/\gamma_e$, derived from the steady state solutions showed at the end of Sec. 1.2 in Chap. 1), we can express Eq. (A.5):

$$\frac{dN}{dt} = \gamma_e N_{th} C_b - \gamma_e N - G|E|^2, \tag{A.7}$$

The rate equations used in all the numerical simulations of this Thesis are:

$$\begin{aligned} \frac{dE}{dt} &= \frac{(1+i\alpha)}{2}\left[G-\gamma\right]E + \kappa_f e^{-i\omega\tau_f} E(t-\tau_f) \\ &+ \sqrt{2\beta N}\,\xi(t) \qquad \text{(A.8)} \\ \frac{dN}{dt} &= \gamma_e N_{th} C_b - \gamma_e N - G|E|^2 \ , \qquad \text{(A.9)} \end{aligned}$$

with $G = \frac{g_N(N-N_0)}{1+s|E|^2}$, in which we take $s = 0$ because we work near threshold values, and $N_{th} = \frac{\gamma}{g_N} + N_0$ [Eq. (1.48) of Chap. 1].

There are some fixed parameters in these rate equations taken into account in all the simulations:

- γ_e: carrier inverse lifetime.
- γ: photon inverse lifetime.
- N_0: number of carriers at transparency.

- g_N: differential gain coefficient.
- α: linewidth enhancement factor.

As far as possible we used experimentally measured parameters, but in many cases we take typical parameter values for the semiconductor lasers used in our experiments.

Table A.1 displays typical parameter values used along the Thesis for AlGaInP laser diodes of λ=635 nm, or λ=650 nm.

Symbol	Parameter	Value
γ_e	Inverse carrier lifetime	6.89×10^{-4} ps^{-1}
γ	Inverse photon lifetime	0.250-0.480 ps^{-1}
N_0	Carrier number at transparency	1.25×10^8
g_N	Differential gain parameter	$1.2 - 1.5 \times 10^{-8}$ ps^{-1}
α	Linewidth enhancement factor	$3 - 4$

Table A.1: *Laser parameters in the low frequency fluctuation regime (Sec. 1.3.2). Other parameters that do not depend intrinsically of the material are: bias current C_b, noise amplitude $\beta \sim 0.5\times10^{-9}$ $ps^{-}1$, feedback time τ_f, and feedback strength κ_f. In the coherence collapse regime (Sec. 1.3.2) parameters are the same except the bias current, that is $C_b >$* 1.9

A.2.1 Carrier recombination

When a semiconductor material is forward-biased (an external voltage is applied), electron and holes diffuse across the p-n junction (Sec. 1.1). In a narrow region, electrons and holes are present simultaneously and can recombine. There are three categories of recombination processes, which can be radiative or non-radiative: Shockley-Read recombination processes (radiative or non-radiative), bimolecular recombina-

tion processes (radiative), and Auger recombination processes (non-radiative) (Liu, 2005):

- Shockley-Read recombination: this process involves only one carrier at a time. It consists in the capture of one carrier, an electron or a hole, by a recombination center (impurity). The net recombination rate is expressed as:

$$A_e \Delta n = A_h \Delta p \tag{A.10}$$

  where A_e and A_h are the Shockley-Read coefficients, and Δn and Δp are the excess of electrons $n - n_0$ and holes $p - p_0$, from the equilibrium n_0 and p_0 values, respectively. The Shockley-Read recombination process can be either radiative or nonradiative, depending on the type of recombination centers involved in the process.

- Bimolecular recombination: involves an electron and a hole at the same time. There are two types:

  - Band-to band, between an electron in the conduction band and a hole in the valence band.
  - Exciton recombination, which is a recombination of an electron and a hole to form an exciton. This exciton can be bounded, localized at an impurity, or it can be a free exciton traveling around the semiconductor.

  The bimolecular recombination processes have the same contribution to the rate of electron recombination than to the rate of hole recombination. This

rate is proportional to the carrier densities and can be expressed as:

$$Bnp \ , \tag{A.11}$$

where B is the bimolecular recombination coefficient, and n and p are the electron and hole concentrations respectively. The bimolecular recombination is a radiative process.

- Auger recombination: the energy produced by a band-to-band recombination of an electron and a hole is taken by a third carrier and transformed to kinetic energy. This is then converted to thermal energy when the carrier is relaxed toward the band edge.

  The Auger process is non-radiative and is a three-body process. It can involve two electrons and a hole, in which case the rate is:

$$C_e n^2 p \ , \tag{A.12}$$

  or two holes and one electron, with a rate:

$$C_h p^2 n \ , \tag{A.13}$$

  where C_e and C_h are the Auger coefficients for electrons and holes, and n and p are the respective carrier densities.

These processes also can happen in the inverse direction, generating in this case free electrons and holes at rates G_e^0 and G_h^0, respectively. Taking into account the three

types of processes, the net recombination rate is:

$$\begin{aligned} R_e &= A_e n + Bnp + C_e n^2 p + C_h n p^2 - G_e^0 \\ R_h &= A_h p + Bnp + C_e n^2 p + C_h n p^2 - G_h^0 \end{aligned} \tag{A.14}$$

Due to the fact that electrons and holes always recombine by pairs, we can write:

$$R = R_e = R_h$$

Where R_e is the net recombination rate for electrons and R_h for holes. When a semiconductor is in thermal equilibrium, the generation rate for electrons and holes is the same and $R = 0$.

The inverse processes of free electrons and holes generation G_e^0 and G_h^0 are:

$$\begin{aligned} G_e^0 &= A_e n_0 + B n_0 p_0 + C_e n_0^2 p_0 + C_h n_0 p_0^2 \\ G_h^0 &= A_h p_0 + B n_0 p_0 + C_e n_0^2 p_0 + C_h n_0 p_0^2 \end{aligned} \tag{A.15}$$

where n_0 and p_0 are the carrier densities (for electrons and holes, respectively) at thermal equilibrium.

The recombination coefficients depend on the carrier concentrations and there are several order of magnitudes of difference between them. Generally A is the largest and C the smallest. At lower carrier concentrations the Shockley-Read processes (A) are important, whereas Auger processes (C) are only important at very high carrier concentrations. Between both limits, bimolecular processes are the important. In general, the B coefficients of direct-gap semiconductors (such as GaAs or InP) are

much larger than those of indirect gap materials such as Si and Ge.

When the concentrations of electrons and holes are higher than their respective equilibrium concentrations, the excess of carriers will relax toward their respective thermal equilibrium values, through recombination processes. The relaxation time constant for excess electrons is the electron lifetime, and for holes the hole lifetime. If the concentration of electrons and holes are very large compared to the density of the recombination centers, we can consider that the excess of minority carriers is equal to the excess of majority carriers ($\Delta n = \Delta p = N$, where N is defined as the density of excess carriers). Assuming that the free electrons and the free holes have the same lifetime, the spontaneous carrier recombination lifetime can be written as:

$$\tau_s = \frac{N}{R} \tag{A.16}$$

The total recombination rate can be expressed in the form:

$$R = R_{rad} + R_{nrad} \tag{A.17}$$

The spontaneous carrier recombination lifetime obeys:

$$\frac{1}{\tau_s} = \frac{1}{\tau_{rad}} + \frac{1}{\tau_{nrad}} \tag{A.18}$$

And the spontaneous carrier recombination rate is defined as:

$$\gamma_e = \frac{1}{\tau_s} \ , \tag{A.19}$$

which doesn't take into account the contributions from the stimulated recombination process.

Assuming that the radiative recombination rate is almost entirely contributed by bimolecular recombination, in thermal equilibrium bimolecular recombination is balanced by bimolecular thermal generation [Eq.(A.15)], which is the same for electron and holes ($G_e^0 = G_h^0 = G_0$). Out of equilibrium, with electron-hole pairs excess, we can write the net radiative recombination rate as:

$$R_{rad} = Bnp - G_0 = Bnp - Bn_0p_0 \ , \tag{A.20}$$

where $G_0 = Bn_0p_0$ because in thermal equilibrium $R_{rad} = 0$, when $n = n_0$ and $p = p_0$.

Whit the excess of carriers defined as $N = n - n_0 = p - p_0$ the radiative carrier lifetime is given as:

$$\tau_{rad} = \frac{N}{R_{rad}} = \frac{1}{B(N + n_0 + p_0)} \tag{A.21}$$

In the limit of low excess of carriers ($N << n_0, p_0$):

$$\tau_{rad} \approx \frac{1}{B(n_0 + p_0)} \tag{A.22}$$

And in the opposite limit ($N >> n_0, p_0$):

$$\tau_{rad} \approx \frac{1}{BN} \tag{A.23}$$

There is a carrier density dependence of the carrier lifetime. Due to the fact that we normally work not very far from threshold, we made an estimation around the threshold value of the carrier density. Taking into account that in a semiconductor laser the carrier density value at threshold (minimum carrier density for lasing condition) is higher than the respective carrier densities at thermal equilibrium, we use Eq. (A.23) to calculate an estimated value of the carrier lifetime, for carrier density value at threshold ($N = N_{th} >> n_0, p_0$).

Finally, due to the assumption of $N = n - n_0 = p - p_0$, we can consider $A_e = A_h = A$, and taking into account that the Auger processes are not very important, due to the large band-gap of the alloys used to build a laser diode ($C \approx 0$), the total spontaneous recombination carrier lifetime reads:

$$\gamma_e = \frac{1}{\tau_s} = A + BN \tag{A.24}$$

From experimental works by Strauss *et al* (1994), the estimated value for the recombination coefficients values for AlGaInP laser are $B = 1.0\ 10^{-10}$ cm^3 s^{-1} and $A = 2.2\ 10^7$ s^{-1}. Estimating the carrier density at threshold as $\sim 6\ 10^{24}$ m^{-3} (Crow and Abram, 1997), the carrier lifetime value considered in the simulations of this Thesis is $\gamma_e \sim 7\ 10^8$ s^{-1}=$7\ 10^{-4}$ ps^{-1}.

A.2.2 Cavity decay rate

The cavity or photon decay rate (γ) is defined as the inverse of the photon lifetime. It is separated into two terms, one describing the internal losses, and the second describing the number of photons that leave the cavity through its mirrors (Petermann,

1988):

$$\gamma = \frac{1}{\tau} = \frac{c}{n}\left[\alpha_i + \frac{1}{2L}\ln\left(\frac{1}{R_1 R_2}\right)\right] , \tag{A.25}$$

where α_i are the internal losses, R_1 and R_2 are the reflectivities of the laser facets, and L the cavity length.

We can assume: $R_1 = R_2 = R$, where R is the reflectivity of the laser/air interface:

$$R = \left(\frac{n_2 - n_1}{n_2 + n_1}\right)^2$$

For AlGaInP lasers, $n_2 = 3.4$ and $n_1 = 1$, and hence $R \sim 0.3$. Finally, taking standard values for these lasers, $\alpha_i \sim 20$ cm^{-1} (typical α_i values range from 10 to 20 cm^{-1}), and $L \sim 450$ μm (see section A.2.4) we obtain $\gamma \sim 0.450$ ps^{-1}.

A.2.3 Population inversion

The optical gain contributed by direct band-to-band transitions from a conduction-band state with energy ϵ_2 to a valence-band state with energy ϵ_1 in a semiconductor is proportional to the density of states. The probability of transition from the higher energy level ϵ_2, to the low energy level ϵ_1: $f_c(\epsilon_2) - f_v(\epsilon_1)$.

The optical gain is positive only if the occupation probability in the conduction band, $f_c(\epsilon_2)$, is higher than the occupation probability in the valence band, $f_v(\epsilon_1)$. This condition leads to an inversion of population in the semiconductor that it is achieved only for strong carrier injection into the active layer, yielding a shift of the quasi-Fermi levels [Eqs. (A.2) and (A.3)] into the conduction or valence bands, due to the voltage bias applied. Using the quasi-Fermi occupation probability for the

conduction and the valence bands defined in Eqs. (A.2) and (A.3) for a transition $h\nu = \epsilon_2 - \epsilon_1$ (Liu, 2005), we obtain:

$$f_c(\epsilon_2) - f_v(\epsilon_1) = f_c(\epsilon_2)[1 - f_v(\epsilon_1)] \left[1 - e^{\frac{(h\nu - \Delta\epsilon_F)}{k_B T}}\right] , \tag{A.26}$$

where $\Delta\epsilon_F = \epsilon_{FC} - \epsilon_{FV}$.

The term $f_c(\epsilon_2)[1-f_v(\epsilon_1)]$ is the probability of transition from an occupied higher state with energy ϵ_2 to an empty state of energy ϵ_1, and by definition it has a value ranging from 0 to 1. The sign of the gain is only determined by the sign of the quantity $(h\nu - \Delta\epsilon_F)$. The condition for a positive gain at any given frequency occurs when the distance between the quasi Fermi levels is larger than the photon energy, and that is larger than the band-gap energy ($\Delta\epsilon_F = \epsilon_{Fc} - \epsilon_{Fv} > h\nu > \epsilon_g = \epsilon_c - \epsilon_v$). The minimum value of the carrier density that fulfills the condition above (determined by $\Delta\epsilon_F = \epsilon_g$, $\epsilon_{Fc} - \epsilon_c = \epsilon_{Fv} - \epsilon_v$) is the transparency carrier density N_{tr}.

It is possible to estimate this value considering that, when a semiconductor is pumped to have a positive gain, electron and hole concentrations are higher than that at the thermal equilibrium ($n > n_0$ and $p > p_0$, therefore $\Delta n \approx n$ and $\Delta p \approx p$). We can approximate: $n \approx p \approx N$, where n and p are the electron and hole concentrations respectively and N is the excess carrier density.

The electron and hole concentrations are defined as:

$$n = \int_{\epsilon_c}^{\infty} \rho_c(\epsilon) f(\epsilon)\, d\epsilon \tag{A.27}$$

$$p = \int_{-\infty}^{\epsilon_v} \rho_v(\epsilon) \left[1 - f(\epsilon)\right] \, d\epsilon \ , \tag{A.28}$$

where $\rho_c(\epsilon)d\epsilon$ and $\rho_v(\epsilon)d\epsilon$ are the number of states per cm^3 in the energy range $d\epsilon$ for the conduction and valence bands respectively, and $f(\epsilon)$ and $[1 - f(\epsilon)]$ are the Fermi distributions describing the probability that a state is filled or empty, respectively.

The electron and hole concentrations considered above can be expressed, taking into account the effective densities of states in the conduction $[N_c(T)]$ and valence $[N_v(T)]$ bands, as:

$$n = N_c \frac{2}{\sqrt{\pi}} F_{1/2}(\xi_c) \tag{A.29}$$

$$p = N_v \frac{2}{\sqrt{\pi}} F_{1/2}(\xi_v) \ , \tag{A.30}$$

where:

$$N_c(T) = 2 \left(\frac{2\pi m_e^* k_B T}{h^2} \right)^{3/2} \tag{A.31}$$

$$N_v(T) = 2 \left(\frac{2\pi m_h^* k_B T}{h^2} \right)^{3/2} \ , \tag{A.32}$$

with m_e^* and m_h^* the effective masses for electrons and holes, and $\xi_c = (\epsilon_{Fc} - \epsilon_c) / k_B T$ and $\xi_v = (\epsilon_v - \epsilon_{Fv}) / k_B T$ giving the Fermi-Dirac integrals as:

$$F_{1/2}(\xi_c) = \int_0^\infty \frac{\xi^{1/2}}{1 + e^{(\xi - \xi_c)}} \, d\xi \tag{A.33}$$

$$F_{1/2}(\xi_v) = \int_0^\infty \frac{\xi^{1/2}}{1 + e^{(\xi - \xi_v)}} \, d\xi \ , \tag{A.34}$$

where $\xi = (\epsilon - \epsilon_c)/k_B T$ is defined for electron density calculations and $\xi = (\epsilon - \epsilon_v)/k_B T$ for hole density calculations.

Considering the inversion condition, that leads to the carrier density at trans-

parency ($\epsilon_{Fc} - \epsilon_c = \epsilon_{Fv} - \epsilon_v$), we can define a value for ξ_{tr} (for which $\xi_c = -\xi_v$), and N_{tr} can be derived from the relation:

$$N_{tr} = N_c F_{1/2}(\xi_{tr}) = N_v F_{1/2}(-\xi_{tr}) \tag{A.35}$$

The values for a GaInP semiconductor material (active region for our AlGaInP laser) are $m_e^* = 0.088 m_0$ and $m_h^* = 0.7 m_0$ (m_0 electron mass)[1]. This leads to the following equality:

$$F_{1/2}(\xi_{tr}) = 22.43 F_{1/2}(-\xi_{tr}) \tag{A.36}$$

We scanned the value of ξ_{tr} to calculate the Fermi-Dirac integral of order 1/2, and we found that the value that matches last equation is $\xi_{tr} \approx 2$.

This leads to the carrier density value at transparency:

$$N_{tr} = 2\left(\frac{2\pi m_e^* k_B T}{h^2}\right)^{3/2} F_{1/2}(\xi_{tr}) = 1.8 \times 10^{24} m^{-3} \ ,$$

using the fact that $F_{1/2}(2) \approx 2.8$.

The number of carriers at transparency is the transparency density multiplied by a standard volume of the active region (V$\approx 100 \mu$m^3), resulting in an adimensional value of $N_0 = 1.8 \times 10^8$. Along this Thesis the value chosen for the numerical simulations was $N_0 = 1.25 \times 10^8$.

[1]Semiconductor constants can be find in: http://www.ioffe.ru/SVA/NSM/

A.2.4 Cavity length

An estimate of the cavity length of a laser can be obtained directly from the laser spectrum. The longitudinal-mode cavity resonances occur at wavelengths:

$$m\lambda_m = 2nL \tag{A.37}$$

where L is the cavity length, λ_m are the different wavelength modes, n is the refractive index, and m an integer. The value of the wavelength change between adjacent modes ($\Delta m = 1$) is given by:

$$\Delta\lambda = \frac{\lambda^2}{2nL} \tag{A.38}$$

And the expression for the cavity length is:

$$L = \frac{\lambda^2}{2n\Delta\lambda} \tag{A.39}$$

For the AlGaInP laser, we experimentally have measured a cavity length of $L \sim 450\mu$m.

It is important to characterize the optical spectrum of a semiconductor laser, due to the substantial variations of the center wavelength with temperature and pump current changes. A change in the temperature of a Fabry-Perot laser causes a refractive index change of the laser material and this causes a shift of the modes sustained by the cavity (Chien, 1993). Another consequence of a change in temperature is a shift of the maximum gain of the laser material which originates a change of the emission wavelength: for increasing temperatures a reduction of the bandgap is produced, resulting in a shift of the gain towards longer wavelengths (Nakamura

et al, 1978). Since the change of the wavelength of the cavity modes and the change of the center wavelength of the optical gain are not synchronous, frequent mode-hops and regions with multimode emission appear. Due to the fact that changes in laser current cause a change of the temperature within the active region of the laser diode (Ito and Kimura, 1980), an increase of the injection current above threshold shows a similar behavior as an increase of the temperature of the laser mount, but the wavelength is coarsely tuned with the temperature and finely tuned with the injection current of the diode.

If we represent the maximum wavelength versus the temperature we can see how the laser diode jumps between discrete wavelength values (Kasukawa *et al*, 1990). Figure A.2 represents the change of the wavelength of the maximum mode for a given pump current, for different temperature values. Several regions with approximately the same slope (each one belonging to one longitudinal mode) are separated by hops of the emitted wavelength which can be to the nearest mode or to a mode relatively far from the original one. A measure of the rate of change of the wavelength with temperature give us important information to delimit the region of the wavelength plateaus.

A.2.5 Gain coefficient

One of the more important parameters to characterize semiconductor lasers is the gain coefficient. In the simulations along the Thesis we used a typical value for a quantum well semiconductor laser, but there are several ways to measure this parameter. In quantum well lasers the gain material per unit length is related to

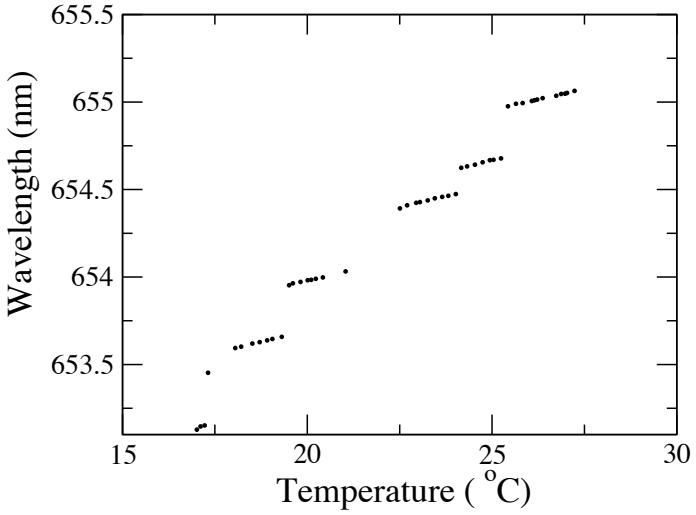

Figure A.2: *Temperature dependence of wavelength of AlgaInP laser diode with 450 μm cavity, for $I_{pump} = 38.01$ mA, resulting in a rate of change in wavelength of* $0.047 nm/^{o}C$.

the carrier number (Liu, 2005):

$$g = g_0 \ln\left(\frac{N}{N_{tr}}\right) \ , \tag{A.40}$$

where $g_0 = \frac{\partial g}{\partial N}\Big|_{N_{tr}} N_{tr}$ is the gain coefficient, with $\frac{\partial g}{\partial N}\Big|_{N_{tr}}$ the differential gain at the transparency carrier density. Taking into account the proportional relation between the carrier number and the pump current below threshold ($N = I\tau_s/ed$), the gain material per unit length is defined as:

$$g = g_0 \ln\left(\frac{I}{I_0}\right) \ , \tag{A.41}$$

where I_0 is the transparency pump current, or the pump current for which the net gain equals the losses in the laser cavity.

A quick way to estimate the optical gain of a semiconductor laser is based on the Fourier transform of the subthreshold optical spectrum (Hofstetter and Thorntom, 1998). This function exhibits a central peak surrounded by higher harmonics symmetrically arranged to the center. The position of these peaks is given by $d = \pm nL/\pi$, where L is the cavity length and d is the optical path length inside the cavity (due to the emission condition of the cavity). The height of these peaks decreases exponentially when the order of the harmonic increases. In a logarithmic scale, there is a constant ratio between the height of the adjacent peaks in the Fourier transform of the subthreshold spectrum. This ratio is called the harmonic amplitude ratio (HAR, or r), and depends on the difference between the mirror loses and the cavity gain ($\beta = g - \alpha_i$):

$$r = R \cdot e^{-\beta L} \ , \tag{A.42}$$

where R is the power reflectivity of the laser mirrors and L stands for the cavity length.

A Fourier transform of the laser spectrum for several values of the pump current below threshold, gives a number of harmonic amplitude ratios, r (see Fig. A.3).

For known R and L values, it is possible to calculate the different loss/gain values for each pumping current. Then, we represent the calculated values of β versus the current values, and fitting with the material gain curve [Eq. (A.41)] we obtain:

$$\beta = g_0 \log\left(\frac{I}{I_0}\right) - \alpha_i \ , \tag{A.43}$$

where g_0 is the gain coefficient, I_0 is the current at transparency, I is the pump

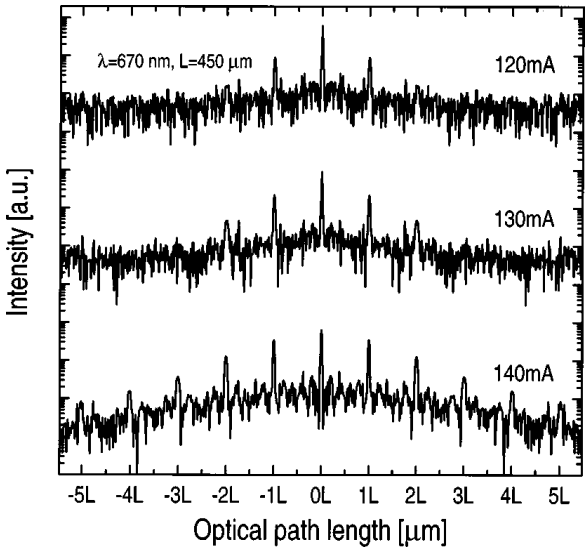

Figure A.3: *Fourier transforms of experimental laser spectra at pump current levels of 120, 130, and 140 mA, for a laser with approximately 150 mA of threshold [from Hofstetter and Thorntom (1998a)].*

current and α_i is the internal loss. We can obtain the g_0 and I_0 values, assuming a value for α_i.

Once g_0 is known, it is possible estimate the renormalized differential gain coefficient used in our simulations, which is related with the nonlinear laser gain $[G(N, |E|^2)]$ by Eq. (1.38).

Taking $g_0 = 200\ cm^{-1}$ from Hofstetter and Thorntom (1998), for instance, and the calculated value of $N_{tr} = 1.8\ 10^24\ \mathrm{m}^{-3}$ in section A.2.3, we have $\left.\frac{\partial g}{\partial N}\right|_{N_{tr}} \simeq 1.1 \times 10^{-20} m^2$ and using Eq. (1.37) the differential gain is:

$$g_N = \frac{c g_N}{n} \simeq 1 \times 10^{-24} \rho m^3 p s^{-1}$$

As we explained in Sec. A.2.3, in our model we use an adimensional value for the number of carriers at transparency (N_0), leading to a renormalization of the differ-

ential gain parameter used in the simulations. Assuming an approximate volume of the active region $V_{active} = 100\mu$ m^3 $= 1 \times 10^{-16}$ m^3, we consider a value of the differential gain coefficient equal to $g_N \simeq 1 \times 10^{-8}$ps^{-1}.

A.3 Light-current characteristics

One of the most important characteristics of a laser diode is the amount of light that it emits for a given pump current. The measurement of the light output of a laser diode as a function of the pump current results in the L-I curve, such as the one shown in Fig. A.4. As the injected current is increased, the laser first shows

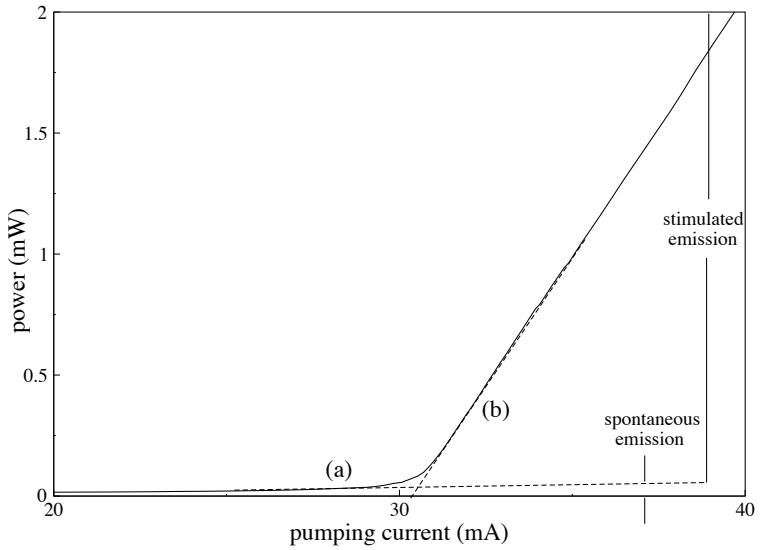

Figure A.4: *Light current characteristic for a solitary laser. Branch (a) and (b) display spontaneous and stimulated emission of the laser diode.*

spontaneous emission and the output power increases very slowly with the pumping current [Fig. A.4 (a)]. At a threshold current (I_{th}), the device begins to emit stimu-

lated radiation and the output power increases quickly (and approximately linearly) with the input current [Fig. A.4 (b)].

A.3.1 Threshold current

The first parameter that we can extract from the L-I curve is the value of the threshold current. The threshold current generally depends on the semiconductor material and on the laser structure. It can be measured by the intersection of the extrapolated spontaneous and laser emission lines, in the L-I curve (in Fig. A.4, (a) and (b) dashed lines). However, the threshold current depends considerably on the size and the cross-sectional area of the laser device. Hence, it is more appropriate to refer to threshold current density (J_{th}) rather than to threshold current (I_{th}). Threshold current density is determined by dividing the experimentally obtained threshold current by the cross sectional area of the laser.

A.3.2 External differential quantum efficiency

It is desirable to generate the most possible quantity of emitted light with the minimum pump current. The external differential laser efficiency, η_d, is a direct measure of ability of the laser to convert the injected current into emitted light, and it is defined as:

$$\eta_d = \frac{\Delta P/\Delta I}{hc/q\lambda} \tag{A.44}$$

where $\Delta P/\Delta I$ is the slope of the L-I curve, h is the Planck's constant, λ is the wavelength and q is the elementary electric charge.

For the L-I curve of Fig. A.4, with a $\lambda = 655.1$ nm, and a slope of 0.21 mW/mA,

we have $\eta_d = 22\%$.

A.3.3 Internal quantum efficiency

The internal quantum efficiency (η_i) is a measure of the efficiency of a laser in converting electron-hole pairs into photons within the laser diode structure. This parameter is independent of the geometry of the device, and thus it is adequate to compare different lasers. The expression that relates the external quantum efficiency (experimentally determined by Eq. (A.44)) and the internal quantum efficiency of a laser is given by (Petermann, 1988):

$$\frac{1}{\eta_d} = \frac{1}{\eta_i}\left[1 + \frac{2\alpha_i}{ln(1/R_1R_2)}L\right] \tag{A.45}$$

where α_i accounts for the internal loss, R_1 and R_2 are the reflectivities at the rear and front respectively laser/air interfaces and L is the cavity length.

Thus, plotting the inverse of the external differential quantum efficiency versus the cavity length, for different lasers of a same wafer semiconductor material, it would be possible to determine the η_i value from the vertical axis intercept point of the linear fit line.

As we mentioned above, internal quantum efficiency is a direct indication of the efficiency of a laser in converting electro-hole pairs (injected current) into photons (light) within the laser diode structure (Mobarman, Appl. Not. Newport, 2007). Not all the photons that are generated find their way out of the device; some of them are re-absorbed due to various internal loss mechanisms. As a result, the internal loss α_i, makes the external quantum differential efficiency smaller than the internal

quantum efficiency. Thus the value of α_i corresponds to the loss of the optical wave propagating through the laser diode cavity. Its value is determined experimentally by measuring the slope of the linear fit of the above expression Eq. (A.45).

A.3.4 Characteristic temperature

The characteristic temperature (T_0) of the laser diode is a measure of the temperature sensitivity of the laser. For high values of T_0, the laser has high threshold current and a weak dependence of η_d with the temperature, and thus it is thermally more stable. The threshold current of a semiconductor laser depends on temperature through:

$$I_{th} = I_c e^{(T/T_0)} \ , \tag{A.46}$$

which describes the empiric exponential increase of the threshold intensity with the temperature, with I_c a constant, and T_0 the characteristic temperature.

Figure A.5 shows the different light-current characteristic curves for a laser diode operating at various temperatures.

After taking the logarithm of Eq. (A.46) and differentiating both sides, we can obtain the value of T_0:

$$\Delta \ln(I_{th}) = \frac{1}{T_0} \Delta T \tag{A.47}$$

$$T_0 = \frac{\Delta T}{\Delta \ln(I_{th})} \tag{A.48}$$

The slope of the fitting values of the increasing temperature versus the natural logarithm of the threshold currents (i.e. obtained by Fig. A.5) gives the characteristic

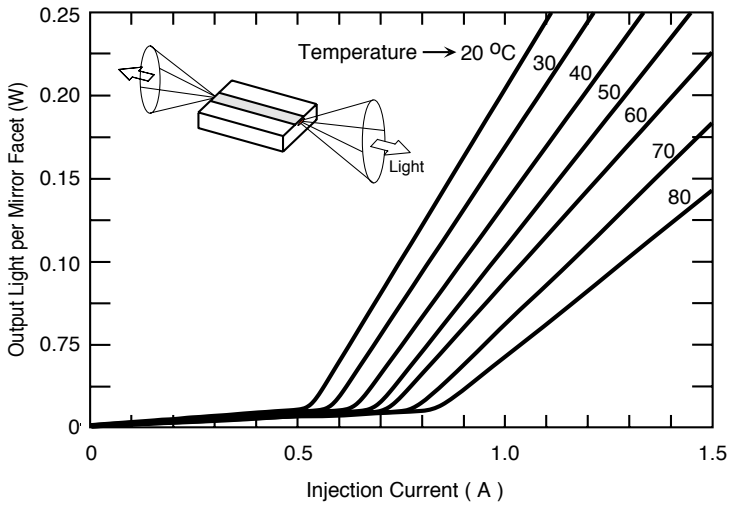

Figure A.5: *Light-current characteristic curves for a laser diode operating in different temperatures (from Mobarman, Appl. Not. Newport (2007)).*

temperature of the laser. Typical characteristic temperatures T_0 for AlGaInP multi-quantum-well lasers range from 100 to 140 K.

A.4 Linewidth enhancement factor

As we introduced in Sec. 1.2, the degree to which changes in the carrier density alter the refractive index and the absorption of the active layer (related with the imaginary part of the refractive index) is characterized by the linewidth enhancement factor α. In other words, the α factor relates the change with the population inversion (N) of the real (n) and imaginary (n'') parts of the refraction index (Henry, 1982):

$$\alpha = \frac{\partial n/\partial N}{\partial n''/\partial N} \tag{A.49}$$

The variations of the imaginary part of the refractive index can be related with gain variations due to changes in the carrier density through the condition for laser emission [Eq. (1.6)] as:

$$\frac{\partial n''}{\partial N} = -\frac{c}{2\omega}\frac{\partial g}{\partial N} \,, \tag{A.50}$$

where $\partial n''/\partial N$ and $\partial g/\partial N$ are the rate of change of the imaginary part of the refraction index and the gain induced by the population inversion, respectively, ω is the emission optical frequency and c the speed of light.

Using Eq. (A.50) the α parameter can quantify the dependence of the gain and refractive index on the population inversion:

$$\alpha = -\frac{\omega}{c}\frac{\partial n/\partial N}{\partial g/\partial N} \tag{A.51}$$

The relation between gain and index variations is shown in Fig. A.6, which represents the gain curves versus frequency (top) and the refractive index versus frequency (bottom) for two kinds of lasers: two-level lasers (left) and semiconductor lasers (right). In two-level lasers, e.g. gas lasers, the gain curve is always symmetric respect to the frequency [Fig. A.6(a)]. Accordingly, the change in the refractive index, n, crosses the zero line exactly at the gain peak. This situation remains unchanged for varying N [Fig. A.6(c)]. Thus, α is always zero in two-level lasers. As we can see in Fig. A.6(b), in semiconductor lasers the gain curve is asymmetric. This is due to the fact that the semiconductor material only absorbs photons above its band-gap (Lasher and Stern, 1964; Henry *et al*, 1981). Consequently, n is different from zero in the vicinity of the gain maximum, but is strongly dependent on N. Any change of N results in a change of n, and the linewidth enhancement factor is

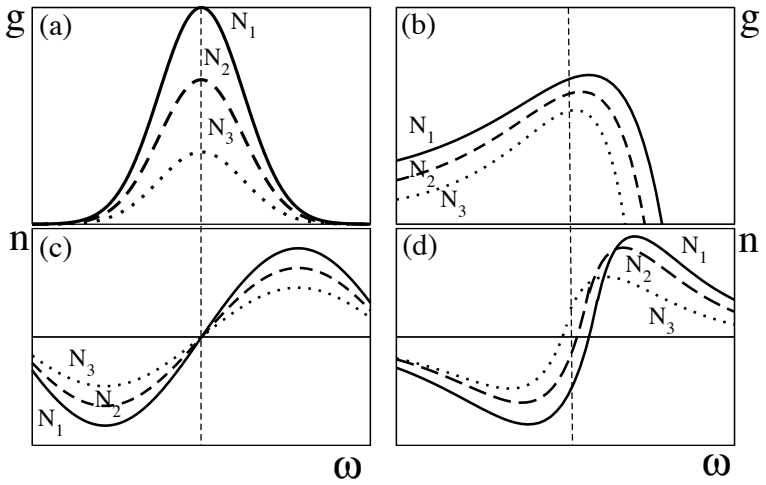

Figure A.6: *Gain curve and refractive index change for a two-level atomic laser (a, c) and for a typical bulk semiconductor laser (b, d); $N_1 > N_2 > N_3$ denote different levels of population inversion. Dotted lines mark the emission wavelength (adapted from Wieczorek* et al *(2005)).*

always nonzero.

The α factor is one of the fundamental parameters of semiconductor lasers. It is responsible for the enhancement of the laser linewidth, and affects the frequency chirp, the modulation response, the injection-locking range, and the effect of optical feedback. If we observe Fig. A.6(d), the refraction index decreases when the population inversion increases at the emission wavelength. The velocity group has to increase to compensate the decrease of the refractive index, and as a consequence the frequency decreases. Due to this, when we have a coherent injection (which causes a decrease of population inversion), the positive value of α results in a frequency downshift. An optimum injection from a transmitter to a receiver laser occurs when the optical frequencies of the two lasers are nearly equal (Sec. 2.1.1). Then the receiver and transmitter optical spectra coincide, and the oscillation frequency of

the receiver is locked to that of the transmitter laser. When the injected frequency is detuned towards higher frequencies from the optimum, the receiver laser output power decreases. The carrier density increases and the refractive index in the active region decreases, which accompany the output decrease. It causes an upshift of the receiver optical frequency, resulting in a partial compensation of the detuning. In contrast, as the injected light frequency is detuned towards the low frequency side, the population inversion increase amplifies the detuning, and the locking between the outputs decrease. Because of this, the laser can achieve locking for negative detuning at a much smaller injected light than for positive detuning (Lang, 1982).

From a dynamical point of view, it is usually said that α couples the intensity variations of the light inside the laser to its phase variations. It is due to the fact that any change on N is reflected in a change of n, which changes the phase of the lasing mode (Masoller, 1997).

There are many reported techniques to measure the value of α. For instance, it is possible to determine α through a measure of the optical spectrum below threshold for different values of the pump current. The α value is then given by the expression (Henning and Collins, 1983):

$$\alpha = \frac{2\pi}{\delta\lambda} \frac{d\lambda_i}{d\{\ln\left[\sqrt{r_i - 1}/\sqrt{r_i + 1}\right]\}} \ , \tag{A.52}$$

where $\delta\lambda$ is the longitudinal mode spacing, $d\lambda_i$ is the increase of wavelength of a mode between two different pump currents, and r_i is :

$$r_i = \frac{P_i + P_{i+1}}{2V_i} \ , \tag{A.53}$$

where P_i and P_{i+1} are the optical power of two consecutive modes, and V_i is the optical power of the valley between them. With this technique it is possible to approximate the α parameter value inside a range that for our lasers lies between 3 and 4.5.

Appendix B

Statistical tools

B.1 Correlations

Correlation is a measure of how related two quantities are. A high correlation means that there is high resemblance between the two data sets being compared. To compare a set of data with itself we use the auto-correlation function. To compare two different data sets we compute the cross-correlation function. When applied to analyze the output intensity of the lasers, these tools reveal useful information about the characteristics of the system, such as the time scales of the dynamics.

In order to calculate the cross-correlation function of two time series $P_1(t)$ and $P_2(t)$, we calculate the covariance (or how much two variables vary togetther) of both series shifted over all the possible values of Δt (lag or delay time), and normalize it to unity:

$$\Gamma_{corr}(\triangle t) = \frac{\langle (P_1(t) - \langle P_1 \rangle)(P_2(t + \triangle t) - \langle P_2 \rangle) \rangle}{\sqrt{\langle (P_1(t) - \langle P_1 \rangle)^2 \rangle \langle (P_2(t) - \langle P_2 \rangle)^2 \rangle}} \tag{B.1}$$

In the case of only one time series $P(t)$, the auto-correlation function is defined as:

$$\Gamma_{auto}(\triangle t) = \frac{\langle (P(t) - \langle P \rangle)(P(t + \triangle t) - \langle P \rangle) \rangle}{\langle (P(t) - \langle P \rangle)^2 \rangle} \tag{B.2}$$

Here the angle brackets indicate time averaging.

B.1.1 Autocorrelation function

With the auto-correlation function one can determine how quickly a signal changes with respect to time, and whether the process repeats itself in a periodic way. To illustrate the characteristics of the auto-correlation function we study the dynamics of typical semiconductor laser configurations.

Figure B.1 shows the auto-correlation function of the numerical time series of

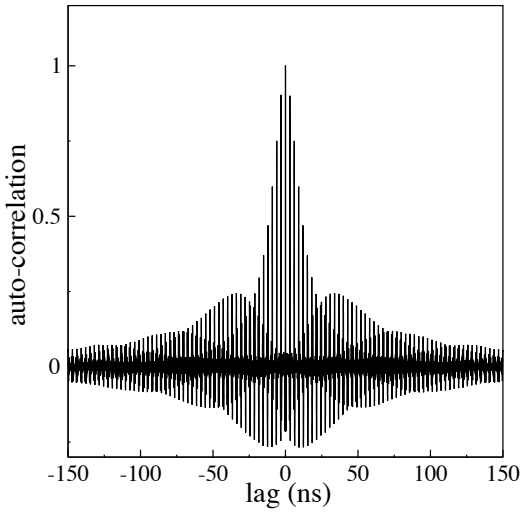

Figure B.1: *Auto-correlation function for a laser with optical feedback ($\tau_f = 3$ ns) in the low frequency fluctuation regime.*

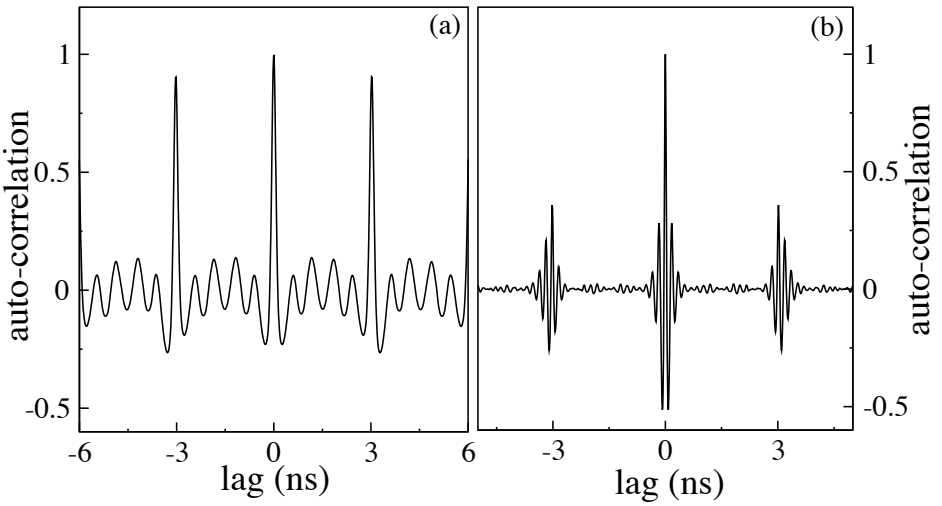

Figure B.2: *Detail of the auto-correlation function for a laser with optical feedback ($\tau_f = 3$ ns): (a) low frequency fluctuation regime, and (b) coherence collapse regime.*

the light intensity emitted by a laser with optical feedback in the low-frequency-fluctuation regime (typical parameters are in Table A.1 of Sec. A.2). The envelope of this function exhibits a maximum at zero (equal to one due to the normalization) and a secondary maximum at a time that corresponds to the mean frequency of the intensity dropouts. A more detailed observation of the auto-correlation function denotes a high correlation for time intervals corresponding to the delay time (τ_f) and multiples of it [Fig. B.2(a)]. Between these secondary peaks, a relatively strong modulation exists, which is absent in the coherence collapse regime [Fig. B.2(b), typical parameters in Table A.1 of Appendix A]. The latter is due to the high irregularity of the coherence collapse regime.

The envelope also decreases much faster in this regime, due to the higher irregularity. The high auto-correlation value at τ_f is an evidence of the existence of memory due to the delay.

B.1.2 Cross-correlation function

When comparing two different signals with the cross-correlation function, one can observe how similar the signals are. When the signals are similar in shape and unshifted with respect to each other, the maximum correlation value occurs at a zero delay time. If one signal is shifted with respect to the other and the signals are periodic, the cross-correlation function takes negative and positive values for the out-of-phase and in-phase coincidences, respectively. In the chaotic case the cross-correlation takes mostly zero values, and it is only high (and positive) for specific values of the shift.

With the cross-correlation function we can observe differences at the output intensities when we change the architecture of the system that are not evident at first sight. The mean feature revealed by the analysis of the cross-correlation function is how the lasers synchronize their output intensities. The highest peak of the cross-correlation function indicates three things: (i) the degree of synchronization, (ii) which laser leads the dynamics, and (iii) the delay between the signals. The height of the maximum peak reveals the degree of synchronization. The location of the peak with respect to zero (at the left or the right), indicates which laser is the leader, and its value reveals the delay between the signals. The fall-off of the envelope is faster or slower depending on the robustness of the synchronization: if the cross-correlation peaks decrease very fast, the series are correlated during only a few roundtrips of the light, and therefore the states of the initial dynamics are weakly correlated after a small time.

The directionality of the coupling between the lasers is also reflected on the cross-correlation function. The relationship between feedbacks and coupling strengths

have high influence in the location of the highest peak. The phase differences of the external cavities are also very important. The position of the peaks and the distance between them will be determined by the feedbacks and coupling times.

There is a large difference between cross-correlation functions depending on the relation between feedback and coupling strengths, even for the same architecture. To see this effect, we now consider the same feedback and coupling time ($\tau_c = \tau_f$) in three numerical simulated cases: unidirectionally coupled lasers with only feedback in the master laser, bidirectionally coupled lasers without feedback, and bidirectionally coupled lasers with feedback in each laser. Figure B.3 shows the

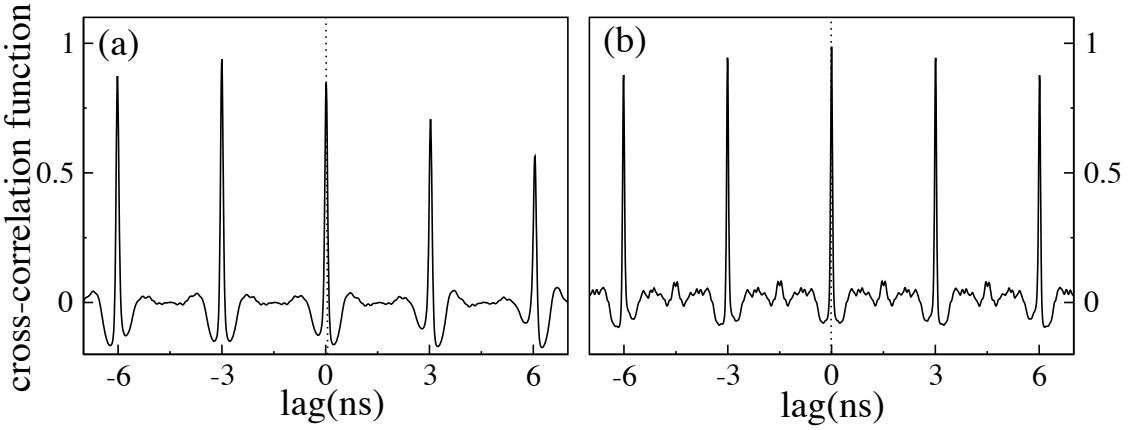

Figure B.3: *Cross-correlation function for unidirectionally coupled lasers with feedback in the emitting laser, in the low frequency fluctuation regime with $\tau_f = \tau_c = 3$ ns: (a) different coupling and feedback strengths $\kappa_c = 80\ ns^{-1}$, $\kappa_f = 30\ ns^{-1}$ and (b) same coupling and feedback strengths $\kappa_c = \kappa_f = 80\ ns^{-1}$.*

calculated cross-correlation function for unidirectionally coupled lasers with only feedback in the master laser. The cross-correlation function shows multiple peaks separated a distance equal to τ_f, with a maximum peak value whose location depends on the relation between the coupling and feedback strengths. Note that here $\tau_c = \tau_f$.

It is possible to distinguish which cavity time affects the distance between peaks calculating the cross-correlation function for the same architecture with different cavity lengths.

Considering higher strength for the coupling than for the feedback, the cross-correlation function shows a highest peak to the left at the coupling time ($-\tau_c$), which indicates that the laser with independent dynamics is the leader [Fig. B.3(a)]. We have a transmission of information from the leader (transmitter) to the laggard (receiver). The leader has the independent dynamics (due to the feedback) and the laggard synchronizes its output to the signal of the leader, with a delay time equal to the time needed by the light to travel between the lasers (Tang and Liu, 2003).

Figure B.3(b), shows the cross-correlation function when we consider the same amount of coupling and feedback strengths. The highest peak occurs at zero lag, $\tau_c - \tau_f$, which corresponds to zero lag for equal feedback and coupling times. In this case the information is transferred instantaneously to the receiver laser (the one without independent dynamics). That is, both signals are synchronized without delay because the light spends the same time to return from the mirror than in traveling to the other laser [see Gross *et al* (2006)].

Figure B.4 represents the cross-correlation for bidirectionally coupled lasers without feedback. We name $\kappa_{1,2}$ and $\kappa_{2,1}$ the two different coupling strengths in each direction. In bidirectionally coupled lasers without feedback, no single laser has independent dynamics, and the chaotic dynamics is induced by the coupling. The cross-correlation function shows multiple peaks separated a distance equal to $2\tau_c$. This can be explained if we take in mind that the signal of one laser synchronizes the other laser whose signal, in turn, is injected into the first one with a delay $2\tau_c$ after

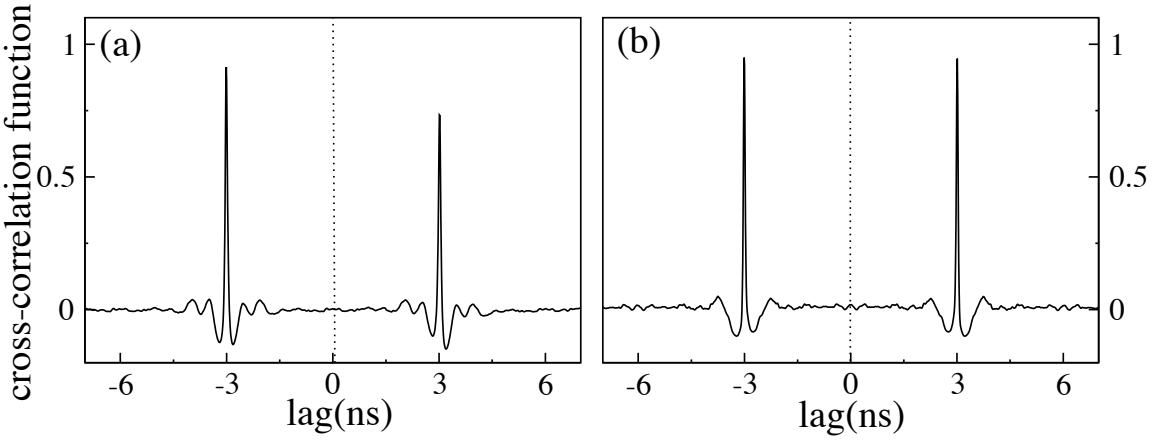

Figure B.4: *Cross-correlation function for bidirectionally coupled lasers without feedbacks in the low frequency fluctuations regime with $\tau_f = \tau_c = 3$ ns: (a) asymmetrical coupling $\kappa_{1,2} = 80\ ns^{-1}$, $\kappa_{2,1} = 30\ ns^{-1}$ and (b) symmetrical coupling $\kappa_{1,2} = \kappa_{2,1} = 80\ ns^{-1}$.*

the emission of the original signal (Heil *et al*, 2001). Figure B.4(a) shows the highest peak at $-\tau_c$ for the asymmetrical situation ($\kappa_{1,2} > \kappa_{2,1}$), with a clear leader in the dynamics of the system. In plot B.4(b) we can see the cross-correlation function for symmetrical coupling strengths ($\kappa_{1,2} = \kappa_{2,1}$). In this case two symmetrical peaks appear at $\pm\tau_c$, showing an alternation of the leader role between both lasers.

This changes in the presence of feedback for each laser. Figure B.5 plots the cross-correlation function for bidirectionally coupled lasers in a symmetrical way ($\kappa_{1,2} = \kappa_{2,1} = \kappa_c$) with the same amount of feedback in each one ($\kappa_{1,1} = \kappa_{2,2} = \kappa_f$). The cross-correlation function shows multiple peaks separated a distance equal to $\tau_c = \tau_f$ (which in the case of different coupling and feedback times corresponds to the minimum of the two quantities), and highest peaks depending on the relation between the coupling and feedback strengths. Figure B.5(a), for $\kappa_c > \kappa_f$, shows two highest peaks at $\pm\tau_c$ due to the fact that the coupling is stronger than the feedback.

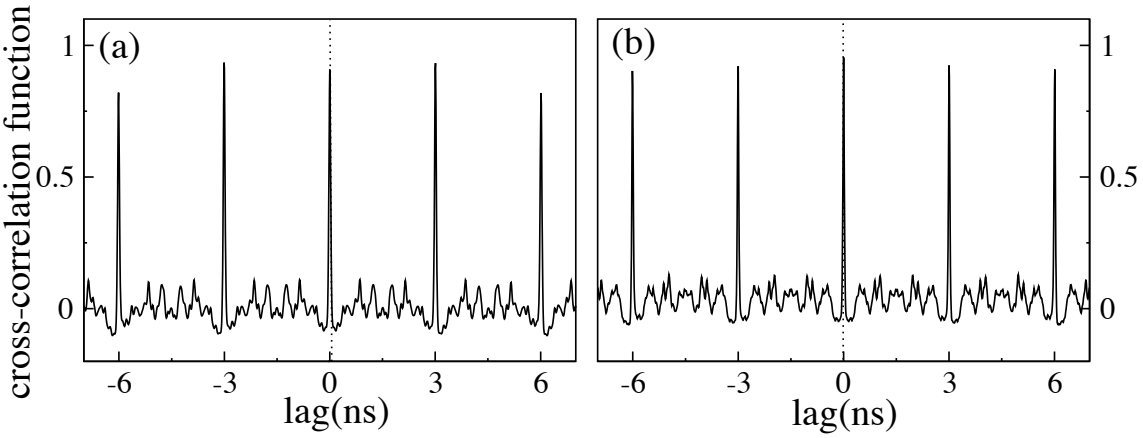

Figure B.5: *Cross-correlation function for bidirectionally coupled lasers with the same amount of feedback in each laser in the low frequency fluctuations regime with* $\tau_f = \tau_c = 3$ *ns: (a) different coupling and feedback strengths* $\kappa_c = 80\ ns^{-1}$, $\kappa_f = 8\ ns^{-1}$ *and (b) same coupling and feedback strengths* $\kappa_c = 80\ ns^{-1}$, $\kappa_f = 80\ ns^{-1}$.

Figure B.5(b) plots the cross-correlation for $\kappa_c = \kappa_f$, showing the zero-lag solution of the system (synchronization without delay). The time needed by the light to affect individually each laser (τ_f) is the same that it needs to travel to the other laser (τ_c). An instantaneous synchronization occurs in this case due to the symmetry of the system (Gross *et al*, 2006).

B.2 Sliding-correlation function

The cross-correlation function is a time-averaged quantity. The expected value of the correlation for any pair of values must be computed by averaging $P_1(t) - P_2(t + \Delta t)$ over the whole duration of the process, where Δt is the lag or delay time between the signals. Sometimes this averaging process hides information. When we need to estimate the time-varying correlation between signals, we calculate the sliding

cross-correlation function. To that end, we divide the signal into sliding windows of a size such that the correlation can be considered stationary on the time scale of the window's width. Then the cross-correlation is computed as a function of the lag within each window, which slides along the time axis to obtain correlations for different time values.

In Fig. B.6 we show the sliding cross-correlation function of numerical simulated series for two different situations: unidirectionally coupled lasers with feedback in one laser [Fig. B.6(a,b)], and bidirectionally coupled lasers [Fig. B.6(c,d)]. In the

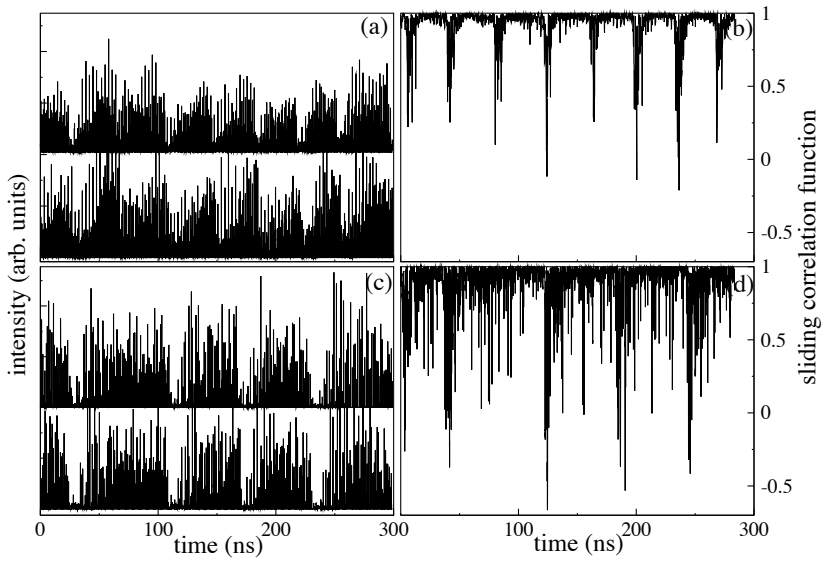

Figure B.6: *Numerical output intensities and sliding cross-correlation function for two unidirectionally coupled lasers with feedback in the emitting laser (a,b), and bidirectionally coupled lasers without feedback (c,d).*

unidirectional case, synchronization is lost during the dropout event, just after the fall of the leader towards zero intensity. The output intensities of both lasers are correlated for a while, but synchronization is lost during short periods of time, which is impossible to detect in the cross-correlation function. If we know the delay time

between both signals (due to a previous calculation of the cross-correlation) we can shift the signals to coincide and calculate the cross-correlation function in an adequate time window. Then we can shift this window along the time axis to see the evolution in time of the cross-correlation function.

Loss of synchronization for bidirectional coupling is revealed by the drop to zero of the sliding correlation, not only during the dropout as in the unidirectional coupling case, but also at intermediate times. The change of the leader in bidirectional coupling produces synchronization loss between the dropouts, as well as during the dropouts themselves.

In summary, the study of the temporal evolution of the cross-correlation function gives more information than provided by the simple evaluation of the cross-correlation function.

Appendix C

Numerical techniques

C.1 Integration of deterministic delay-differential equations

Delay differential equations (DDE) can be classified in different ways, depending on the type of delay (constant, variable, or state dependent), or the number of delays (finite number for discrete DDEs, or a continuum number of delays for distributed DDEs). We consider the case of multiple constant delays:

$$\begin{aligned} \dot{y}(t) = &\quad f\left[t, y(t), y(t-\tau_1), ...y(t-\tau_n)\right] \\ y(t) = &\quad \phi(t) \qquad t \in [-\tau_{max}, 0] \end{aligned} \tag{C.1}$$

where the delays are $\tau_i > 0$.

We can solve a system of finite dimension if we have the initial conditions of the

state variables. For a DDE system, at every temporal step we need the past history of the variables between $-\tau_{max}$ and 0, where τ_{max} is the maximum value of the delay of the system (Bellen and Zennaro, 2003).

Let us consider, without loss of generality, the case of a single delay:

$$\begin{aligned} \dot{y}(t) = &\quad f\left[t, y(t), y(t-\tau)\right] \\ y(t) = &\quad \phi(t) \qquad t \in [-\tau, 0] \end{aligned} \tag{C.2}$$

The initial way to work with this type of equations is the same as for ordinary differential equations (ODEs), but for $t < 0$ the variable is an arbitrary initial function, and for $t > 0$ the solution is determined by the differential equation. ODE solvers consider the first derivative as continuous: any discontinuity would be propagated and enhanced in each time step. The discontinuity at $t = 0$ in Eq. (C.2) forces us to vary the way of solve the problem in the case of DDE's.

The way to face up to the problem is dividing the total simulation time into time intervals of length τ and solving each time interval with an ODE solver. This leads to an approximation to the solution of the DDE in that interval, which can be used to find an approximate solution on the next time interval.

Figure C.1 displays a scheme of the time divisions used to integrate Eq. (C.2). The major time divisions into intervals of length τ are denoted by $1\tau, 2\tau$...., etc. The integration of each interval of length τ requires a division into n subintervals of length h, which is the integration time step of the algorithm. These divisions can be expressed as:

$$t_i = t_0 + ih \qquad \text{for } i = 0 \text{ to } n \ ,$$

for each interval time of length τ. As the first initial condition we define a vector of

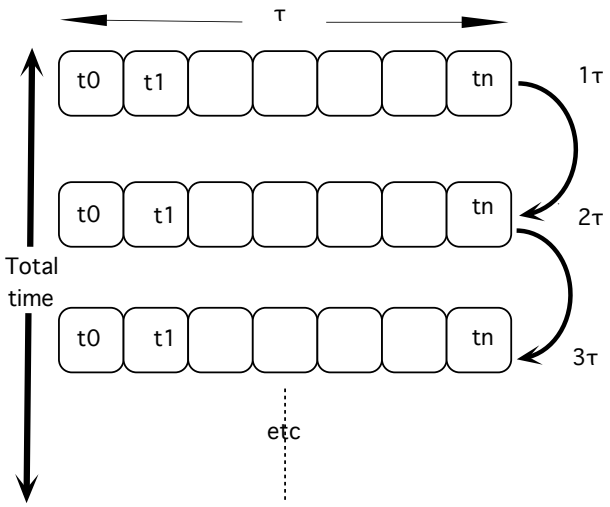

Figure C.1: *Division of total time into time intervals of length τ. Each interval is divided in n steps of length h, to apply the ODE algorithm. The initial condition for the first interval τ is defined as zero value, and each subsequent interval τ uses the value integrated at the previous interval.*

dimension $n = \tau/h$, which will be used to find the approximate solution of the first time interval 1τ. Then we fill the first 1τ vector with these values, and use them as initial condition to integrate the next time interval 2τ, and so on until the last τ interval.

The numerical algorithm used to integrate the τ intervals is very similar to the ones used to integrate ODEs, but introducing this delayed function into the algorithm.

Using the differential equation (C.2), we can determine the instantaneous rate of change of y at time t_0:

$$\dot{y}(t_0) = f\left(t_0, y(t_0), y(t_0 - \tau)\right) = f\left(t_0, y_0, y_{\tau 0}\right) \tag{C.3}$$

It is expected that the rate of change of the function remains near of $f(t_0, y_0, y_{\tau 0})$ for t close to t_0. Then we can approximate the function defined in the first time interval 1τ, y_1, for each small step h as:

$$\begin{aligned} t_1 &= t_0 + h \\ y_1 &= y_0 + f(t_0, y_0, y_{\tau 0})(t_1 - t_0) = y_0 + hf(t_0, y_0, y_{\tau 0}) \end{aligned} \tag{C.4}$$

and for a t close to t_i we can approximate the rate of change of the function for the next step τ to:

$$y_{i+1} = y_i + hf\left(t_i, y_i, y_{i\tau}\right) \tag{C.5}$$

where $y_i = y(t_i)$ is the function evaluated a time step h before and $y_{i\tau} = y(t_i - \tau)$ is the function evaluated a time step h before but from the previous τ division. That is the Euler's method, where h is the step size.

An improved variation of the Euler's method consists in approximating the function by the average of the values at t_i and t_{i+1} to find the rate of change of the function. This results in:

$$\begin{aligned} k &= y_i + hf(t_i, y_i, y_{i\tau}) \\ y_{i+1} &= y_i + \frac{h}{2}\left[f\left(t_i, y_i, y_{i\tau}\right) + f\left(t_{i+1}, k, y_{i+1,\tau}\right)\right] \end{aligned} \tag{C.6}$$

This is called the improved Euler algorithm or the Heun method. Heun's method is based on the evaluation of an approximation of $f(t_{i+1}, k, y_{i+1,\tau})$ by replacing the value of k with an estimate derived from the original Euler method, with the resulting above iteration scheme. In evaluating the mean value over one step h, the error

will be of order h^2.

C.2 Integration of the noise term

In our case, we have to implement the integration of a multiplicative noise in a delay differential equation (San Miguel and Toral, 2000). We have a system of the form:

$$\begin{aligned} \dot{y}(t) = &\quad f\left[t, y(t), y(t-\tau)\right] + g[t, y(t)]\zeta(t) \\ y(t) = &\quad \phi(t) \qquad t \in [-\tau, 0] \ , \end{aligned} \tag{C.7}$$

where $\zeta(t)$ is a Gaussian white noise with zero mean $[\langle\zeta(t)\rangle = 0]$, and correlation $\langle\zeta(t)\zeta^*(t')\rangle = 2\delta(t-t')$.

In our system, the noise term is not directly affected by the delay. That is $g[t, y(t)]$ does not depend on $y(t-\tau)$, and therefore we can consider the integration of the noise as an added term in the algorithm of the delay differential equation. Then we can apply the approximated algorithm:

$$\begin{aligned} k &= y_i + hf(t_i, y_i, y_{i\tau}) + h^{1/2}u(t)g(t_i, y_i) \\ l &= y_i + hf(t_i, y_i) \\ y_{i+1} &= y_i + \frac{h}{2}\left[f(t_i, y_i, y_{i\tau}) + f(t_{i+1}, k)\right] + \frac{h^{1/2}u(t)}{2}\left[g\left(t_i, y_i\right) + g\left(t_{i+1}, l\right)\right] \end{aligned} \tag{C.8}$$

which is known as the stochastic Heun method. The advantage of the stochastic Heun method is that it treats better the deterministic part, and avoids some instabilities of the Euler's method.

Bibliography

Adachi, S., H. Kato, A. Moki, and K. Ohtsuka, 1994, *Refractive index of* $(Al_xGa_{1-x})_{0.5}In_{0.5}P$ *quaternary alloys*, J. Appl. Phys. **75**, 478.

Agrawal, G. P. and N. K. Dutta, 1986, *Long wavelength semiconductor lasers*, ed. Van Nostrand Reinhold, New York.

Ahlers, V., U. Parlitz, and W. Lauterborn, 1998, *Hyperchaotic dynamics and synhronization of external cavity semiconductor lasers*, Phys. Rev. E **58**, 7208.

Alferov, Zh., 2000, *Double heterostructure lasers: early days and future perspectives*, IEEE J. Select. Top. Quant. Electron. **6**, 832.

Annovazzi-Lodi, V., S. Donati, and M. Manna, 1994, *Chaos and locking in a semiconductor laser due to external injection*, IEEE J. Quant. Electron. **30**, 1537.

Annovazzi-Lodi, V., S. Donati, and A. Scire, 1996, *Synchronization of chaotic injected-laser systems and its application to optical cryptography*, IEEE J. Quantum Electron. **32**, 953.

Annovazzi-Lodi, V., S. Donati, and A. Scire, 1997, *Synchronization of chaotic lasers*

by optical feedback for cryptographic applications, IEEE J. Quantum Electron. **33**, 1449.

Argyris, A., D. Syvridis, L. Larger, V. Annovazzi-Lodi, P. Colet, I. Fischer, J. García-Ojalvo, C. R. Mirasso, L. Pesquera, and K. A. Shore, 2005, *Chaos-based communications at high bit rates using commercial fibre-optic links*, Nature **437**, 343.

Atay, F. M., 2003, *Distributed delays facilitate amplitude death of coupled oscillators*, Phys. Rev. Lett. **91**, 094101.

Balenzuela, P. and J. García-Ojalvo, 2005, *Neural mechanism for binaural pitch perception via ghost stochastic resonance*, Chaos **15**, 023903.

Bartussek, R. and P. Hänggi, 1994, *Stochastic resonance in optical bistable systems*, Phys. Rev. E **49**, 3930.

Basov, N. G., 1968, *Dynamics of injection lasers*, IEEE J. Quantum Electron. **4**, 855.

Bellen, A. and M. Zennaro, 2003, *Numerical methods for delay differential equations*, Clarendon Press.

Benzi, R., S. Sutera, and A. Vulpiani, 1981, *The mechanism of stochastic resonance*, J. Phys. A **14**, L453.

Besnard, P., B. Meziane, and G. M. Stephan, 1993, *Feedback phenomena in a semiconductor laser induced by distant reflectors*, IEEE J. Quantum Electron. **29**, 1271.

Boccaletti, S., J. Kurths, G. Osipov, D. L. Valladares, and C. S. Zhou, 2002, *The synchronization of chaotic systems*, Phys. Rep. **366**, 1.

Boccaletti, S., V. Latora, Y. Moreno, M. Chavez, and D. U. Hwang, 2006, *Complex networks: structure and dynamics*, Phys. Rep. **424**, 175.

Bogatov, A. P., P. G. Eliseev, and B. N. Sverdlov, 1975, *Anoumalous interaction of spectral modes in a semiconductor laser*, IEEE J. Quantum Electron. **11**, 510.

Bryant, H. L. and J. P. Segundo, 1976, *Spike initiation by transmembrane current: a white-noise analysis*, J. Physiol. **260**, 279.

Broom, R. F., E. Mohn, C. Risch, and R. Salathê, 1970, *Microwave self-modulation of a diode laser coupled to an external cavity*, IEEE J. Quantum Electron. **6**, 328.

Buldú, J. M., J. García-Ojalvo, C. R. Mirasso, M. C. Torrent, and J. M. Sancho, 2001, *Effect of external noise correlation in optical coherence resonance*, Phys. Rev. E **64**, 051109.

Buldú, J. M., J. García-Ojalvo, M. C. Torrent, R. Vicente, T. Pérez, and C. R. Miraso, 2002, *Entrainment of optical low-frequency fluctuations is enhanced by coupling*, Fluct. and Noise Lett. **3**, L127.

Buldú, J. M., J. García-Ojalvo, C. R. Mirasso, and M. C. Torrent, 2002a, *Stochastic entrainment of optical power dropouts*, Phys. Rev. E **66**, 021106.

Buldú, J. M., R. Vicente, T. Pérez, C. R. Miraso, M. C. Torrent, and J. García-Ojalvo, 2002b, *Periodic entrainment of power dropouts in mutually coupled semiconductor lasers*, Appl. Phys. Lett. **27**, 5105.

Buldú, J. M., 2003, *Entrainment of semiconductor lasers: noise, modulation and synchronization*, PhD Thesis, Universitat Poltècnica de Catalunya, Terrassa.

Buldú, J. M., D. R. Chialvo, C. R. Mirasso, M. C. Torrent, and J. García-Ojalvo, 2003, *Ghost resonance in a semiconductor laser with optical feedback*, Europhys. Lett. **64**, 178.

Buldú, J. M., J. García-Ojalvo, and M. C. Torrent, 2004, *Delay-induced resonances in an optical system with feedback*, Phys. Rev. E **61**, 046207.

Buldú, J. M., M. C. Torrent, and J. García-Ojalvo, 2005, *Demultiplexing chaos from multimode semiconductor lasers*, IEEE J. Quantum Electron. **41**, 164.

Buldú, J. M., C. M. Gonzalez, J. Trull, M. C. Torrent, and J. García-Ojalvo, 2005a, *Coupling-mediated ghost resonance in mutually injected lasers*, Chaos **15**, 013103.

Buldú, J. M., T. Heil, I. Fischer, M. C. Torrent, and J. García-Ojalvo, 2006, *Episodic synchronization via dynamic injection*, Phys. Rev. Lett. **96**, 024102.

Bulsara, A., E. W. Jacobs, T. Zhou, F. Moss, and L. Kiss, 1991, *Stochastic resonance in a single neuron model: theory and analog simulation*, J. Theor. Biol. **152**, 531.

Calvo, O., D. R. Chialvo, V. M. Eguiluz, C. R. Mirasso, and R. Toral, 2004, *Anticipated synchronization: a metaphorical linear view*, Chaos **14**, 7.

Calvo, O. and D. R. Chialvo, 2006, *Ghost stochastic resonance in an electronic circuit*, Int. J. Bif. Chaos **16**, 731.

Ciszak, M., O. Calvo, C. Masoller, C. R. Mirasso, and R. Toral, 2003, *Anticipating*

the response of excitable systems driven by random forcing, Phys. Rev. Lett. **90**, 204102.

Coffman, K., W. D. McCormick, and H. L. Swinney, 1986, *Multiplicity in a chemical reaction with one-dimensional dynamics*, Phys. Rev. Lett. **56**, 999.

Colet, P. and R. Roy, 1994, *Digital communication with synchronized chaotic lasers*, Opt. Lett. **19**, 2056.

Chialvo, D. R. and A. V. Apkarian, 1993, *Modulated noisy biological dynamics. Three examples*, J. Stat. Phys. **70**, 375.

Chialvo, D. R., O. Calvo, D. L. Gonzalez, O. Piro, and G.V. Savino, 2002, *Subharmonic stochastic synchronization and resonance in neuronal systems*, Phys. Rev. E **65**, 050902(R).

Chialvo, D. R., 2003, *How we hear what is not there: a neural mechanism for the missing fundamental illusion*, Chaos **13**, 1226.

Chien, R. L., 1993, *Shift of mode-hopping wavelength in single-mode semiconductor lasers*, Appl. Spectrocopy **47**, 1716.

Crow, G. C. and R. A. Abram, 1997, *Monte Carlo simulations of carrier transport in AlGaInP laser diodes*, IEEE J. Quantum Electron. **33**, 1551.

Cuomo, K. M. and A. V. Oppenheim, 1993, *Circuit implementation of synchronized chaos with applications to communications*, Phys. Rev. Lett. **71**, 65.

Cuomo, K. M., A. V. Oppenheim, and S. H. Strogatz, 1993, *Synchronization of*

Lorenz based chaotic circuits with applications to communications, IEEE Trans. Circ. Syst. II **40**, 626.

Debnath, G., T. Zhous, and F. Moss, 1989, *Remarks on stochastic resonance*, Phys. Rev. A **39**, 4323.

Dellunde, J., 1996, *Gain-switching and current modulation of semiconductor lasers with optical injection*, PhD Thesis, Universitat Politècnica de Catalunya, Terrassa.

Dente, G. C., P. S. Durkin, K. A. Wilson, and Ch. E. Moeller, 1988, *Chaos in the coherence collapse of semiconductor lasers*, IEEE J. Quantum Electron. **24**, 2441.

Dicke, R. H., 1958, *Molecular amplification and generation systems and methods*, U. S. Patent 2,851,652.

Donati, S. and C. R. Mirasso, 2002, *Special issue on optical chaos and applications to cryptography*, IEEE J. Quantum Electron. **38**, 1138.

Dumke, W. P., 1962, *Interband transitions and maser action*, Phys. Rev. **127**, 1559.

Edmonds, H. D. and A. W. Smith, 1970, *Second-harmonic generation with the GaAs laser*, IEEE J. Quantum Electron. **6**, 356.

Eguia, M. C., G. B. Mindlin, and M. Guidici, 1998, *Low-frequency fluctuations in semiconductor lasers with optical feedback are induced with noise*, Phys. Rev. E **58**, 2636.

Eguia, M. C. and G. B. Mindlin, 1999, *Semiconductor laser with optical feedback: from excitable to deterministic low-frequency fluctuations*, Phys. Rev. E **60**, 1551.

Eurich, C. W., A. Thiel, and L. Fahse, 2005, *Distributed delays stabilize ecological feedback systems*, Phys. Rev. Lett. **94**, 158104.

van Exter, M. P. and J. P. Woerdman, 1992, *Determination of the α-factor of a Fabry-Perot-type semiconductor laser by injection locking*, Elect. Lett. **28**, 1607.

Fauve, S. and F. Heslot, 1983, *Stochastic resonance in a bistable system*, Phys. Lett. A **97**, 5.

Fischer, I., G. H. M. van Tartwijk, A. M. G. Levine, W. Elsässer, E. Göbel, and D. Lenstra, 1996, *Fast pulsing and chaotic itinerancy with a drift in the coherence collapse of semiconductor lasers*, Phys. Rev. Lett. **76**, 220.

Fischer, I., Y. Liu, and P. Davis, 2000, *Synchronization of chaotic semiconductor laser dynamics on subnanosecond time scales and its potential for chaos communication*, Phys. Rev. A **62**, 011801(R).

Fischer, I., R. Vicente, J. M. Buldú, M. Peil, C. R. Mirasso, M. C. Torrent, and Jordi García-Ojalvo, 2006, *Zero-lag long-range synchronization via dynamical relaying*, Phys. Rev. Lett. **97**, 123902.

Fujiwara, M., K. Kubota, and R. Lang, 1981, *Low-frequency intensity fluctuation in laser diodes with external optical feedback*, Appl. Phys. Lett. **38**, 217.

Gammaitoni, L., E. Menichella-Saetta, S. Santuchi, F. Marchesoni, and C. Presilla, 1989, *Periodically time-modulated bistable systems: stochastic resonance*, Phys. Rev. A **40**, 2114.

Gammaitoni, L., P. Hänggi, P. Jung, and F. Marchesoni, 1998, *Stochastic resonance*, Rev. Mod. Phys. **70**, 223.

García-Ojalvo, J. and J. M. Sancho, 1999, *Noise in spatially extended systems*, Springer, New York.

García-Ojalvo, J., J. Casademont, C. R. Mirasso, M. C. Torrent, and J. M. Sancho, 1999, *Coherence and synchronization in diode-laser arrays with delayed global coupling*, Int. J. Bifurcation Chaos **9**, 2225.

García-Ojalvo, J., M. B. Elowitz, and S. H. Strogatz, 2004, *Modeling a synthetic multicellular clock: repressilators coupled by quorum sensing*, PNAS. Proc. of the Nat. Academy of Sci. of Unit. States of Amer. **101**, 10955.

Giacomelli, G., M. Guidici, S. Balle, and J. R. Tredicce, 2000, *Experimental evidence of coherence resonance in an optical system*, Phys. Rev. Lett. **84**, 3298.

Giudici, M., C. Green, G. Giacomelli, U. Nespolo, and J. R. Tredicce, 1997, *Andronov bifurcation and excitability in semiconductor lasers with optical feedback*, Phys. Rev. E **55**, 6414.

Giudici, M., C. Green, G. Giacomelli, U. Nespolo, and J. R. Tredicce, 1998, *Reply to "Comment on 'Andronov bifurcation and excitability in semiconductor lasers with optical feedback'*, Phys. Rev. E **58**, 4043.

Glass, L., 2001, *Synchronization and rhythmic processes in physiology*, Nature **410**, 277.

Goedgebuer, J. P., L. Larger, and H. Porte, 1998, *Optical cryptosystem based on synchronization of hyperchaos generated by a delayed feedback tunable laser diode*, Phys. Rev. Lett. **80**, 2249.

González, C. M., M. C. Torrent, and J. García-Ojalvo, 2007, *Controlling the leadder-laggard dynamics in delay-synchronized lasers*, Chaos **17**, 033122.

González, C. M., C. Masoller, M. C. Torrent, and J. García-Ojalvo, 2007a, *Synchronization via clustering in a small delay-coupled laser network*, Europh. Lett. **79**, 64003.

González, C. M., J. M. Buldú, M. C. Torrent, and J. García-Ojalvo, 2007b, *Processing distributed inputs in coupled excitable lasers*, Phys. Rev. A **76**, 053824.

Gordon, J. P., H. J. Zeiger, and C. H. Townes, 1954, *Molecular microwave oscillator and new hyperfine structure in microwave spectrum of NH_3*, Phys. Rev. Lett. **95**, 282.

Grohs, J., S. Apanasevich, P. Jung, H. Ißler, D. Burak, and C. Klingshirn, 1994, *Noise-induced switching and stochastic resonance in optically nonlinear CdS crystals*, Phys. Rev. A **49**, 2199.

Gross, N., W. Kinzel, I. Kanter, M. Rosenbluh, and L. Khaykovich, 2006, *Synchronization of mutually versus unidirectionally coupled chaotic semiconductor lasers*, Opt. Comm. **267**, 464.

Hall, R. N., G. E. Fenner, J. D. Kingsley, T. J. Soltys, and R. O. Carlson, 1962, *Coherent light emission from GaAs junctons*, Phys. Rev. Lett. **9**, 366.

Hänggi, P., P. Talkner, and M. Borkovec, 1990, *Reaction-rate theory: fifty years after Kramers*, Rev. Mod. Phys. **62**, 251.

Hayashi, I., M. B. Panish, P. W. Foy, and S. Sumsky, 1970, *Junction lasers which operate continuously at room temperature*, Appl. Phys. Lett. **17**, 109.

Hawks, J. and I. Latimer, 1995, *Lasers: theory and practice*, Prentice & Hall Europe.

Heil, T., I. Fischer and W. Elsäßer, 1998, *Coexistence of low-frequency fluctuations and stable emission on a single high-gain mode in semiconductor lasers with external optical feedback*, Phys. Rev. A **58**, R2672.

Heil, T, I. Fischer, W. Elsäßer, J. Mulet, and C.R. Mirasso, 1999b, *Statistical properties of low-frequency fluctuations during single-mode operation in distributed-feedback lasers: experiments and modeling*, Opt. Lett. **24**, 1275.

Heil, T., I. Fischer and W. Elsäßer, 1999a, *Influence of amplitude-phase coupling on the dynamics of semiconductor lasers subject to optical feedback*, Phys. Rev. A **60**, 634.

Heil, T., I. Fischer, and W. Elsäßer, 2000, *Stabilization of feedback induced instabilities in semiconductor lasers*, J. Opt. B: Quantum Semiclass. Opt. **2**, 413.

Heil, T., I. Fischer, W. Elsäßer, J. Mulet, and C. R. Mirasso, 2001, *Chaos synchronization and spontaneous symmetry-breaking in symmetrically delay-coupled semiconductor lasers*, Phys. Rev. Lett. **86**, 795.

Heil, T., 2001, *Delay dynamics in semicondcutor lasers. Feedback and coupling induced instabilites, stabilization, and synchronization*, PhD Thesis, Technische Universität Darmstadt, Darmstadt.

Heil, T., J. Mulet, I. Fischer, C. R. Mirasso, M. Peil, P. Colet, and W. Elsäßer, 2002, *ON/OFF phase shift keying for chaos-encrypted communication using external-cavity semiconductor lasers*, IEEE J. Quantum Electron. **38**, 1162.

Henry, C. H., R. A. Logan, and K. A. Bertness, 1981, *Spectral dependence of the change in refractive index due to carrier injection in Ga As lasers*, J. Appl. Phys. **52**, 4457.

Henry, C. H., 1982, *Theory of the linewidth of semiconductor lasers*, IEEE J. Quantum Electron. 18, 259.

Henry, C. H. and R. F. Kazarinov, 1986, *Instability of semiconductor lasers due to optical feedback from distant reflectors*, IEEE J. Quantum Electron. 22, 294.

Henning, I. D. and J.V. Collins, 1983, *Measures of the semiconductor laser linewidth broadening factor*, Elect. Lett. **19**, 927.

Herrero, R., M. Figueras, J. Rius, F. Pi, and G. Orriols, 2000, *Experimental observation of the amplitude death effect in two coupled nonlinear oscillators*, Phys. Rev. Lett. **84**, 5312.

Hirota, O. and Y. Suematsu, 1979, *Noise properties of injection laser reflected waves*, IEEE J. Quantum Electron. **15**, 142.

Hofstetter, D. and R. L. Thorntom, 1998, *Measurement of optical cavity properties in semiconductor lasers by Fourier analysis of the emission spectrum*, IEEE J. Quantum Electron. **34**, 1914.

Hofstetter, D. and R. L. Thorntom, 1998a, *Loss measurements on semiconductor lasers by Fourier analysis of the emission spectra*, Appl. Phys. Lett **72**, 404.

Hohl, A., A. Gavrielides, T. Erneux, and V. Kovanis, 1997, *Localized synchronization in two coupled nonidentical semiconductor lasers*, Phys. Rev. Lett. **78**, 4745.

Hohl, A., A. Gavrielides, T. Erneux, and V. Kovanis, 1999, *Quasiperiodic synchronization for two delay-coupled semiconductor lasers*, Phys. Rev. A **59**, 3941.

Homar, M., M. San Miguel, and S. Balle, 1993, *Semiconductor lasers with weak optical feedback: spectral properties and frequency-dependent losses*, Opt. Lett. **18**, 1329.

Horsthemke, W. and R. Lefever, 1984, *Noise induced transitions*, Springer, Berlin.

Huber, D. and L. S. Tsimring, 2005, *Cooperative dynamics in a network of stochastic elements with delayed feedback*, Phys. Rev. E **71**, 036150.

Hui, R., A. D'Ottavi, A. Mecozzi, and P. Spano, 1990, *Novel measurement technique of α factor in DFB semiconductor lasers by injection locking*, Elect. Lett. **26**, 997.

Ito, M. and T. Kimura, 1980, *Carrier density dependence of refractive index in AlGaAs semiconductor lasers*, IEEE J. Quantum Electron. **16**, 910.

Izhikevich, E. M., 2005, *Polychronization: Computation with Spikes*, Neural Comp. **18**, 245.

Javan, A., W. R. Bennett, and D. R. Herriot, 1961, *Population inversion and continuous optical maser oscillation in a gas discharge containing a He-Ne mixture*, Phys. Rev. Lett. **6**, 106.

Kasukawa, A., N. Matsumoto, I. J. Murgatroy, T. Fukushima, S. Kashiwa, and H Okamoto, 1990, *Temperature dependence of emission wavelength in $1.3\mu m$ GaInAsP/InP grin SHC MQW laser diodes grown by MOCVD*, Semicond. Sci. Techmol. **5**, 498.

Keener, J. and J. Snyder, 1998, *Mathematical Physiology*, Springer, New York.

Kim, M. Y., R. Roy, J. L. Aron, T. W. Carr, and I. B. Schwartz, 2005, *Scaling behavior of laser population dynamics with time-delayed coupling: theory and experiment*, Phys. Rev. Lett. **94**, 088101.

Klein, E., N. Gross, M. Rosenbluh, W. Kinzel, L. Khaykovich, and I. Kanter, 2006, *Stable isochronal synchronization of mutually coupled chaotic lasers*, Phys. Rev. E **73**, 066214.

Kozyreff, G., A. G. Vladimirov, and P. Mandel, 2000, *Global coupling with time delay in an array of semiconductor lasers*, Phys. Rev. Lett. **85**, 3809.

Krauskopf, B., S. Wieczorek, and D. Lenstra, 2000, *Different types of chaos in an optically injected semiconductor laser*, Appl. Phys. Lett. **77**, 1611.

Kroemer, H., 1963, *A proposed class of heterojunction injection lasers*, Proc. IEEE **51**, 1782.

Kuhn, T. S., 1978, *Black-Body Theory and the quantum discontinuity, 1894-1912*, University of Chicago Press.

Lasher, G. and F. Stern, 1964, *Spontaneous and stimulated recombination radiation in semiconductors*, Phys. Rev. Ser. II **133**, A533.

Lang, R. and K. Kobayashi, 1980, *External optical feedback effects on semiconductor injection laser properties*, IEEE J. Quantum Electron. **16**, 347.

Lang, R., 1982, *Injection locking properties of a semiconductor laser*, IEEE J. Quantum Electron. **18**, 976.

Lee, M. W., J. Paul, C. Masoller, and K. A. Shore, 2006, *Observation of cascade complete-chaos synchronization with zero time lag in laser diodes*, J. Opt. Soc. Amer. B **23**, 846.

Lenstra, D., B. H. Verbeek, and A. J. Den Boef, 1985, *Coherence collapse in single-mode semiconductor lasers due to optical feedback*, IEEE J. Quantum Electron. **21**, 674.

Levine, A. M., G. H. M. van Tartwijk, D. Lenstra, and T. Erneux, 1995, *Diode lasers with optical feedback: stability of the maximum gain mode*, Phys. Rev. A **52**, R3436.

Li, Y., Y. Wang, and A. Wang, 2008, *Message filtering characteristics of semiconductor laser as receiver in optical chaos communications*, Opt. Comm. **281**, 2656.

Lindner, B., J. García-Ojalvo, A. Neiman, and L. Schimansky-Geier, 2004, *Effects of noise in excitable systems*, Phys. Rep. **392**, 321.

Liu, J. M., 2005, *Photonic devices*, University Press, Cambridge.

Liu, Y. and P. Davis, 2000, *Synchronization of chaotic mode hopping*, Opt. Lett. **25**, 475.

Liu, Y., Y. Yakiguchi, P. Davis, T. Aida, S. Saito, and J. M. Liu, 2002, *Experimental observation of complete chaos synchronization in semiconductor lasers*, App. Phys. Lett. **80**, 4306.

Liu, J., H. Chen, and S. Tang, 2002a, *Synchronized chaotic optical communications at high bit rates*, IEEE J. Quantum Electron. **38**, 1184.

Locquet, A., F. Rogister, M. Sciamanna, P. Mégret, and M. Blondel, 2001, *Two types of synchronization in unidirectionally coupled chaotic external-cavity semiconductor lasers*, Phys. Rev. E **64**, 045203(R).

Locquet, A., C. Masoller, P. Mégret, and M. Blondel, 2002, *Comparison of two types of synchronization of external-cavity semiconductor lasers*, Opt. Lett. **27**, 31.

Locquet, A., C. Masoller, and C. R. Mirasso, 2002a, *Synchronization regimes of optical-feedback-induced chaos in unidirectionally coupled semiconductor lasers*, Phys. Rev. E **65**, 056205.

Longtin, A., A. Bulsara, and F. Moss, 1998, *Time interval sequences in bistable systems and noise induced transmission of neural information*, Phys. Rev. Lett. **67**, 656.

Maiman, T. H., 1960, *Stimulated optical radiation in ruby*, Nature **187**, 493.

Mainen, Z. F. and T. J. Sejnowski, 1995, *Reliability of spike timing in neocortical neurons*, Science **268**, 1503.

Manjarrez, E., P. Balenzuela, J. Garcia-Ojalvo, E. E. Vasquez, L. Martinez, A. Flores, and C. R. Mirasso, 2006, *Phantom reflexes: muscle contractions at a frequency not physically present in the input*, BioSystems **90**, 379.

Manrubia, S. C. and A. S. Mikhailov, 1999, *Mutual synchronization and clustering in randomly coupled chaotic dynamical networks*, Phys. Rev. E **60**, 1579.

Manrubia, S. C., A. S. Mikhailov, and D. H. Zanette, 2004, *Emergence of dynamical order*, World Scientific, Singapore.

Marino, F., M. Giudici, S. Barland, and Salvador Balle, 2002, *Experimental evidence of stochastic resonance in an excitable optical system*, Phys. Rev. Lett. **88**, 040601.

Maritan, A. and J. R. Banavar, 1994, *Chaos, noise, and synchronization*, Phys. Rev. Lett. **72**, 1451 (see also comment from Pikovsky (Pikovsky, 1994)).

Martínez Avila, J. F., R. Vicente, J. R. Rios Leite, and C. R. Mirasso, 2007, *Synchronization properties of bidirectionally coupled semiconductor lasers under asymmetric operating conditions*, Phys. Rev. E. **75**, 066202.

Masoller, C., 1997, *Implications of how the linewidth enhancement factor is introduced on the Lang and Kobayashi model*, IEEE J. Quantum Electron. **33**, 796.

Masoller, C., 1997a, *Comparison of the effects of nonlinear gain and weak optical feedback on the dynamics of semiconductor lasers*, IEEE J. Quantum Electron. **33**, 804.

Masoller, C. and N. B. Abraham, 1998, *Stability and modulation properties of a semiconductor laser with weak optical feedback from a distant reflector*, Phys. Rev. A **57**, 1313.

Masoller, C., 2001, *Anticipation in the Synchronization of Chaotic Semiconductor Lasers with Optical Feedback*, Phys. Rev. Lett. **86**, 2782.

Masoller, C. and A. C. Marti, 2005, *Random delays and the synchronization of chaotic maps*, Phys. Rev. Lett. **94**, 134102.

McNamara, B., K. Wiesenfeld, and R. Roy, 1988, *Observation of Stochastic Resonance in a Ring Laser*, Phys. Rev. Lett. **60**, 2626.

Mirasso, C. R., P. Colet, and P. García-Fernández, 1996, *Synchronization of chaotic semiconductor lasers: application to encoded communications*, IEEE Phot. Techn. Lett. **8**, 299.

Mirasso, C. R., 2000, *Fundamental issues of nonlinear laser dynamics*, edited by B. Krauskopf and D. Lenstra, American Insitute of Physics **548** of *AIP Conf. Proc.*, chap. 6.

Mirasso, C. R., J. Mulet, and C. Masoller, 2002, *Chaos shift-keying encryption in chaotic external-cavity semiconductor lasers using a single-receiver scheme*, IEEE Phot. Techn. Lett. **14**, 1041.

Mobarham, K. S., 2007, "Test and characterization of laser diodes: determination of principal parameters", Application notes of Newport corporation.

Mørk, J., B. Tromborg, and P. L. Christiansen, 1988, *Bistability and low frequency fluctuations in semiconductor lasers with optical feedback: a theoretical analysis*, IEEE J. Quantum Electron. **24**, 123.

Mørk, J., J. Mark and B. Tromborg, 1990, *Route to chaos and competition between relaxation oscillations for a semiconductor laser with optical feedback*, Phys. Rev. Lett. **65**, 1999.

Mørk, J., B. Tromborg, and J. Mark, 1992, *Chaos in semiconductor lasers with optical feedback: theory and experiment*, IEEE J. Quantum Electron. **28**, 93.

Moser, M., R. Winterhoff, C. Geng, I. Queisser, F. Scholz, and A. Dörnen, 1994, *Refractive index of* $(Al_xGa_{1-x})_{0.5}In_{0.5}P$ *grown by metalorganic vapor phase epitaxy*, Appl. Phys. Lett. **64**, 235.

Mulet, J. and C. R. Mirasso, 1999, *Numerical statistics of power dropouts based on the Lang-Kobayashi model*, Phys. Rev. E **59**, 5400.

Mulet, J., C. Masoller, and C. R. Mirasso, 2002, *Modeling bidirectionally coupled single-mode semiconductor lasers*, Phys. Rev. A **65**, 063815.

Murakami, A. and J. Ohtsubo, 2002, *Synchronization of feedback-induced chaos in semiconductor lasers by optical injection*, Phys. Rev. A **65**, 033826.

Nakamura, M., K. Aiki, N. Chinone, R. Ito, and J. Umeda, 1978, *Longitudinal-mode behaviors of mode-stabilized $Al_xGa_{1-x}As$ injection lasers*, J. Appl. Phys. **49**, 4644.

Nakamura, Y., F. Tominaga, and T. Munakata, 1994, *Clustering behavior of time-delayed nearest-neighbor coupled oscillators*, Phys. Rev. E **49**, 4849.

Nathan, M. I., W. P. Dumke, G. Burns, F. H. Dill, and G. J. Lasher, 1962, *Stimulated emission of radiation from GaAd p-n junctions*, Appl. Phys. Lett. **1**, 62.

Neiman, A., L., Schimansky-Geier, A. Cornell-Bell, and F. Moss, 1999, *Noise enhanced phase synchronization in excitable media*, Phys. Rev. Lett. **83**, 4896.

Ohtsubo, J., 2002, *Chaotic dynamics in semiconductor lasers with optical feedback*, ed. by E. Wolf, Progress in Optics **44**, Elsevier, Amsterdam.

Otsuka, K., T. Ohtomo, T. Maniwa, H. Kawasaki, and J. Y. Ko, 2003, *Noise-driven switching and chaotic itinerancy among dynamic states in a three-mode intracavity second-harmonic generation laser operating on a Λ transition*, Chaos **13**, 1014.

Palenzuela, C., R. Toral, C. Mirasso, O. Calvo, and J. Gunton, 2001, *Coherence resonance in chaotic systems*, Europhys. Lett. **56**, 347.

Pantev, C., T. Elbert, B. Ross, C. Eulitz, and E. Terhardt, 1996, *Binaural fusion and the representation of virtual pitch in the human auditory cortex*, Hearing Res. **100**, 164.

Paoli, T. L., J. E. Ripper, A. C. Morosini, and N. B. Pantel, 1975, *Suppression of intensity self-pulsations in CW junction lasers by frequency-selective optical feedback*, IEEE J. Quantum Electron. **11**, 525.

Park, S. H., S. Kim, H. B. Pyo, and S. Lee, 1999, *Phase synchronization in the forced Lorenz system*, Phys. Rev. E **60**, 4962.

Pecora, L. M. and T. L. Carroll, 1990, *Synchronization in chaotic systems*, Phys. Rev. Lett. **64**, 821.

Pecora, L. M. and T. L. Carroll, 1991, *Driving systems with chaotic signals*, Phys. Rev. A **44**, 2374.

Pecora, L. M., T. L. Carroll, G. A. Johnson, D. J. Mar, and J. F. Heagy, 1997, *Fundamentals of synchronization in chaotic systems, concepts and applications*, Chaos **7**, 520.

Peil, M., T. Heil, I. Fischer, and W. Elsäßer, 2002, *Synchronization of chaotic semiconductor laser systems: a vectorial coupling-dependence scenario*, Phys. Rev. Lett. **88**, 174101.

Peil, M., 2006, *Dynamics and synchronization phenomena of semiconductor lasers with delayed optical feedback: utilizing nonlinear dynamics for novel applications*, PhD Thesis, Technische Universität Darmstadt, Logos Verlag Berlin, Darmstadt.

Petermann, K., 1988, *Laser diode modulation and noise*, Kluwer Academic Press.

Petermann, K., 1995, *External optical feedback phenomena in semiconductor lasers*, IEEE J. Sel. Top. Quantum Electron. **1**, 480.

Pikovsky, A. S., 1994, *Comment on "Chaos, noise, and synchronization"*, Phys. Rev. Lett. **73**, 2931.

Pikovsky, A. S. and J. Kurths, 1997, *Coherence resonance in a noise-driven excitable system*, Phys. Rev. Lett. **78**, 775.

Pikovsky, A., M. Rosenblum, and J. Kurths, 2003, *Synchronization: a universal concept in nonlinear sciences*, Cambridge University Press, Cambridge, England.

Proktov, A. M., 1958, *Molecular amplifier and generator for sub-millimeter waves*, Soviet Phys. JETP Englisch Transl. **34**, 1658.

Pyragas, K., 1983, *Predictable chaos in slightly perturbed unpredictable chaotic systems*, Phys. Lett. A **181**, 203.

Quist, T. M., R. J. Keyes, W. E. Krag, B. Lax, A. L. McWhorter, R. H. Rediker, and H. J. Zeiger, 1962, *Semiconductor maser of GaAs*, Appl. Phys. Lett. **1**, 91.

Reddy, D. V. R., A. Sen, and G. L. Johnston, 1998, *Time delay induced death in coupled limit cycle oscillators*, Phys. Rev. Lett. **80**, 5109.

Rees, P., P. S. Spencer, I. Pierce, S. Sivaprakasam, and K. A. Shore, 2003, *Anticipated chaos in a nonsymmetric coupled external cavity laser system*, Phys. Rev. A **68**, 033818.

Risch, Ch. and C. Voumard, 1977, *Self-pulsation in the output intensity and spectrum*

of GaAs-AlGaAs cw diode lasers coupled to a frequency-selective external optical cavity, J. Appl. Phys. **48**, 2083.

Rogister, F., A. Locquet, D. Pieroux, M. Sciamanna, O. Deparis, P. Mégret, and M. Blondel, 2001, *Secure communication scheme using chaotic laser diodes subject to incoherent optical feedback and incoherent optical injection*, Opt. Lett. **26**, 1486.

Rogister, F. and R. Roy, 2007, *Localized excitations in arrays of synchronized laser oscillators*, Phys. Rev. Lett. **98**, 104101.

Rosenblum, M. G., A. S. Pikovsky, and J. Kurths, 1997, *From phase to lag synchronization in coupled chaotic oscillators*, Phys. Rev. Lett. **78**, 4193 .

Roy, R. and K. S. Thornburg, 1994, *Experimental synchronization in chaotic lasers*, Phys. Rev. Lett. **72**, 3502.

Russell, D. P, 1987, *An introduction to the development of the semiconductor laser*, IEEE J. Quantum Electron. **23**, 651.

Ryan, A. T., G. P. Agrawal, G. R. Gray, and E. C. Gage, 1994, *Optical-feedback-induced chaos and its control in multimode semiconductor lasers*, IEEE J. Quantum Electron. **30**, 668.

Sacher, J., W. Elsäßer, and E. O. Gobel, 1992, *Intermittency in the coherence collapse of a semiconductor laser with external feedback*, Phys. Rev. Lett **63**, 2224.

Sacher, J., D. Baums, P. Panknin, W. Elsäßer, and E. O. Gobel, 1992, *Intensity instabilities of semiconductor lasers under current modulation, external light injection, and delayed feedback*, Phys. Rev. A **45**, 1893.

San Miguel, M. and R. Toral, 2000, *Stochastic effects in physical systems*, Review Paper, Inst. and Non. Str. VI, E. Tirapegui, J. Martinez, and R. Tiemann, Kluwer Ac. Publishers **35**, 230.

Sánchez, E., M. A. Matías, and V. Pérez-Muñuruzi, 1997, *Analysis of synchronization of chaotic sytems by noise: an experimental study*, Phys. Rev. E **56**, 4068.

Sánchez-Diaz, A., C.R. Mirasso, P. Colet, and Garcia-Fernández, 1999, *Encoded Gbit/s digital communications with synchronized chaotic semiconductor lasers*, IEEE J. Quantum Electron. **35**, 292.

van der Sande, G., G. Verschaffelt, J. Danckaert, and C. R. Mirasso, 2005, *Ghost stochastic resonance in vertical-cavity surface-emitting lasers: experiment and theory*, Phys. Rev. E **72**, 016113.

Sano, T.,1994, *Antimode dynamics and chaotic itinerancy in the coherence collapse of semiconductor lasers with optical feedback*, Phys. Rev. A **50**, 2719.

Schäfer, C., M. G. Rosemblum, H. H. Abel, and J. Kurths, 1999, *Synchronization in the human cardiorespiratory system*, Phys. Rev. E **60**, 857.

Schawlow, A. L. and C. H. Townes, 1958, *Infrared and optical masers*, Phys. Rev. **112**, 1940 .

Schouten, J. F., R. J. Ritsma, and B. L. Cardozo, 1962, *Pitch of the residue*, J. Acoust. Soc. Am. **34**, 1418.

Schuster, H. G. and P. Wagner, 1989, *Mutual entrainment of two limit cycle oscillators with time delayed coupling: general and mathematical physics*, Prog. Theor. Phys. **81**, 939.

Shahverdiev, E. M., S. Sivaprakasam, and K. A. Shore, 2002, *Inverse anticipating chaos synchronization*, Phys. Lett. A **292**, 320.

Sigg, J., 1993, *Effects of optical feedback on the light-current characteristics of semiconductor lasers*, IEEE J. Quantum Electron. **29**, 1262.

Sivaprakasam, S. and K. A. Shore, 1999, *Demonstration of optical synchronization of chaotic external cavity laser diodes*, Opt. Lett. **24**, 466.

Sivaprakasam, S. and K.A. Shore, 1999a, *Signal masking for chaotic optical communication using external-cavity diode lasers*, Opt. Lett. **24**, 1200.

Sivaprakasam, S., E. M. Shahverdiev, P. S. Spencer, and K. A. Shore, 2001, *Experimental demonstration of anticipating synchronization in chaotic semiconductor lasers with optical feedback*, Phys. Rev. Lett. **87**, 154101.

Sivaprakasam, S., J. Paul, P. S. Spencer, P. Rees, and K. A. Shore, 2002, *Regimes of chaotic synchronization in external-cavity laser diodes*, IEEE J. Quantum Electron. **38**, 1155.

Sivaprakasam, S., J. Paul, P. S. Spencer, P. Rees, and K. A. Shore, 2003, *Nullfied time-of-flight lead-lag in synchronization of chaotic external-cavity laser diodes*, Opt. Lett. **28**, 1397.

Strauss, U., W. W. Rühle, H. J. Queisser, K. Nakano, and A. Ishibashi, 1994, *Band-to-band recombination in $Ga_{0.5}In_{0.5}P$*, J. Appl. Phys. **75**, 8204 .

Strogatz, S. H. and I. Stewart, 1993, *Coupled oscillators and biological synchronization*, Sci. Am. Mag. **269**, 102.

Sugawara, T., M. Tachikawa, T. Tsukamoto, and T. Shimizu, 1994, *Observation of synchronization in laser chaos*, Phys. Rev. Lett. **72**, 3502.

Sukow, D. W. , T. Heil, I. Fischer, A. Gavrielides, A. Hohl-AbiChedid, and W. Elsäßer, 1999, *Picosecond intensity statistics of semiconductor lasers operating in the low-frequency fluctuation regime*, Phys. Rev. A **60**, 667.

Sukow, D. W. and D. J. Gauthier, 2000, *Entraining power-dropout events in an external cavity semiconductor laser using weak modulation of the injection current*, IEEE J. Quantum Electron. **36**, 175.

Takiguchi, Y., Y. Liu, and J. Ohtsubo, 1998, *Low-frequency fluctuation induced by injection-current modulation in semiconductor lasers with optical feedback*, Opt. Lett. **23**, 1369.

Takiguchi, Y., H. Fujino, and J. Ohtsubo, 1999, *Experimental synchronization of chaotic oscillations in externally injected semiconductor lasers in low-frequency fluctuation regime*, Opt. Lett. **24**, 1570.

Tanguy, Y., J. Houlihan, G. Huyet, E. A. Viktorov, and P. Mandel, 2006, *Synchronization and clustering in a multimode quantum dot laser*, Phys. Rev. Lett. **96**, 053902.

Tang, S. and J. M. Liu, 2003, *Experimental verification of anticipated and retarded synchronization in chaotic semiconductor lasers*, Phys. Rev. Lett. **90**, 194101.

van Tartwijk, G. H. M. and D. Lenstra, 1995, *Semiconductor laser with optical injection and feedback*, Quantum. Semiclass. Opt. **7**, 87.

van Tartwijk, G. H. M., A. M. Levine, and D. Lenstra, 1995a, *Sisyphus effect in semiconductor lasers with optical feeback*, IEEE J. Sel. Top. Quantum. Electron. **1**, 466.

van Tartwijk, G. H. M. and G. P. Agrawal, 1998, *Laser instabilities: a modern perspective*, Prog. Quantum Electron **22**, 43.

van Tartwijk, G. H. M. and I. Fischer, 1998, *Comment on "Andronov bifurcation and excitability in semiconductor lasers with optical feedback'*, Phys. Rev. E **58**, 4041.

van Tartwijk, G. H. M. and D. Lenstra, 1998, *Low-frequency fluctuations in semiconductor lasers with optical feedback*, Asian J. Phys. **7**, 562.

Tkach, R. W. and A. R. Chraplyvy, 1986, *Regimes of feedback effects in* 1.5 μm *distributed feedback lasers*, J. Light. Techn. **4**, 1655.

Toral, R., C. R. Mirasso, E. Herdández-García, and O. Piro, 2001, *Analitical and numerical studies of noise-induced synchronization of chaotic systems*, Chaos **11**, 665.

Tromborg, B., J. H. Osmundsen, and H. Olesen, 1984, *Stability analysis for a semiconductor laser in an external cavity*, IEEE J. Quantum Electron. **20**, 1023.

Tromborg, B., H. Olesen, X. Pan, and S. Saito, 1987, *Transmission line description of optical feedback and injection locking for Fabry-Perot and DFB lasers*, IEEE J. Quantum Electron. **23**, 1875.

Uchida, A., S. Yoshimori, M. Shinozuka, T. Ogawa, and F. Kannari, 2001, *Chaotic on-off keying for secure communications*, Opt. Lett. **26**, 866.

Uchida, A., T. Heil, Y. Liu, P. Davis, and T. Aida, 2003, *High-frequency broad-band signal generation using a semiconductor laser with a chaotic optical injection*, IEEE J. Quantum Electron. **39**, 1462.

Uchida, A., Y. Liu, and P. Davis, 2003a, *Characteristics of chaotic masking in synchronized semiconductor lasers*, IEEE J. Quantum Electron. **39**, 963.

Uchida, A., R. McAllister, and R. Roy, 2004, *Consistency of nonlinear system response to complex drive signals*, Phys. Rev. Lett. **93**, 244102.

Uchida, A., F. Rogister, J. Garcia-Ojalvo, and R. Roy, 2005, *Synchronization and communication with chaotic laser systems*, Prog. Opt **48**, 203.

Vahala, K., Ch. Harder, and A. Yariv, 1983, *Observation of relaxation resonance effects in the field spectrum of semiconductor lasers*, Appl. Phys. Lett. **42**, 211.

Vicente, R.,T. Perez, and C. R. Miraso, 2002, *Open-versus closed-loop performance of synchronized chaotic external-cavity semiconductor lasers*, IEEE J. Quantum Electron. **38**, 1197.

Vicente, R., C. R. Miraso, and I. Fischer, 2007, *Simultaneous bidirectional message transmission in a chaos-based communication scheme*, Opt. Lett. **32**, 403.

Voss, H. U., 2000, *Anticipating chaotic synchronization*, Phys. Rev. E **61**, 5115.

Wang, W., I. Z. Kiss, and J. L. Hudson, 2000, *Experiments on arrays of globally coupled chaotic electrochemical oscillators: synchronization and clustering*, Chaos **10**, 248.

Weiss, C. O. and R. Vilaseca, 1991, *Dynamics of lasers*, VCH Verlagsgesellschaft, Weinheim, Germany.

Wieczorek, S., B. Krauskopf, T. B. Simpson, and D. Lenstra, 2005, *The dynamical complexity of optically injected semiconductor lasers*, Phys. Rep. **416**, 1.

Wiesenfeld, K., and F. Jaramillo, 1998, *Minireview of stochastic resonance*, Chaos **8**, 539.

van Wiggeren, G. D. and R. Roy, 1998, *Communication with chaotic lasers*, Science **279**, 1198.

van Wiggeren, G. D. and R. Roy, 1998a, *Communication with optical chaotic waveforms*, Phys. Rev. Lett. **81**, 3547.

van Wiggeren, G. D. and R. Roy, 1999, *Chaotic communications using time-delayed optical systems*, Int. J. Bif. and Chaos **9**, 2129.

Winful, H. G. and L. Rahman, 1990, *Synchronized chaos and spatiotemporal chaos in arrays of coupled lasers*, Phys. Rev. Lett. **65**, 1575.

White, J. K. and J. V. Moloney, 1999, *Multichannel commuicaiton using infinite dimensional spatiotemporal chaotic system*, Phys. Rev. A **59**, 2422.

Wu, L., S. Zhu, and Y. Ni, 2007, *Combination of two basic types of synchronization in a coupled semiconductor laser system*, Eur. Phys. J. D **41**, 349.

Wunsche, H. J., S. Bauer, J. Kreissl, O. Ushakov, N. Korneyev, F. Henneberger, E. Wille, H. Erzgraber, M. Peil, W. Elsässer, and I. Fischer, 2005, *Synchronization*

of delay-coupled oscillators: a study of semiconductor lasers, Phys. Rev. Lett. **94**, 163901.

Yamada, M., 1983, *Transverse and longitudinal mode control in semiconductor injection lasers*, IEEE J. Quantum Electron. **19**, 1365.

Yamada, M. and H. Fujisaka, 1983, *Stability theory of synchronized motion in coupled-oscillator systems. II*, Prog. Theor. Phys. **70**, 1240.

Yamada, M. and H. Fujisaka, 1984, *Stability theory of synchronized motion in coupled-oscillator systems. III*, Prog. Theor. Phys. **72**, 885.

Yanchuk, S., 2005, *Discretization of frequenies in delay coupled oscillators*, Phys. Rev. E **72**, 036205.

Yariv, A., 1989, *Quantum Electronics*, John Wiley & Sons, New York.

Yeung, M. K. S. and S. H. Strogratz, 1999, *The delay in Kuramoto model of coupled oscillators*, Phys. Rev. Lett. **82**, 648.

Zhou, C. and J. Kurths, 2002, *Noise induced phase synchronization and synchronization transitions in chaotic oscillators*, Phys. Rev. Lett. **88**, 230602.

Zhou, B. B. and R. Roy, 2007, *Isochronal synchrony and bidirectional communications with delay-coupled oscillators*, Phys. Rev. E **75**, 026205.

LIST OF PUBLICATIONS

- "Coupling-mediated ghost resonance in mutually injected lasers", J. M. Buldú, C. M. González, J. Trull, M. C. Torrent, and J. García-Ojalvo, Chaos **15**, 013103 (2005).

- "Processing distributed inputs in coupled excitable lasers", C. M. González, J. M. Buldú, M.C. Torrent, and J. García-Ojalvo, Phys. Rev. A **76**, 053824 (2007).

- "Controlling the leadder-laggard dynamics in delay-synchronized lasers",C. M. González, M. C. Torrent, and J. García-Ojalvo, Chaos **17**, 033122 (2007).

- "Synchronization via clustering in a small delay-coupled laser network", C. M. González, C. Masoller, M. C. Torrent, and J. García-Ojalvo, Europh. Lett. **79**, 64003 (2007).

- "Quasiperiodic transition to chaos of two mutually coupled lasers", C. M. González, T. Berkvens, I. Fischer, M. C. Torrent, and J. García-Ojalvo, in preparation.

- "Isochronal solution induced by external noise in two muttually coupled semiconductor lasers", C. M. González, I. Fischer, M. C. Torrent, and J. García-Ojalvo, in preparation.